www.emu.ee
Eesti Maaülikool
Estonian University of Life Sciences

THE CHARACTERIZATION AND MODELLING OF THE DYNAMIC BEHAVIOR OF HARD-TO-MACHINE ALLOYS

RASKESTI LÕIKETÖÖDELDAVATE METALLISULAMITE DEFORMATSIOONI KIRJELDAMINE JA MODELLEERIMINE

TÕNU LEEMET

A Thesis
for applying for the degree of Doctor of Philosophy
in Production Engineering

Väitekiri
Filosoofiadoktori kraadi taotlemiseks
tootmistehnika erialal

Tartu 2012

EESTI MAAÜLIKOOL
ESTONIAN UNIVERSITY OF LIFE SCIENCES

Eesti Maaülikool
Estonian University of Life Sciences

THE CHARACTERIZATION AND MODELLING OF THE DYNAMIC BEHAVIOR OF HARD-TO-MACHINE ALLOYS

RASKESTI LÕIKETÖÖDELDAVATE METALLISULAMITE DEFORMATSIOONI KIRJELDAMINE JA MODELLEERIMINE

TÕNU LEEMET

A Thesis
for applying for the degree of Doctor of Philosophy
in Production Engineering

Väitekiri
Filosoofiadoktori kraadi taotlemiseks
tootmistehnika erialal

Tartu 2012

Institute of Technology
Estonian University of Life Sciences

According to verdict No 22 of November 20, 2012, the Doctoral Committee of the Engineering Sciences of the Estonian University of Life Sciences has accepted this for thesis for the defence of degree of Doctor of Philosophy in Production Engineering.

Opponent: **Professor Jānis Rudzītis** Dr. habil. hc. ing.
Institute of Mechanical Engineering
Riga Technical University

Opponent: **Jüri Majak**, doc. math.
Faculty of Mechanical Engineering
Tallinn University of Technology

Supervisor: **Professor Jüri Olt**, Dr. Sc.(Eng)
Estonian University of Life Sciences

Defence of the thesis:
Estonian University of Life Sciences, Institute of Technology, room B136, Kreutzwaldi 56, Tartu, on 21 December, 2012, at 12.00.

Publication of this dissertation is supported by the Estonian University of Life Sciences.

ISBN 978-9949-484-62-1

CONTENTS

LIST OF ORIGINAL PUBLICATIONS

I Siemers, C., Zahra, B., **Leemet, T.**, Rösler, J. Development of Advanced beta-Titanium Alloys. Proceedings of the 8th AMMT'09 Conference, St. Petersburg, Russia, (Vol. 1; 2009; 1; pp. 461-468).

II **Leemet, T.**, Hokka, M., Kuokkala, V.T., Olt, J. Behavior of Ti-15-3 alloy at wide range of strain rates and temperatures. Proceedings of 8th International Conference of DAAAM Baltic Industrial Engineering. 19-21st April 2012, Tallinn, ESTONIA, pp. 668-673.

III Hokka, M., Shrot, A., **Leemet, T.**, Baeker, M., Kuokkala, V.-T. Dynamic Behavior and Numerical Modeling of Titanium 15-3-3-3 Alloy. Proceedings of SEM XII International Congress & Exposition on Experimental and Applied Mechanics Measurement Challenges for New Structures and Materials. Hilton Orange County/Costa Mesa, Costa Mesa, CA USA June 11-14, 2012

IV Hokka, M., **Leemet, T.**, Shrot, A., Baeker, M., Kuokkala, V.-T. Modeling of the Dynamic Behavior of Hard-to-Machine Alloys. Proceedings of DYMAT 2012 - 10th International Conference on the Mechanical and Physical Behaviour of Materials under Dynamic Loading 2nd-7th, 2012, Freiburg, Germany

V Hokka, M., **Leemet, T.**, Shrot, A., Baeker, M., Kuokkala, V.-T. Characterization and Numerical Modeling of High Strain Rate Mechanical Behavior of Ti-15-3 Alloy for Machining Simulations. Materials Science and Engineering A. Nr. 550 (2012), pp. 350-357.

AUTHOR'S CONTRIBUTION

The author was involved in the planning of experimental work. Author conducted described experimental studies, data analyzes and results formatting. For interpretation of the results, valuable contribution was given by Dr. Mikko Hokka. Author worked on constitutive modeling of the flow behavior. Preliminary investigations for the applicability of original Johnson-Cook model and that of an empirical fitting model were leaded by the author. Author was there to initiate modifications to the original Johnson-Cook model. Dr. Mikko Hokka and M.Sc. Aviral Shrot gave valuable contribution in concluding the modified modeling approach. Experimental work and following analyses of the results for cutting force measurement were conducted by author. The original manuscript of thesis was written by the author and commented by Dr. Mikko Hokka and prof. Jüri Olt. All the attached papers were also commented by the co-authors.

LIST OF SYMBOLS AND ABBREVIATIONS

A	Yield stress in the Johnson-Cook material model
A_b	Cross-sectional area of the pressure bar
A_s	Cross-sectional area of the specimen
B	Material parameter in the Johnson-Cook material model
C	Strain rate factor parameter in the Johnson-Cook material model
C_0	Longitudinal elastic wave velocity
C_p	Specific heat capacity of a material
E	Young's modulus
E_T	Thermal energy
n	Strain hardening exponent in the Johnson-Cook material model
m	Thermal-softening exponent in the Johnson-Cook material model
k	Strain softening exponent in the modified Johnson-Cook model.
k_B	Boltzmann'z constant ($1.38 \cdot 10^{-23}$ J/atom·K)
L_s	Specimen length
L_{st}	Striker length
T	Absolute temperature
t	Time
T_r	Room temperature, absolute
T_{ref}	Reference temperature in the Johnson-Cook material model
v_{st}	Striker velocity
β	Fraction of mechanical energy that is converted into heat
ε	Strain
ε_e	Engineering strain
ε_i	Incident axial strain
ε_r	Reflected axial strain
ε_t	Transmitted axial strain
ε_T	True strain
$\dot{\varepsilon}$	Strain rate
$\dot{\varepsilon}_{ref}$	Reference strain rate in the Johnson-Cook material model
ΔG	Thermal energy
ΔG_M	Mechanical energy
ΔG_T	Thermal energy
σ	Stress
σ_a	Adiabatic stress in modified Johnson-Cook equation
σ_e	Engineering stress

σ_i	Isothermal stress in modified Johnson-Cook equation
σ_T	True stress
ρ	Density of the material

DAQ	Data Acquisition System
DMS	Department of Materials Science
EDM	Electric discharge machining
FMINSEARCH	Matlabs built-in multidimensional unconstrained nonlinear optimization function
HT-SHPB	High temperature Split Hopkinson Pressure Bar
LVDT	Linear variable differential transformer
MATLAB	Programming application for engineering disciplines
MES	Mechanical Equation of State
PID	Proportional-integrative-differential control, controller
TUT	Tampere University of Technology
SHPB	Split Hopkinson Pressure Bar
VAR	Vacuum arc remelting

INTRODUCTION

Today there is an increasing number of applications where construction material are being deformed fast i.e. at a high rate. Good examples are high-speed material forming and cutting operations, car crashes, vibrations of structures and buildings during earth-quakes, and various aerospace applications. In addition there are numerous applications from the defense industry. In these kinds of applications in particular, the dependence of material properties on the strain rate must be known to justify materials selection and to facilitate modeling and simulation of the material behavior.

Titanium alloy Ti-15V3Cr3Al3Sn, commercially known as Ti 15 3, is a metastable beta-titanium alloy, first introduced in 1978 by the American company USAF. Beta titanium alloys like Ti 15 3 show a unique combination of high strength, high ductility, and low density. The most important industries using these alloys are the aerospace, power generation, and chemical industries. Continuous demand for higher safety and lower CO_2 emissions make titanium alloys attractive for the automotive industry as well, but so far their use has been rather limited due to the high cost of the material (Leyens & Peters 2003; Bhattacharjee 2007). The relatively high price of titanium alloys, compared to other construction materials, has two principal reasons: 1) the production costs of the raw material and 2) the costs related to the manufacturing of the components. In some instances, up to 50% of the material has to be removed with different machining processes (Siemers 2009), which can be very time consuming and therefore expensive due to the generally poor machinability of titanium alloys. Automated high speed machining of Ti 15 3 is hampered by two key factors: first, the continuous chip production, due to which the operator must continuously interfere with the process to remove the chips manually, and second, the accelerated wear of the cutting tools due to the adiabatic heating and poor heat conductivity of the metal, which in turn causes insufficient geometrical and surface tolerances of the workpiece (Siemers 2009).

Nickel-base alloys are mostly used in high-temperature applications whenever steels or titanium alloys cannot be applied anymore. In general steels are known to lose their mechanical strength at elevated temperatures. Above around 550 °C oxidation resistance of titanium is insufficient. For

example, engine applications in aviation and power engineering demand excellent mechanical properties at temperatures above 600 °C (Ezugwu 2003).

Alloy 625 belongs to the group of austenitic Nickel-Chromium-Molybdenum alloys. It has excellent resistance to oxidation up to 850 °C and corrosion resistance in a broad range of corrosive conditions, for example jet engine environments and many other aerospace and chemical processes applications. Its superior corrosion resistance in sea water environments leads to practical usage of the alloy in marine and offshore applications, whenever stainless steels cannot be applied anymore.

During manufacturing of Alloy 625 products, up to 50% of the forged semi-finished parts have to be removed by different machining operations. Machining of these alloys is considered to be difficult because of their mechanical properties and behavior. Cutting forces are high because material retains strength and hardness to reasonably high temperatures (Ezugwu 1999; Fang 2003). Nickel-based superalloys are known to posses strong and rapid strain hardening, which can further increase the cutting forces (Dudzinski 2004). Moderate thermal conductivity of these alloys can result in adiabatic heating and increased tool temperatures which accelerates tool wear, thus adding yet one more component to the cost composition of the production. Additionally, the formation of long continuous chips instead of short segmented ones cuts down production automation ability and enhances possible tool wear and inaccuracies in the geometry of the detail.

The machinability of hard-to-machine alloys can be improved by developing so-called free machining alloys with better chip formation properties, by developing better tools, and by enhancing machining procedures, which can be greatly assisted by proper modeling of the material behavior and simulation of the machining process.

Nowadays it is considered that in the technological development process in general an optimum ratio between physical testing and numerical simulations should be found. It has also been pointed out that due to the ongoing growth in the available computing power, in the future majority of the testing needed in the development phase will be done via numerical simulations. For the simulations to provide realistic and trustworthy outcome, it is essential to have a correct constitutive relation or descrip-

tion of the behavior of the material as input. In the specific case of metal machining, dynamic plasticity needs to be described with constitutive equations, which are mathematical expressions showing the dependencies of flow stress on variables describing the state of the material and the deformation conditions.

AIM AND OBJECTIVES OF THE STUDY

Metastable beta titanium alloys have huge industrial potential especially for the aerospace industry. However, most titanium alloys have low thermal conductivity and overall high chemical reactivity at high temperatures. This can cause problems in machining if the material adheres to the machining tools (Rahman 2006; Hartung 1982; Jawaid 1999). When machining, the adiabatic heating can easily increase the temperature of the billet material and the tool by several hundreds of degrees and lead to rapid tool wear and increased machining expenses. In addition it is observed that at low cutting speeds the chip formation in the machining of titanium alloys tends to be continuous, meaning that in the worst case the machining needs to be stopped and the chip removed manually to avoid tool damage and to guarantee geometrical accuracy of the detail. Essentially similar issues and phenomena are present during the machining of several nickel based superalloys. That is why most titanium alloys and nickel based superalloys are classified as hard-to-machine materials, and the majority of the total fabrication costs of geometrically complex components can be due to the high machining costs. Therefore, improving the machinability of these alloys by improving the machining technology can significantly reduce the overall manufacturing costs of components. Simulations have become the major tool for designing and analyzing technological processes. In the specific case of machining, reliable finite element simulations need material models that can mathematically reproduce the essential features of the material behavior. Material behavior is influenced by strain rate and temperature, which can have significant effects on the strength and strain-hardening behavior of the material.

The aim and purpose of this study is to:

1) experimentally characterize titanium alloy Ti-15-3 Alloy 625 at a wide range of strain rates and temperatures;
2) analyze the effects of strain rate and temperature on to the mechanical behavior of Ti-15-3 and Alloy 625 alloys
3) to work on the development of a mathematical model describing the plastic flow behavior of Ti-15-3 alloy. A model that when implemented in the simulations would provide good agreement with machining experiments;
4) perform preliminary cutting force measurements for Ti-15-3 and Alloy 625 using the Split Hopkinson Pressure Bar technique.

List of the tasks to be solved to reach the aim:

1. Overview about the mechanics of plastic deformation of metals will be given.
2. Overview about the materials testing methods, especially ones for high rate testing, will be given.
3. Overview about the theory of modeling will be given.
4. Experimental work for determining the flow behavior or Ti-15-3 and Alloy625 will be conducted.
5. Analysis of experimental data resulting from experimental work will be conducted.
6. Method for determining the parameters in the constitutive equation will be developed.
7. Proper modification due to the thermal softening effect on the constitutive equation will be developed if needed.
8. Extrapolative power of the model will be investigated.
9. Material model with determined parameter values will be proposed and analyzed.
10. Chip morphology will be experimentally investigated.
11. Orthogonal cutting forces will be experimentally determined and compared with results from simulations.

In overall three novel and significant features can be attributed to the current study:

1. Experimental characterization of the mechanical behavior at compression of titanium alloy Ti-15-3 and Alloy 625 in a wide range of strain rates and temperatures. Including the usage of the Split Hopkinson Pressure Bar technique.
2. Modification of the classical Johnson-Cook material model. A novel method is developed to build model for complex forming operation using data from uni-axial compression tests. Physical modification is introduced to the phenomenological Johnson-Cook material model.
3. Novel experimental technique for cutting force measurements is investigated using the Split Hopkinson Pressure Bar technique.

1. THEORETICAL BACKROUND

1.1. Dislocation dynamics

The strain rate dependence of flow stress in crystalline materials at low and intermediate strain rates is explained by thermally a activated dislocation motion. A steep upturn in the flow stress is often observed at higher strain rates. This rapid increase of strength can be explained by the phenomena caused by the viscous drag on dislocations at higher dislocation glide velocities. Temperature also affects the material behaviour by changing the available thermal energy and character of the obstacles for the dislocations. Changes in the material temperature can, in turn, happen for both external and internal reasons. During deformation only 5 to 10% of imparted energy is consumed for restructuring the defect (dislocation) structure of the material, and most of the work is dissipated as heat. When the strain rate increases, there simply is not enough time for the heat to escape from the deforming material, and the isothermal conditions of low strain rate deformation change towards more adiabatic during deformation at higher strain rates. As a consequence, the deformation may become highly localized at very narrow regions within the specimen. For example, in the cutting experiments with Ti-15-3 the alloy was shown to develop these so-called adiabatic shear bands (**I**).

Plastic deformation in crystalline materials is caused by different mechanisms or by different combinations of them. The most important mechanisms being:
- dislocation slip(glide),
- mechanical twinning,
- martensite reaction,
- creep,
- others.

Movement of dislocations as predominant from the point of view of the strain rate and temperature dependent plasticity, will be discussed further. Dislocations are defects in the structure of the material. It has been shown (Isaac 1998) that the plastic deformation behavior of the material can generally be divided into three strain rate regimes depending on the effects of dislocation kinetics. Thermally activated processes are controlling dislocation motion at low and intermediate strain rates. Depending

on the specific material, flow stress in this range has a moderate dependence on the strain rate. At around a strain rate of 10^3 s^{-1} the majority of the metals exhibit a considerable upturn in the flow stress value. The exact limiting value is different for materials. In this region dislocation drag controlled deformation mechanisms take place. Increasing the strain rate even higher leads to a mechanism where dislocation speed is close to the speed of sound waves and relativistic effects start to take effect. Regions of thermally activated dislocation motion and that of viscous drag are pictured in Figure 1.

Strain rate and temperature depended plasticity of the metals in a temperature range far below melting temperature is determined by the mobility of the dislocations. Movement of dislocations is hindered by different obstacles and thereby the strength of the material is increased (Meyers 1994; Hirth 1968).

In the material, the periodic lattice and defects that are present almost all the time, constitute energy barriers for dislocations to overcome. Depending on the "size" of the barrier, division into short and long range obstacles is made. For the plastic deformation to proceed, enough energy has to be available for dislocation to overcome the barrier. Fun-

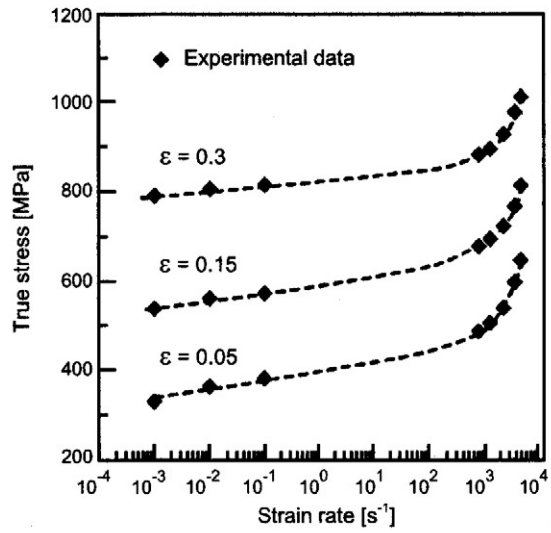

Figure 1. The flow stress as a function of the strain rate at three constant strain values. Material AISI 304 stainless steel (after Lee 2001).

damentally, energy for dislocations can be provided from two sources: externally applied stress and/or thermal vibration energy (Meyers 1994; Hirth 1968; Courtney 2000; Hosford 2006). External stress can provide energy for overcoming obstacles of both types. Thermal vibration energy can only assist in overcoming barriers of a short-range type. From here a further distinction can be made, namely long-range obstacles are classified as athermal ones and short-range ones as thermal. This principle can be illustrated with the following formula (Equation 1), a thermal obstacle with an energy barrier value of ΔG will be overcome if the mechanical ΔG_M and thermal ΔG_T energy of dislocation sum up to sufficient value.

$$\Delta G = \Delta G_M + \Delta G_T \tag{1}$$

For a given temperature T, the probability for overcoming a thermal obstacle can be estimated by Equation 2 (Meyers 1994)

$$p_B = \exp\left(-\frac{\Delta G_T}{k_B T}\right) \tag{2}$$

Where k_B is the Boltzmann constant. From the equation it can be concluded that the more thermal energy, $E_T = k_B T$ there is available at any instant, the more probable it is for the dislocation to overcome the thermal obstacle, and in this way causing the temperature dependency of the plasticity.

In addition to the above, thermal energy ΔG_T will be provided only when there is a sufficient timeperiod available. As dislocations themselves are in constant oscillation, with frequency $\upsilon_0 \sim 10^{11}$ Hz (Kocks *et al.* 1975), frequency with which a dislocation successfully overcomes an obstacle can be written, Equation 3 (Meyers 1994).

$$\nu_1 = \nu_0 p_B = \nu_0 \cdot \exp\left(-\frac{\Delta G_T}{k_B T}\right) \tag{3}$$

Time balance of the running dislocation has two components: so called running and waiting times (Curtze 2009). The former meaning the time that it takes for a dislocation to move from one obstacle to another. The latter gives the time that dislocation 'waits' in front of the barrier for a sufficient amount of energy to become available. This effect can be summarized with Equation 4 (Curtze 2009).

$$\Delta t = \Delta t_r + \Delta t_w \propto \frac{\Delta \bar{l}}{\dot{\varepsilon}} \tag{4}$$

Where Δt, Δt_r and Δt_w represent overall time, running and waiting times; Δl and $\dot{\varepsilon}$ are for length and strain rate accordingly. This should be interpreted that the higher the strain rate, the less time there is for the dislocation to receive the necessary amount of energy, ΔG_T, thus decreasing dislocation mobility and increasing the strength.

The shear stress t needed to move the dislocation can be divided to two parts as expressed by Equation 5 (Meyers 1994)

$$\tau = \tau_A + \tau^* \tag{5}$$

Where τ_A is the athermal component that can be due to external stress only, and τ^* is the thermal component i.e. part of the external stress that is for overcoming thermal obstacles.

$$\tau_T = \tau(0K) - \left(\tau_A(T) + \tau^*(T)\right) \tag{6}$$

Equation 6 expresses the amount of which the critical shear stress is lowered with the assistance of thermal energy (Curtze 2009).

The effects of the strain rate and temperature together on the plasticity of metals are summarized on Figure 2. Together with increasing temperature the thermal component τ^* decreases until certain critical temperature T_C. From there on all obstacles left are athermal in nature and internal thermal energy can't be of further assistance.

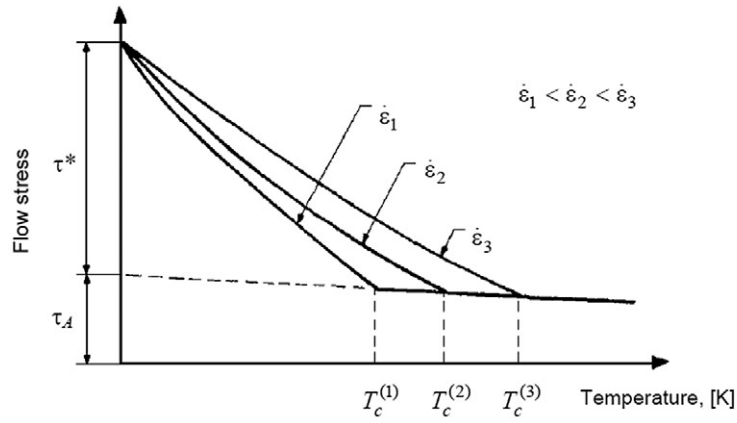

Figure 2. A schematic presentation of the temperature and strain rate effects on the flow stress of crystalline materials (Meyers 1994).

1.2. Effects of adiabatic heating

When a specimen is being deformed plastically, the majority of the work done is transformed into heat. According to (Meyers 1994) up to 90% and more of mechanical work of plastic deformation is converted into heat. Complementary temperature rise during the deformation process can be estimated with Equation 7, where ρ is the density of the material, C_p specific heat capacity of the material and β is a coefficient indicating the fraction of work that is converted to heat. Commonly used value for β is 0.9.

$$\Delta T = \frac{\beta}{\rho \cdot C_p} \int \sigma \cdot d\varepsilon \tag{7}$$

Depending on the loading rate and heat conductivity of the material being tested, different influences on the behavior can be observed due to the adiabatic heating effect. At low strain rates, there is enough time for the heat to dissipate into the surrounding environment, causing little effect in the temperature of the specimen under test, resulting in what is said to be isothermal testing. As for high rate loading, there is not sufficient time for the heat to dissipate and the accumulating heat will affect the behavior. That is known as an adiabatic testing condition. The most notable effect of adiabatic heating is the effect of thermal softening (Zener 1944) that is responsible for the decrease or even loss of strain hardening capability of the material. On the microstructural level this softening effect can be partly due to the formation of slip bands i.e. concentrated areas of deformation within the material. Ti-15-3 is being considered as a moderate heat conductor and has been reported to exhibit slip bands in the microstructure (Spotz 2011)

1.3. Modeling the material behavior

First it is important to distinguish that different areas in material behavior demand specific constitutive equations to be used (Klepaczko 2009). Only some of the material behaviors are listed below with remarks on mathematical approximation methods used for description:

i) isotropic elasticity – Hooks law,
ii) non-isotropic elasticity – specific formulations,
iii) rate-independent plasticity together with temperature dependency – Mises yield criterion and others,

iv) rate-dependent plasticity, without temperature dependency – many theories,
v) rate and temperature dependent plasticity – many specific formulations.

In the general theory of constitutive modeling, usually a division of the models into two main groups is made. The first group constitutes of phenomenological equations. These are relations developed by synthesis of experimental results together with several rounds of iterations for model optimization. In essence it is a curve-fitting technique resulting in a mathematical description of the plastic flow behavior of a particular material. It is a common understanding that a phenomenological equation possesses rather limited predictive power, meaning that they are only to be considered and used in the same range as experimental data was measured.

The second group of equations is built based on the physical principles of material behavior, hence often called physically based models. Dislocation dynamics, thermally activated processes, diffusion, recrystallization etc. are physical processes to be considering when developing physically based constitutive models for rate and temperature dependent plasticity. The major drawback here is that the number of parameters in the equation can grow beneath the practical capabilities of engineering applications. In addition there remain issues with experimental determination of the parameters. On the other hand physical models have in principle capability for being able to predict the behavior outside of the experimentally tested range. A comparison of the 'predictive' or 'extrapolative' powers of the two underlying modeling principles has been the subject of numerous studies (Nemat-Nasser 2005). There are also many good physical models available in the literature today. However, for reasons not too clear yet, physical models are not implemented in commercial computer codes to a considerable extent (Klepaczko 2009).

In addition to the two principles mentioned above, there is a third approach described in the literature. Structure-Mechanical models as they are called. The governing principle here is that modeling tries to incorporate physical reasoning and microstructural effect from the materials science together with empirical flow behavior. Some consistent research on modeling plastic flow behavior of Ti-15-3 on the basis of thermally activated processes is available in the literature (Ogawa 1997). An extensive

overview about the recent developments in the field of structure-mechanical modeling can be found from the handbook by Totten *et al.* 2004.

The fourth and perhaps most straight forward approach is to use direct measurement data in the numerical computations.

In engineering practice, constitutive equations with strain, strain rate and temperature as the variables have proved to be most useful for simulating industrial processes. The concept of mechanical equation of state (MES) has been the underlying principle in the development of the majority of the commercial solutions. The MES concept is based on the assumption that mechanical stress, strain, strain rate and temperature constitute a single unique surface in space. General mathematical form can be expressed as Equation 8.

$$\sigma = f(\varepsilon, \dot{\varepsilon}, T) \tag{8}$$

Where σ, ε, $\dot{\varepsilon}$ and T are true plastic stress, true plastic strain, true plastic strain rate and absolute temperature.

There is a myriad of specific constitutive models developed following Equation 8 and available from the literature. Here only two of the most widespread general forms are presented. Equation 9 shows a form of constitutive equation where three separate functions are set up in a multiplicative manner.

$$\sigma(\varepsilon, \dot{\varepsilon}, T) = f(\varepsilon) \cdot f(\dot{\varepsilon}) \cdot f(T) \tag{9}$$

Another approach on modeling rate and temperature dependent plastic flow behavior is following an assumption of the additive built-up of the model, Equation 10.

$$\sigma(\varepsilon, \dot{\varepsilon}, T) = g_1(\varepsilon) + g_2(\dot{\varepsilon}, T) \tag{10}$$

This way several effects of the behavior can be incorporated into one model because the number of additives in the model can be infinite in theory. It has been concluded (Klepaczko 2009) that model of the specific additive form has the highest potential for commercial usage, Equation 11.

$$\sigma(\varepsilon,\dot{\varepsilon},T)=g_1(\varepsilon,\dot{\varepsilon},T)+g_2(\dot{\varepsilon},T) \tag{11}$$

First term, g_1, is for describing the strain rate and temperature dependent strain hardening. As g_2 is for considering the immediate strain rate and temperature effects e.g. the deep upturn in the flow stress value around the strain rate of 10^3 s^{-1} at a constant temperature for the majority of the metals.

Rämo, (Rämo *et al.* 2009) have shown good results using a special form of the additive form for simulations. An empirical fitting model was created using polynomials for sub-functions g_i. Equation 12 presents an example of the overall structure of the developed model. The strength of this method is that within the tested range of strains, strain rates and temperatures, the model is accurate assuming that a sufficient set of testing results is available for the range. Although the number of parameters is excessive, optimization algorithms can be developed for automated coefficient estimation.

$$\sigma(\varepsilon,\dot{\varepsilon},T)=\sum_{i=1}^{n}a_i\varepsilon^i+\sum_{j=1}^{n}b_i\dot{\varepsilon}^j+\sum_{k=1}^{n}c_kT^k+h \tag{12}$$

A good model should be able to reproduce the real material behavior well enough, be mathematically simple, and to have an optimum (small) number of material parameters. The history effect present in the loading path violates the very fundamental assumption of the MES concept (Klepaczko 2009). Namely, it has been experimentally proved that for real materials there is no single unique surface for a set of stress, strain, strain rate and temperature values. In practical engineering, compromises are needed and typically simplified models are used that still provide acceptable accuracy for practical applications.

1.3.1. Johnson-Cook Model

Arguably, in the practical engineering, the most widely used phenomenological constitutive equation is the Johnson-Cook model, Equation 13 (Shrot 2010; Hokka 2008).

$$\sigma(\varepsilon,\dot{\varepsilon},T)=\left(A+B\cdot\varepsilon^n\right)\left(1+C\cdot\ln\left[\frac{\dot{\varepsilon}}{\dot{\varepsilon}_{ref}}\right]\right)\left(1-\left[\frac{T-T_r}{T_m-T_r}\right]^m\right) \tag{13}$$

which describes the flow stress as a multiplication of three terms. The first term represents the dependence of flow stress on strain, the second

Table 1. The Johnson-Cook model.

$$\left(A + B \cdot \varepsilon^{n}\right) \qquad \left(1 + C \cdot \ln\left(\frac{\dot{\varepsilon}}{\dot{\varepsilon}_{ref}}\right)\right) \qquad \left(1 - \left[\frac{T - T_r}{T_m - T_r}\right]^{m}\right)$$

Elasto-plastic term	Viscosity term	Thermal softening term
A yield stress	C strain rate factor	T_r room temperature
B pre-exponential factor	$\dot{\varepsilon}_{ref}$ reference strain rate	T_m melting temperature
n work-hardening exponent		m thermal-softening exponent

term on strain rate, and the third on temperature. It includes five independent material parameters that are to be determined from a set of tests performed at different strain rates and temperatures. Components and explanation of the terms in the Johnson-Cook model are given in Table 1 (Shrot 2010; Hokka 2008).

The first three parameters A, B, and n are determined by fitting a Ludvig's type equation, the first term in the model, on the so-called reference stress-strain curve (often the curve obtained at room temperature at the strain rate of 1 s^{-1}, where the conditions are still isothermal for most materials). The remaining two parameters are then determined by fitting the model to the measured data at different temperatures and strain rates.

The model however, has a fundamental problem in that it assumes the parameters to be independent of each other, which for most materials and deformation conditions is not the case when implemented to the wide range of strain rates and temperatures (**V**; Samantary *et al*. 2009). Johnson-Cook model assumes a continuous strain hardening rate together with an increasing strain rate. Several studies have shown that it is not the case with many of the materials (Hokka 2008; Nemat-Nasser 2005; Liang 1999; Khan 1999). However, the Johnson-Cook model is still broadly used mostly because of its simplicity and availability of the parameters for many materials. The number of parameters is effectively low and they are readily available from standard and easily reproducible tests.

1.4. Mechanical testing of metals

In essence all mechanical testing of materials is following the same governing principle. An external force or load is applied to the specimen made of interested material and the behavior of the specimen is then investigated in detail. Different applications in materials testing demand a wide range of testing equipment with versatile capabilities. A key factor in distinguishing between testing methods is the time dependent rate of applied external force, as that is responsible for the creation of conditions under which a specimen under a test will deform. The common testing methods together with strain rate ranges, equipment and conditions are depicted in Figure 3.

The common range on testing, so to say, is the strain rate region of 10^{-4} to 10^{-1} s^{-1} with quasi-static conditions. For loading, testing frames with an either electromechanical screw driven beam or servo hydraulic actuator are used. Creep tests and quasi-static tests are mainly conducted at the ambient temperature. A wide range of specialized furnaces, climate chambers make it possible to experiment with different environmental conditions. Strain is usually measured directly from the specimen via strain gauge. Conventional servohydraulic systems are limited around loading rate 1 s^{-1}. For higher strain rates i.e. higher loading rates dynamic effects caused by inertia need to be accounted for (Nemat-Nasser 2001). Special hydraulic testing machines are developed to cover the intermediate region from 10^{-1} to 10^{-2} s^{-1}. Split Hopkinson Pressure Bar (SHPB)

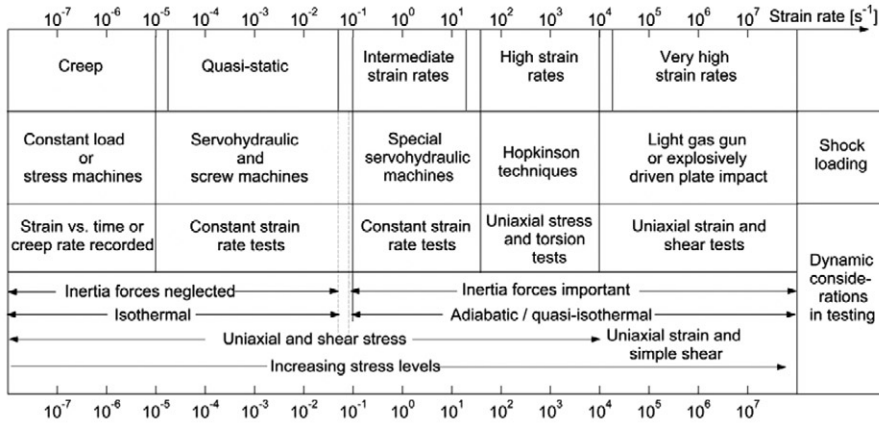

Figure 3. Overview of common testing techniques, their corresponding strain rate range and the conditions during testing (Nemat-Nasser 2001).

technique has been the prevailing method for high strain rate testing in between 10^{-2} to 10^{-4} s^{-1}. The following chapters will give detailed overview about the SHPB technique. Mechanical testing with very high strain rates relies on the usage of explosives.

1.5. Deformation mechanics at high rate testing

During low strain rate testing all parts of the specimen are in stress equilibrium. The loading rate is then sufficiently low to allow the buildup of a uniform stress field. The situation differs in the case of higher loading rates where wave propagation effects have to be considered. Figure 4 explains the situation in more detail, looking at a specimen under the uni-axial compression test.

The bulk specimen can be divided into incremental elements of height dy_0 and cross-sectional area A_0. Initially, at time t_0, the element is positioned at some arbitrary height y. Additionally it is assumed that no forces are acting on the specimen. Loading the specimen will cause displacement u in the position and also a modification in the dimensions of the element, A and dy consequently. Force acting on the upper face of the element along the y-axis being $F+dF$, and on the lower face against the y-axis, F. Displacement u is caused by the difference in the two forces, dF and is described by the Newton's second law of motion, Equation 14.

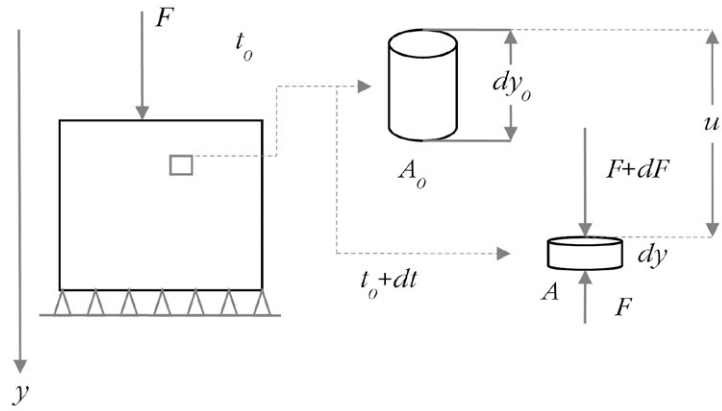

Figure 4. Schematic illustration of the deformation of a compressive specimen by a stress wave (after Curtze 2009 and Nemat-Nasser 2001).

$$dF = m \cdot a = \rho A_0 dy_0 \left(\frac{d^2 u}{dt^2} \right) \quad (14)$$

Where ρ is the density of the material, A_0 and dy_0 initial cross-sectional area and axial length. Equation 14 shows that for a test conducted with a low rate the acceleration term decreases and the state of force equilibrium is achieved. The situation is different for high rate, speed testing. Higher loading rates lead to the increase of force difference, *dF*. Considering that the specimen constitutes a large number of elements, differences in every element lead to overall inequality of forces and also stresses. Thus the specimen is not under the force equilibrium anymore. The same applies for stress and strain. Since stress is following directly from force, stress and strain are interrelated too. All of these variables are not uniform along the axis of the specimen during high rate testing. Deformation of the specimen can't be described with stress equilibrium as with quasi static testing, the wave phenomenon has to be considered. In practice the wave propagation phenomenon start taking effect from strain rates of 1 s^{-1}.

For high strain rate testing e.g. for SHPB system, stress wave is travelling along the specimen and also the rest of the testing system. Some few reverberations are needed to achieve stress equilibrium in compression testing at SHPB. Ring up time or time until the equilibrium is reached can be shortened via shaping the stress pulse. A pulse with a rectangular shape causes longer ringing than one which is more trapezoidal shape. The SHPB technique is based on an ability to record elastic stress wave travelling within long slender cylindrical bars. This uni-axial wave propagation is governed by 1D-wave equation.

1.6. The SHPB technique at ambient and elevated temperatures

There are several methods for high strain rate testing including, for example, drop tower tests and cam plastometers. However, the most commonly used testing method at strain rates between 10^2 and 10^4 s^{-1} is the Split Hopkinson Pressure Bar (SHPB) technique.

1.6.1. SHPB device for testing at ambient temperature

Figure 5 illustrates schematically the construction of a typical compression SHPB device. The device typically consists of two 1-2 m long metal bars with a diameter of 10-25 mm, and a striker bar, usually made of the

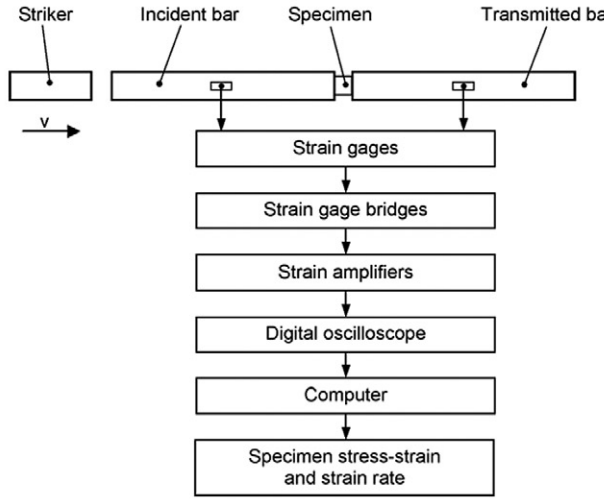

Figure 5. SHPB system schematically (Apostol 2007).

same material and with the same diameter as the stress bars. When the striker bar is shot against the free end of the incident stress bar, the impact generates a stress pulse that propagates in the incident bar towards the specimen, which is sandwiched between the incident and transmitted bars. As the stress pulse reaches the bar-specimen interface, part of the pulse is reflected back as a wave of tension while part of it is transmitted through the specimen to the transmitted bar. The specimen is deformed plastically at a high strain rate as the pulse travels through it. Stress, strain, and strain rate in the specimen can be calculated from the three elastic stress pulses, incident, reflected, and transmitted pulses, measured from the pressure bars using strain gages and recorded with a digital oscilloscope. For cutting down the ringing time in the system, a fourth bar may be installed. It is called the momentum trap bar and in principle it is acting like a damper for the waves travelling back and forth in the incident and transmitted bar.

When considering elastic stress pulse traveling along a cylindrical bar dispersion has to be counted for. It is caused by lateral inertia of the bars and it results in undesired modification of the pulse shape. Pulse measured from the midpoint of the pressure bars is not pulse acting on the boundary surface of the bar-specimen. However, mathematically dispersion correction is done using Banckroft's method. Additional mechanical improvement is achieved with usage of pulse shaping. Usu-

ally a thin disk of soft material e.g. copper is placed between the striker and incident bar. This way the rise time of the pulse is increased and that results in suppressed dispersion effects, since some of the highly dispersive short wavelengths are canceled. In addition, oscillations on the pulses are decreased and equilibrium stress within the specimen is achieved at lower strain values. On the counterpart, longer rise time leads to a non constant strain rate. Choosing between suitable pulse shaper dimensions and material remains a matter of experience together with trial and error (Nemat-Nasser 2001).

1.6.2. SHPB technique at elevated temperatures

Conducting high strain rate tests at elevated temperatures is challenging due to several practical and scientific reasons. The test setups found in the literature can be divided into two basic methods: 1) heating up all or short sections of the incident and transmitted bars together with the specimen, and 2) heating the specimen only while keeping the bars at room temperature throughout the test. The first method involves an inherent problem that limits its usable temperature range: when heating up the bars their physical properties change, which affects the strength of the bars and the speed of the elastic waves distorting the measured stress pulses. The change in the speed of the wave is difficult to account for and the necessary mathematical or mechanical corrections are complicated. Restrictions to the second technique are set by the allowed contact time of the hot specimen with the cold bars before the impact. The contact time can be minimized by a special manipulation system for the bars and the specimen and using, for example, a furnace or a radiation heater outside the axis of the bars. The essence of this method is to bring the hot specimen and the cold bars into contact just a fraction of a second before the impact of the striker on the input bar. Both the control and timing of the specimen heating and the movements of the bars and the specimen are very critical and can only be done using computer controlled systems.

2. EXPERIMENTAL STUDY

Mechanical behavior of Ti-15-3 and Alloy 625 was investigated in a wide range of strain rates and temperatures. For the sake of clarity and unambiguous understanding, the following division of experimental work was used throughout the study. In Table 2 a categorization is presented that is referred to as the testing matrix. This picture shows that different experimental techniques were used to perform the experimental part of the study.

Table 2. Testing matrix. Sub-categorization of experimental work performed in this study.

High Strain Rate at Room Temperature (HSR@RT)	Low Strain Rate at Room Temperature (LSR@RT)
Strain rate range: 10^3 - $4{\cdot}10^3$ s^{-1} Temperature: all tests started at room temperature 23 °C Equipment used: Split Hopkinson Pressure Par (SHPB) system	Strain rate range: 10^{-3} - 1 s^{-1} Temperature: all tests started at room temperature 23 °C Equipment used: industrial servo-hydraulic testing machines
Low Strain Rate at High Temperature (LSR@HT)	High Strain Rate at High Temperature (HSR@HT)
Strain rate range: 10^{-3} - 1 s^{-1} Temperature: 400 - 1000 °C Equipment used: industrial servo hydraulic testing machines with high temperature furnace	Strain rate range: 10^3 - $4{\cdot}10^3$ s^{-1} Temperature: 400 - 1000 °C Equipment used: Split Hopkinson Pressure Par (SHPB) system with high temperature capabilities

2.1. Materials

β-titanium alloys like Ti-15V-3Al-3Sn-3Cr (Ti-15-3) have a combination of low density, high strengths and ductility. These materials are very important in the fields of aerospace applications. In addition, β-titanium alloys exhibit the lowest Young's modulus of all classes of titanium alloys. This makes them interesting for the medical implant technology on the side of the 'traditional" titanium industries like aerospace and power generation (Boyer 1994).

The alloy Ti-15V-3Al-3Cr-3Sn investigated in the project was produced at GfE Metalle and Materialien GmbH in Germany. Titanium sponge

coming from Kazakhstan has been first mixed with two alloys (85V-15Al and 50V-40Cr-10Al) and pure Sn and was compacted to an electrode of diameter 120 mm. Then the electrode was molten into a first ingot (diameter 160 mm) in a VAR furnace followed by single VAR remelting step. The final ingot was 200 mm in diameter. These round bars were deformed at 850 °C by rotary swaging in several steps to a final diameter of about 78 mm. The bars were water-quenched from 700 °C to an 'as received state' (Rokicki *et al*. 2010). Compression specimens of 6 mm in diameter and 6 mm to 8 mm in length were EDM machined from a round bar with diameter of 70 mm.

Nickel-based superalloys are normally used in high-temperature applications whenever steels (due to a drop in mechanical properties at elevated temperature) or titanium alloys (due to potentially insufficient oxidation resistance above 550 °C) cannot be applied anymore. In aerospace engine applications or in stationary gas turbines, excellent mechanical properties are needed at temperatures above 600 °C in combination with corrosion and oxidation resistance (Sims *et al*. 1987).

Material studied in the current work was nickel-based Alloy 625 produced by ThyssenKrupp VDM (Alloy 625, brand name: Nicofer® 6020 hMO), following the specifications UNS NO6625 Grade 1, 2.4856 and ASTM B 446-03. The chemical composition of alloy is presented in Table 3. The material has been forged from a diameter of approximately 200 mm to a final diameter of 80 mm at 1080 °C. Followed by a heat treatment at 975 °C for 0.45 hours, after that it is water quenched to a soft annealed condition. Compression specimens of 6 mm in diameter and 6 mm to 8 mm in length were EDM machined from a round bar with a diameter of 70 mm.

Table 3. Chemical composition of the Alloy 625 (Siemers *et al*. 2011).

	Ni	Cr	Mo	Nb	Fe	Ti	Al	Mn	Si	Co	C	Ta	S	P
Max wt%	Bal	22.10	9.10	3.43	4.73	0.33	0.21	0.11	0.10	0.08	0.03	0.01	0.001	0.006

2.2. The Split Hopkinson pressure bar at DMS of TUT

The compression SHPB test system built at the Department of Materials Science of Tampere University of Technology (TUT) is pictured in Figure 6. It uses pressure bars made of high strength steel (YS ~ 1100

Figure 6. The compressive SHPB equipment at TUT. The computer together with components of the data acquisition system (DAQ) is seen at the front. The set up of pressure bars together with stanchions built on the I-beam are just behind.

MPa), Maraging steel (YS ~ 1850 MPa), or high strength aluminum alloy 7075 (YS ~ 500 MPa). Compression behavior of materials can be studied in a strain rate range of $2 \cdot 10^2$-10^4 s^{-1} by varying the length and the impact velocity of the striker bar and the length of the specimen. For data acquisition, a pair of strain gauges is bonded on both the incident and the transmitted bar. The signals are amplified using a signal conditioner with a bandwidth of 500 kHz and recorded on a 12-bit 10Msample digital oscilloscope. Test data is downloaded to a PC and processed further with MATLAB based calculation routines.

The setup mainly used in this study consists of 22 mm diameter high strength Maraging steel incident, transmitted, and striker bars. Proper alignment of the three bars relative to each other is essential. Incident and transmitted pressure bar are supported by the stanchions, which can be regulated in y- and z- directions. The lengths of the incident, transmitted, and momentum trap bars were 1200 mm each, and the length of the striker bar varied between 200 mm and 400 mm. At room temperature an experiment is performed simply by placing the cylindrical specimen

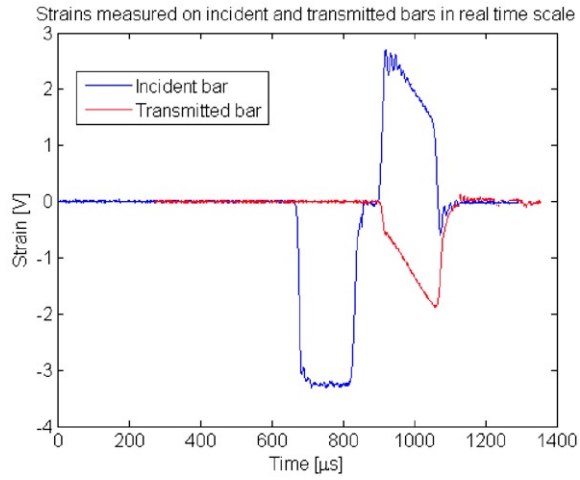

Figure 7. Typical output data from the strain gauges of SHPB (Curtze 2009).

between the lubricated ends of the incident and transmitted bars, and then impacting the striker bar to the free end of the incident bar. The impact velocity of the striker is adjusted by changing the launching pressure and measured using three IR sender receiver pairs. The impact of the striker creates a stress pulse that propagates in the incident bar at the speed of sound (~4900 m/s), and when the stress pulse reaches the bar-specimen interface, part of the pulse is transmitted through the specimen into the transmitted bar, whereas the remaining part of the incident stress pulse is reflected back to the incident bar as a wave of tension. The incident, reflected, and transmitted stress pulses are measured with strain gages bonded on the surface of the stress bars, and the signals are amplified and recorded using Kyowa CDV 700A series signal conditioner and Yokogawa DL 708 high sampling rate digital oscilloscope. Figure 7 demonstrates typical shapes of the measured raw curves.

The stress, strain, and strain rate in the specimen are calculated from the dispersion corrected stress pulses using Equations 15-17. The numerical dispersion correction used is from the developments of Gorman, (Gorman 1997).

Average engineering stress in the specimen:

$$\sigma(t) = \frac{A_b E \varepsilon_t(t)}{A_s} \tag{15}$$

Average engineering strain in the specimen:

$$\varepsilon(t) = \frac{2C_0}{L_s}\int_0^t \varepsilon_r(t)dt \tag{16}$$

Average engineering strain rate in the specimen:

$$\dot{\varepsilon} = \frac{2C_0\varepsilon_r(t)}{L_s} \tag{17}$$

Where A_b is the cross-sectional area of the pressure bars, E is the Young's modulus of the bar material, $\varepsilon_i(t)$, $\varepsilon_r(t)$ and $\varepsilon_t(t)$ the incident, reflected and transmitted axial strains measured in the bars as a function of time, A_s the cross-sectional area of the specimen, C_0 the longitudinal elastic wave velocity in the bars and L_s the length of the specimen.

Engineering stresses, strains and strain rates calculated with equations above are converted to true values using Equations 18-20:

$$\sigma_T = \sigma_e(1+\varepsilon_e) \tag{18}$$

$$\varepsilon_T = \ln(1+\varepsilon_e) \tag{19}$$

$$\dot{\varepsilon}_T = \frac{d\varepsilon_T}{dt} \tag{20}$$

A summary of the compressive Split Hopkinson Pressure Bar system capabilities in the Department of Materials Science in Tampere University of Technology is given in Table 4.

In essence, SHPB device is an open loop device. An estimation of the output values can be predicted. For rough control, the following equations can be used. Inputs variable by the operator are the length and the impact velocity of the striker bar and the length of the specimen. The amplitude of the elastic wave in the bars is proportional to the striker velocity, v_{st}, at the moment of the impact, Equation 21. Length of the

Table 4. SHPB system capabilities at TUT.

Type of loading	Compression
Duration of the loading pulse [s]	50 ... 200·10^{-6}
Strain rate range [s^{-1}]	10^2...10^4
Load range [kN]	0...250
Specimen dimension [mm]	D<22; h~0.5...12
Temperature range [°C]	-150...1000

striker bar, L_{st}, determines the duration of the loading pulse, Equation 22 i.e. integration time in Equation 16.

$$\sigma = \frac{v_{st} E_B}{2C_0} \tag{21}$$

$$\Delta t = \frac{2L_{st}}{C_0} \tag{22}$$

2.3. High Temperature SHPB System at TUT

The fully computerized high temperature SHPB (HT-SHPB) system at TUT is constructed using the idea of only heating the specimen and keeping the other components of the testing system at room temperature. The specimen is first placed in a specimen holder using a ceramic wool support ring. The specimen holder is then pushed into the furnace by a pneumatic manipulation system. When the specimen has reached the desired test temperature, the manipulator rapidly retracts the specimen at high speed from the furnace to the centerline of the bars. The striker bar is shot, and just before it hits the incident bar, a transmitted bar manipulator pushes the bars and the specimen together. This way the maximum contact time of less than 50 ms is ensured between the hot specimen and the cold bars. The specimen is heated by a small resistive tube furnace with a maximum temperature of around 1000 °C. The entrance of the furnace is shielded with a special pneumatically controlled shutter to protect the bars from the heat. During heating of the specimen, a flow of inert gas is maintained to prevent the specimen from oxidizing. The specimen temperature is measured directly from the surface of the specimen using a K-type thermocouple touching the surface of the specimen. Figure 8 gives a schematic illustration of the testing steps during a test with the HT-SHPB at TUT.

In addition to the described HT-SHPB, a conceptually new and different heating system was designed and constructed during the time of this thesis project (Kuokkala *et al.* 2010). The principle difference is in the method and time of the specimen heating. Hence, the new heating system is the so called 'rapid-heating' system, because compared with the radiation furnace based system, heating times are several magnitudes lower. In the rapid-heating system the specimen is sandwiched between

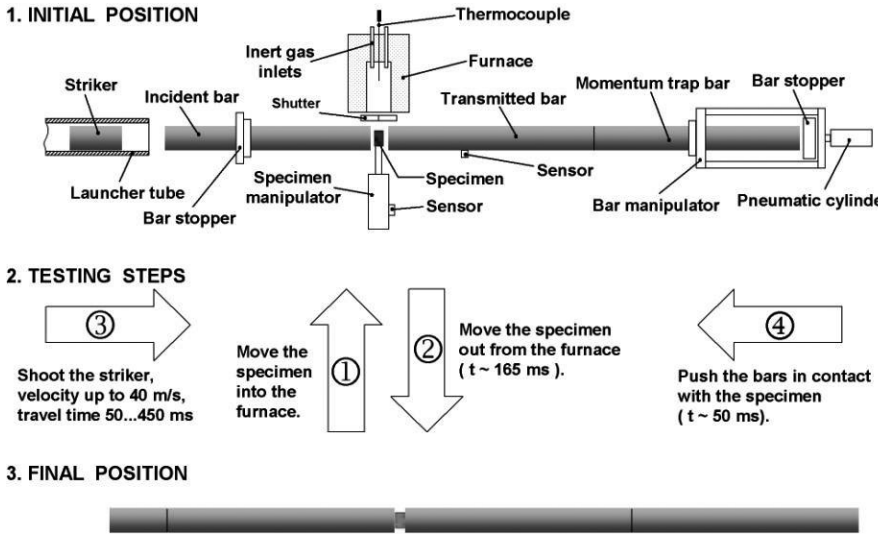

Figure 8. Schematics of the testing stages during a test with the HT-SHPB system (Apostol 2007; Apostol *et al*. 2003).

the electrodes and the current is driven through the system to heat up the specimen. Motivation for the development was to investigate if the time spent at an elevated temperature has any effect on the mechanical behavior due to potential changes in the microstructure.

2.4. Quasi-static compression testing

For tests in the LSR@RT and LSR@HT areas (see Table 2), industry standard servo-hydraulic materials testing machines were used. Room temperature tests were conducted with the Instron 8800 series testing system with the nominal loading capacity of 100 kN. Considering the high strength of tested materials, special compression anvils were locally manufactured to withstand the high forces foreseen for those tests. Strain was measured directly from the specimen via strain gauge.

High temperature test were performed on the MTS 810 100kN testing system. PID-controlled induction coil together with high-frequency supply unit was used as the heating element. Temperature feedback was red with thermocouple directly in contact with the specimen surface. For the

high temperature test a pair of special pushrods was designed and manufactured. Attention had to be paid for the heat dissipation as otherwise the strength of the rods themselves would have not been sufficient to withstand testing forces without deforming themselves. Pushrods with interior cooling circuits where cold water from the tap acted as an agent for the heat exchanger were developed. Direct strain measurements from the specimen during the high temperature low strain rate testing was compromised because the pushrods tended to lose their axiality during the test process. Therefore readings from the strain gauge were considered as unreliable. Measurements from the built-in LVDT were used for strain calculations instead.

2.5. U-shape test

For simulation and model verification a special test was devised. The principle was taken from orthogonal cutting and modified to be implemented on the SHPB system. Usage of "U-shape" specimen together with standard industrial cutting blades made it possible to perform cutting-force measurements on the SHPB equipment. U-shape test specimen together with the cutting tool is shown in Figure 9. For testing, the cutting tool is simply inserted between the arms of the 'U'-shaped specimen, and the specimen-tool assembly is arranged between the incident and transmitted bars, resulting in chip formation between the arms when an elastic pulse initiated by striker impacting the free end of the incident bar, forces the tool to move inside the arms of the specimen, Figure 10.

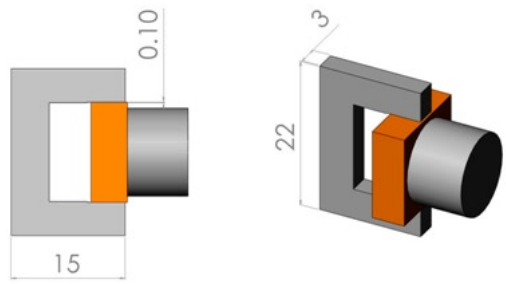

Figure 9. U-shape specimen for cutting force measurement experiments. Dimensions in millimeters are illustrative.

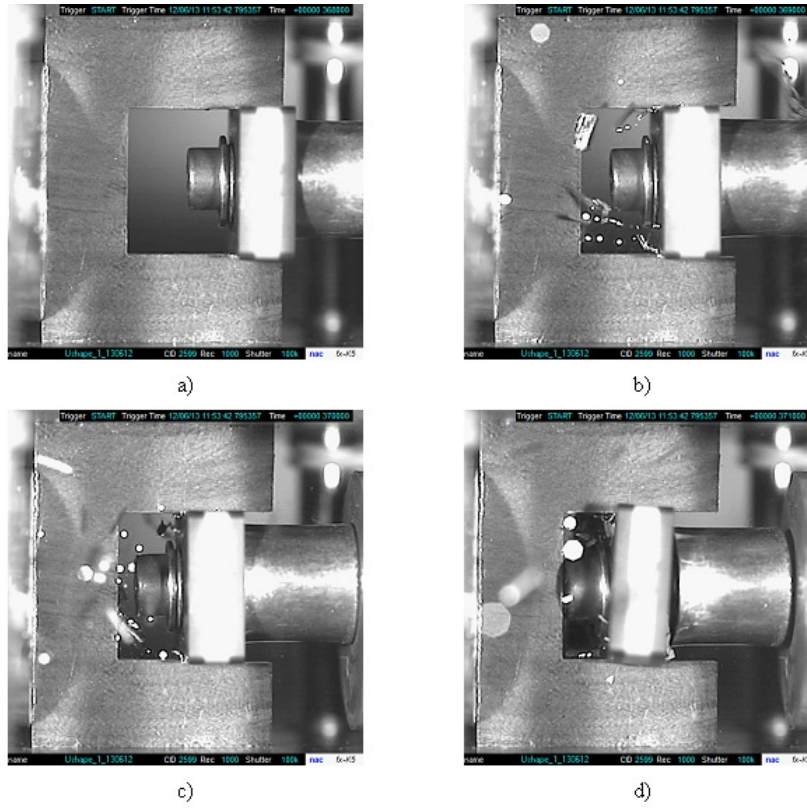

Figure 10. High-speed camera images, a-d, of the U-shaped experiment. Photography by Dmitri Gomon.

Transmitted bar signal $\varepsilon_t(t)$ is used to evaluate dynamic cutting force, Equation 23. Additionally, normalizations, as cutting force per cutting length and per cutting area i.e. so called cutting stress, were estimated.

$$F(t) = \sigma(t) \cdot A_S = A_b \cdot E \cdot \varepsilon(t) \qquad (23)$$

The actual cutting depth was measured post mortem under stereo microscope. In Figure 11 an example U-type specimen is pictured and photographed before and after testing. It is also showing that the test didn't result in symmetrical chip formation on both arms of the "U". This kind of asymmetry was noticed for the majority of the tests and thus prevented the usage of nominal depth values in calculations.

For the chip morphology investigation, quick-stop metal cutting experiments were performed at the Institute of Materials Science, Technische

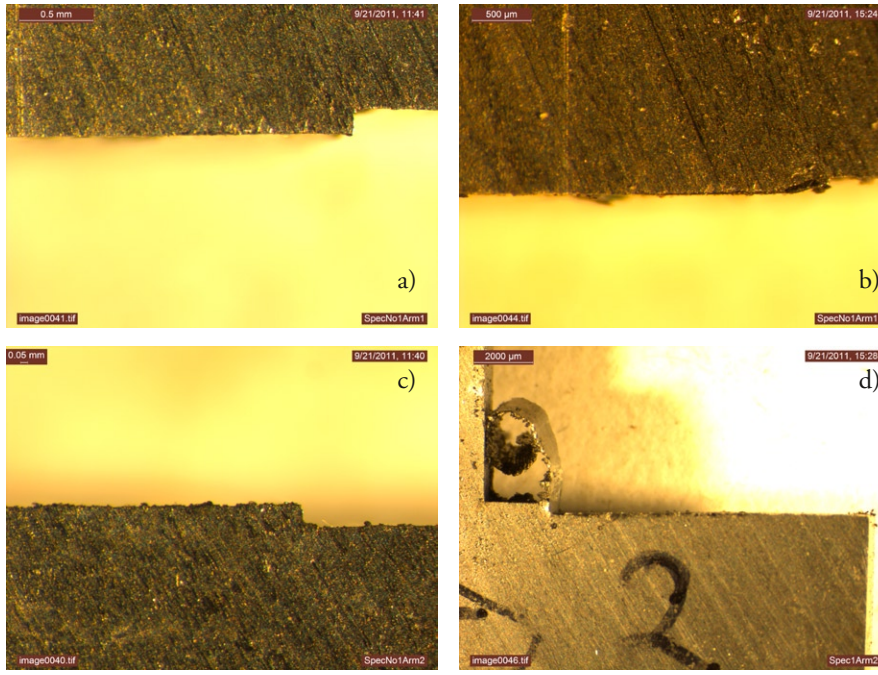

Figure 11. Photograph showing the two arms of the U-type specimen before (a, c) and after (b, d) test.

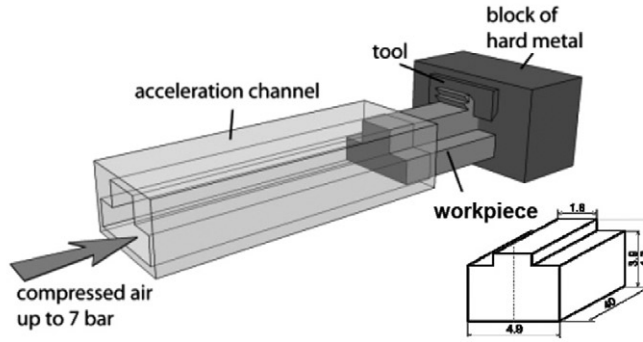

Figure 12. Experimental set-up of a quick-stop experiment set up in the Institute of Materials Science, Technische Universität Braunschweig, Germany. Photo copy from Ciemers *et al*. 2009.

Universität Braunschweig, Germany. In principle it is a device where the specimen made of material under investigation is shot against a stationary, proportionally much heavier, block with the cutting tool attached to it, Figure 12. Yielding root chip and its morphology is investigated with different means of microscopy.

3. MODELING TI-15-3 ALLOY

The ultimate goal of the modeling work done in the study was for the assistance and verification of the numerical cutting simulations. Two distinguishable factors to be matched were ship morphology and magnitude of cutting forces involved. Strains, strain rates and temperatures seen in the vicinity of the chip removal are known to be in the range of 800%, 10^5 s^{-1} and 900 °C, accordingly (Rösler *et al.* 2005). It is obvious that direct experiments for model parameter determination are practically impossible. In general, the model is built using available testing results in combination with some amount of potential model modification.

At first, an attempt was made to find a single set of values for the Johnson-Cook model parameters over the whole studied range of strain rates and temperatures. From this straight forward approach possible short-comings of the model in cutting simulations could be identified. The first initial set of values was obtained from room temperature low strain rate tests. Several rounds of iterations were made, during which the initial set was compared to the experimental results obtained at different strain rates and temperatures. As a result of fitting, the model into the compression test data according to Table 2, following a set of material parameters for the Johnson Cook model (Table 5) was found to give the best fit at the strain rate range of 10^{-3} - $4{\cdot}10^3$ s^{-1} and the temperature range of 295-1273 K

Tabel 5. Parameters for the Johnson Cook model for Titanium 15-3 alloy for the whole testing range according to Table 2 (**II**).

A	B	n	C	M	T_{ref} [°C]	T_m[°C]	$\dot{\varepsilon}$ [s^{-1}]
754	882	1.3	0.02	0.7	23	1669	10^{-3}

Figure 13 shows the comparison of the experimental stress-strain curves and the curves calculated using the preliminary model with parameters according to Table 5. The calculated values match well with the measured data at the reference conditions, i.e., room temperature and strain rate of 10^{-3} s^{-1}. However, the model does not predict the material behavior at higher strain rates and elevated temperatures, and the calculated stresses are in clear mismatch with experimental behavior. In principle, the fit is significantly improved if only relatively narrow ranges of strain rate and temperature are used. Therefore it is obvious that for suitable practical

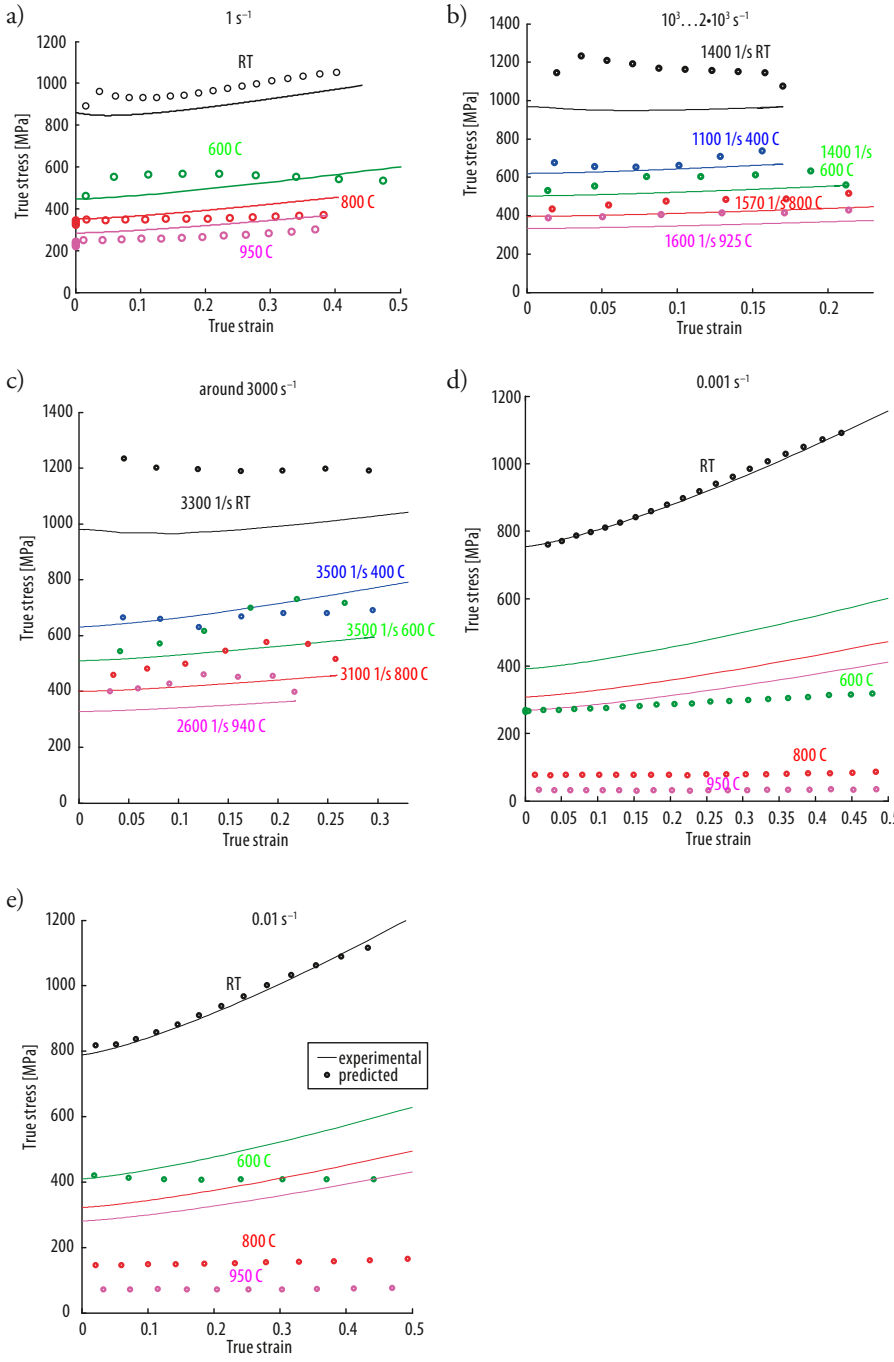

Figure 13. Comparison of model prediction and experimental results for different strain rates and temperatures – a)1 s^{-1}; b)10^3 - $2{\cdot}10^3$ s^{-1}; c) ~ $3{\cdot}10^3$ s^{-1}; d) 10^{-3} s^{-1}; e)10^{-2} s^{-1}.

application separate sets of Johnson-Cook parameters should be used for different strain rate and temperature regimes.

The main reason for the Johnson-Cook model not to be capable of reproducing the true stress-strain response of Ti-15-3 is related to the strain hardening behavior of this material that deviates considerably from the shape of the parabolic strain hardening term i.e. the first term in the multiplicative set-up of the Johnson-Cook material model. Furthermore, interdependence of the Johnson-Cook model parameters on each other limits the usability of the model to narrower ranges of strain rates and temperatures. For any positive value of parameter 'C', the strain hardening rate predicted by the model increases with the strain rate. For the Ti-15-3 alloy this seems not to be the case, as the strong adiabatic heating decreases the strain hardening rate rapidly at strain rates higher than 1 s^{-1}.

Identified parameters were checked for numerical cutting simulations without success. Namely, from the chip morphology Ti-15-3 is known to produce segmented chips (**I**; Rokici *et al*. 2010; Siemers *et al*. 2011). Model, according to Table 5 produces continuous chips instead. Chip segmentation has its roots in the effect of adiabatic heating present during plastic deformation. Titanium alloys are considered to be moderate heat conductors. During the severe plastic deformation present at the primary cutting zone heat accumulates and results in a considerable temperature gradient within the base material. In effect it is changing the overall homogeneity of the material and results in the creation of zones of severe plastic deformation or adiabatic shear bands as they are called (**I**). For model improvement the next logical step was to limit the testing range used for finding model parameters. HSR@RT was chosen as the testing base since it coincides closest to the conditions seen in practical machining i.e. regular machining is done at room temperature. On the other side low strain rates should be excluded too as they are not likely to occur during machining. In addition, extrapolative or predictive capability of the model has to be accounted for as the conditions of the experimental tests differ significantly from those during actual cutting. Various material models are presented in the literature that are modified Johnson-Cook equations with extra parameters and terms for a pronounced strain softening effect (Sima 2010; Calamaz 2008; Hua 2004; Calamaz 2010). Modifications are there to supplement thermal softening and make it possible to develop segmentation in the chip.

In conclusion, following two aspects of modified modeling approach were formed (**III-V**):

– usage of so called adiabatic modification of the Johnson-Cook model in the simulations, Equation 24.

$$\sigma_a = \left(A + B \cdot \varepsilon^n\right)\left(1 + C \ln \frac{\dot{\varepsilon}}{\varepsilon_{ref}}\right)\left[1 - \left(\frac{T + \left((\beta/\rho c)\int_0^{\varepsilon} \sigma d\varepsilon\right) - T_{ref}}{T_m - T_{ref}}\right)^m\right] \quad (24)$$

– identification, that parameters in Equation 24 are to be determined from isothermal (σ_i) flow curves that in turn need to be calculated from experimentally measured adiabatic (σ_a*) flow curves, Equation 25.

$$\sigma_i = \frac{\sigma_a *}{\left[1 - \left(\frac{T + \left((\beta/\rho c)\int_0^{\varepsilon} \sigma d\varepsilon\right) - T_{ref}}{T_m - T_{ref}}\right)^m\right]} \quad (25)$$

Following direct works of Dr. Mikko Hokka and M.Sc Aviral Shrot, Table 6 is giving an overview of the parameters found to give the best solution towards machining simulations of Ti-15-3 alloy.

Tabel 6. Parameters for the modified Johnson Cook equation for Ti-15-3 (**III-V**).

A	B	n	C	M	T_{ref} [°C]	T_m [°C]	$\dot{\varepsilon}$ [s^{-1}]	β	C_p [J/(kgK)]	ρ [kg/m^3]
984	380	0.3	0.069	1.1	23	1669	1400	0.9	500	4760

The measurement data, adiabatic stress and isothermal stress are pictured in Figure 14. An example of extrapolation towards higher strains is presented in Figure 14 b, where two strain rates 3300 s^{-1} and 1 s^{-1} have been modeled by Dr.Mikko Hokka and M.Sc Aviral Shrot.

The described model proved to give good results for orthogonal cutting simulations, meaning that simulated chips had a similar morphology with physical ones. The calculated cutting forces were equal in magnitude compared with experimental measurements. Further developments of the model could be carried out via inverse parameter determination (Shrot 2003).

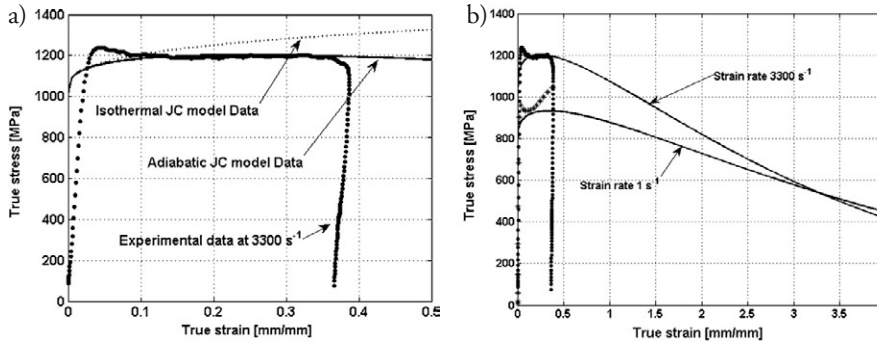

Figure 14. Experimental and modeled flow curves Ti-15-3 alloy. a) isothermal, adiabatic and measured flow curves at 3300 s^{-1}; b) experimental data together with prediction of the model for strain rates 1 s^{-1} and 3300 s^{-1} (**III-V**). Photo courtesy of Dr. Mikko Hokka.

Another attempt was made for the developing model describing the mechanical behavior of Ti-15-3 in the whole tested range of strains, strain rates and temperatures. Following conclusion made about the Johnson-Cook model lacking the ability for covering such a range, an empirical fitting model was developed, Equation 26. Optimization was done via utilizing MATLABS built-in multidimensional unconstrained nonlinear optimization function FMINSEARCH.

$$\sigma(\varepsilon,\dot{\varepsilon},T)=\sum_{i=1}^{5}a_i\varepsilon^i+b\ln(\dot{\varepsilon})+\sum_{k=1}^{3}c_kT^k+h \qquad (26)$$

With found coefficients as in Table 7.

Table 7. Coefficients in the empirical fitting model, Equation 26.

a_1	a_2	a_3	a_4	a_5	b	c_1	c_2	c_3	h
-6981	18637	-16897	5556	-234	26	1e-06	-0.002	0.184	1094

In Figure 15 data points from experimental data are plotted in comparison with points calculated by the empirical fitting model according to Equation 26. The fit, as seen, is arguably good and it gives a reasonable reason for suggesting it for the usage in the applications where conditions met the ones covered by physical testing.

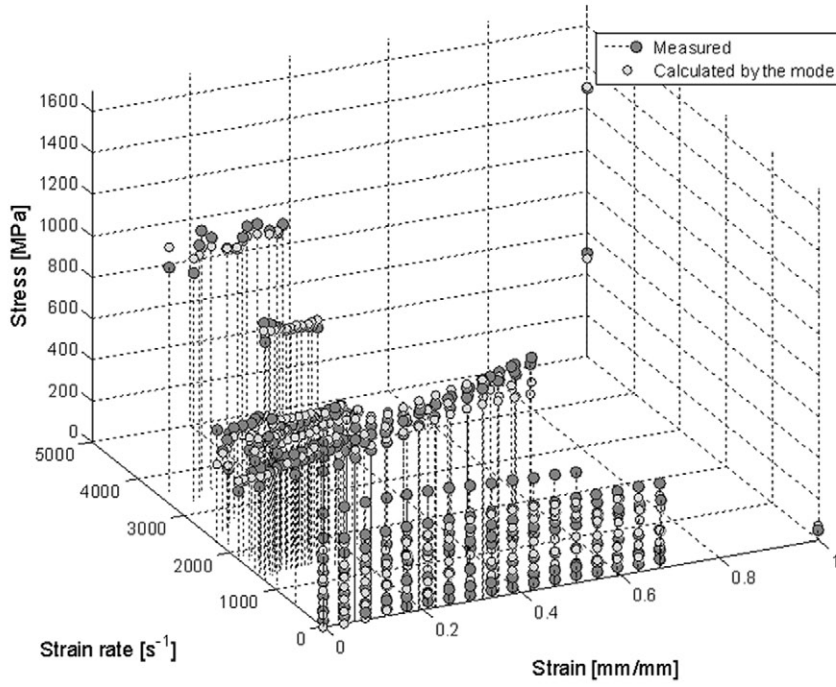

Figure 15. Comparison of experimentally measured points on flow curves against ones calculated by the empirical fitting model, Equation 26.

Modeling dynamic plasticity for Alloy 625 fell out from the scope of this study.

4. MECHANICAL BEHAVIOR AND CUTTING FORCE MEASUREMENTS

The mechanical behavior of the Ti-15-3 and Alloy 625 was characterized by compression tests at strain rates from quasi static performed on servo hydraulic testing machines to high strain rates using the SHPB technique. Specimens were wire cut from as received ingot to cylinders of a diameter of 8 mm and length either 8 mm or 6 mm. This length to diameter ratio stays between 0.5 and 1, which is considered as an optimum range for minimizing effects of specimen friction and inertia (Davies 1963).

4.1. Results on the Ti-15-3 alloy

The mechanical properties of Ti-15-3-3-3 alloy were investigated in compression tests at a wide range of strain rates and temperatures. Test results showing the static and dynamic response of the Ti-15-3 alloy at different temperatures are show in the Figure 16.

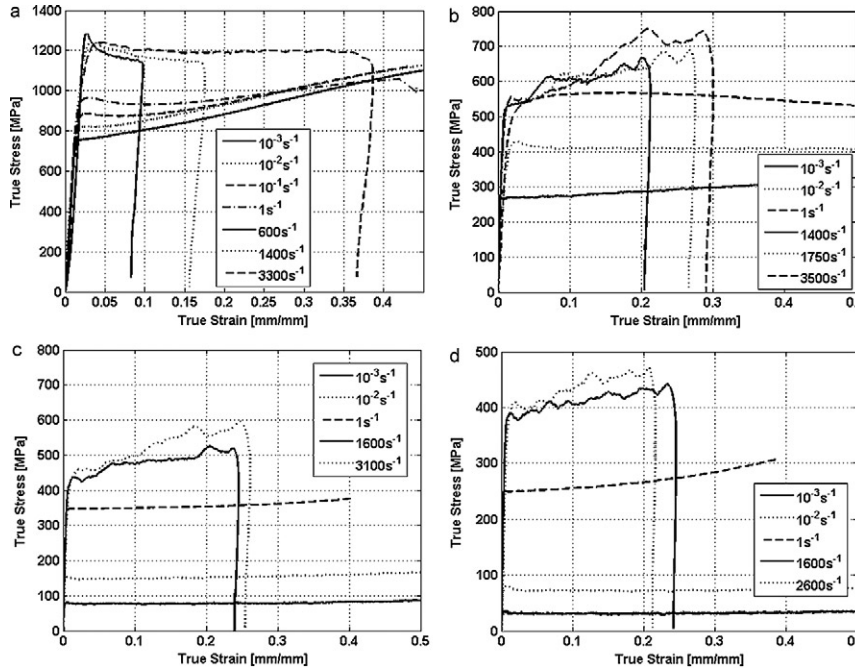

Figure 16. True compression stress-strain flow curves for Ti-15-3 at (a) room temperature, (b) 600 °C, (c) 800 °C and (d) 950 °C . Photo courtesy of Dr. Mikko Hokka.

At room temperature, the material shows very strong strain rate dependence and the yield strength increases from about 750 MPa at the strain rate of 10^{-3} s^{-1} to about 1200 MPa at the strain rate of 3300 s^{-1}. At low strain rates at room temperature, the alloy strain hardens strongly, but the hardening rate quickly decreases as the strain rate is increased, and at higher strains the strength of the material at the strain rate of 10^{-3} is actually higher than at the strain rate of 1 s^{-1}. This behavior is most likely due to the adiabatic heating and consequent thermal softening during the higher rate deformation. At higher temperatures, the strength of the material is clearly lower than at room temperature, and the hardening behavior is also slightly different. The pronounced yield behavior consistently observed at high strain rates at room temperature is not observed anymore at higher temperatures. At elevated temperatures (Figure 16 b-d), the strain hardening rate is clearly lower at low strain rates than at the higher strain rates. The strain rate sensitivity of the material is also higher at elevated temperatures than at room temperature. The strain hardening rate, however, decreases when the temperature is further increased from 400 °C, and at the highest test temperature of 925 °C, the work hardening rate is already very low, most likely due to the fast dynamic recovery taking place at high temperatures.

4.2. Results on Alloy 625

The results from the compression tests on Alloy 625 are shown in Figure 17. The yield strength of the material varies between 490 MPa at low strain rates and 690 MPa at the highest strain rate of 4600 s^{-1} at room temperature. At all strain rates strong strain hardening continues up to about 25% of strain, after which it starts to slowly decrease. The observed strain hardening rate seems to be quite insensitive to strain rate. Figure 17 b shows true stress strain curves for Alloy 625 measured at the strain rate of 1000 s^{-1} at different temperatures. It is observed that no essential change in the response of the material is observed when the temperature is increased from room temperature to 200 °C. Yield behavior is noticeable as it changes from smooth and continuous yielding to discontinuous and pronounced yielding at temperatures between 200 °C and 570 °C. The low strain rate tests at high temperatures showed indications of serrated flow, which is an indication of dynamic strain aging during the test.

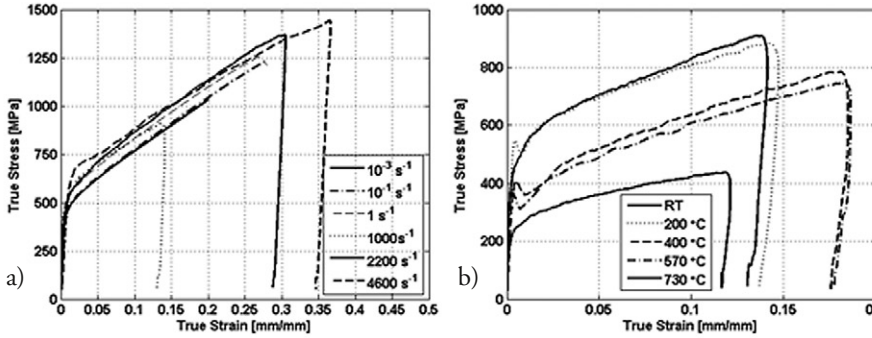

Figure 17. The results the compression tests Alloy 625: a) the stress strain curves measured at room temperature, b) the stress strain curves measured at different temperatures at the strain rate of 1000 s^{-1} (**IV**). Photo courtesy of Dr. Mikko Hokka.

4.3. U-shape experiments

Motivation for performing U-shape cutting experiments on SHPB system, was to get an experimental estimation for the cutting stress magnitude. This value of the cutting stress can then be compared with the ones received from the simulations. A good match between those two cutting stress values is also an indication about the quality of the constitutive model used for numerical simulations. As illustrated in Figure 18, for Ti-15-3 2200 MPa was estimated for the average cutting stress seen in the U-shaped experiments performed at the cutting speed of 15 m/s. The given orthogonal cutting speed was chosen because when this value is converted into a conventional cutting speed value, it corresponds to the limit of the so called high speed machining. Numerical simulation with the same linear cutting speed estimate the cutting stress to be 2000 MPa (**V**). The difference in the magnitude of the two values can at least partly be explained with the mis-match in the frictional conditions in the simulated and experimental setups (**V**).

For Ti-15-3 chip morphology investigations were done using quick-stop metal cutting experiments together with analyses under light microscopy and scanning electron microscopy. Ti-15-3 alloy showed to produce segmented chips at all tested cutting conditions, Figure 19 (**I**).

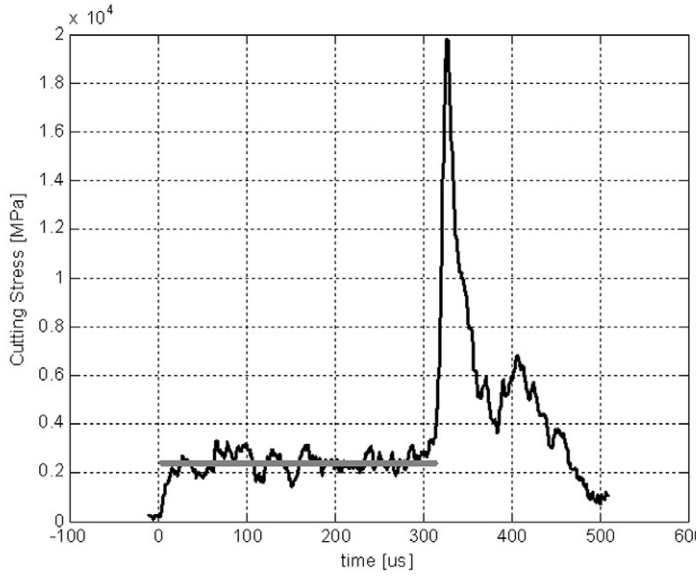

Figure 18. Cutting stress in time, measured from U-shaped specimen of Ti-15-3 with cutting speed of 15 m/s.

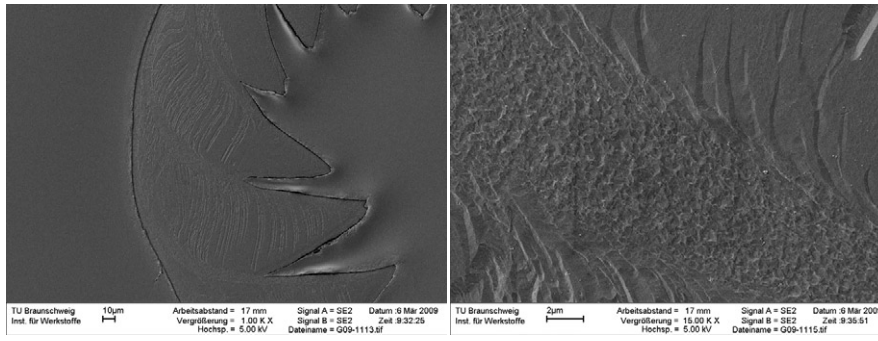

Figure 19. From a) the overall segmentation of chip is seen; b) is a close-up view into a primary shear zone with new nano-crystalline structure (**I**).

U-shaped specimens were also used for experimental determination of the cutting stress for Alloy 625. For orthogonal cutting speed 21 m/s average cutting stress is 1650 MPa, Figure 20.

U-shaped tests on SHPB have the potential to become a significant tool for the experimental works in the machining branch of the materials mechanics field. However more analyses are needed for the evaluation

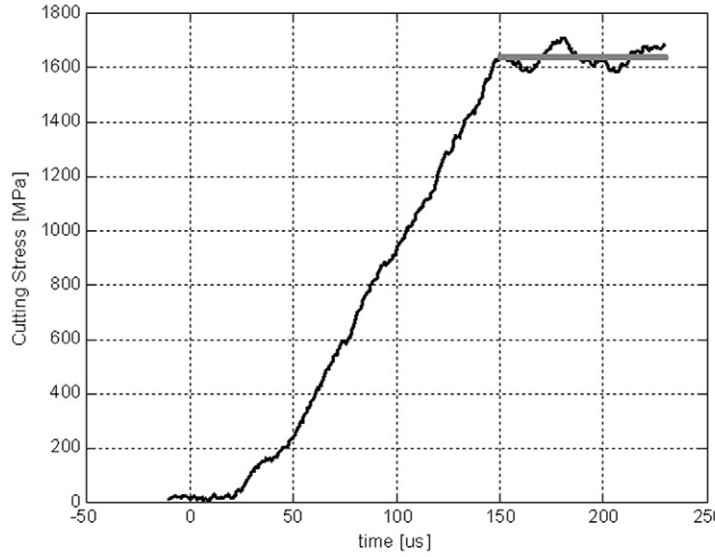

Figure 20. Cutting stress in time, measured from U-shaped specimen of Alloy 625 with cutting speed of 21 m/s.

of the method itself. Effects of specimen geometry are to be investigated and clarified. From the current study it remained unclear to what extent this method can be used to describe the dependence of cutting stress on cutting speed, as further research is needed here. Other potential usage of the method can be determination of possible cutting parameter-dependent change in the chip formation mechanism from continuous chips to segmented chips.

5. SUMMARY AND CONCLUSIONS

In this study the mechanical behavior of two superior alloys, Ti-15-3 and Alloy 625, was investigated. Motivation for the study has its roots in the poor machinability of the selected materials. Based on the data about mechanical behavior, a material model can be built and tested in numerical simulations. This assists in the completion of understanding and advancing issues involved in the machining process.

This study can be concluded with the following statements:

1) titanium alloy Ti-15-3 was experimentally characterized at a wide range of strain rates and temperatures. Alloy 625 was experimentally investigated only in the region of high strain rates for room and elevated temperatures,

2) mechanical properties of both alloys were verified to have considerable dependence on strain rate and temperature,

3) developments of a mathematical model describing the plastic flow behavior of Ti-15-3 alloy at a wide range of temperatures and strain rates were performed. No single set of Johnson-Cook parameter values was found to be able to describe the mechanical behavior of Ti-15-3 over the studied wide range of strain rates and temperatures. Therefore the model parameters have to be defined for narrower regions of strain rate and temperature to yield acceptable fits between the calculated and experimental stress strain curves. The conventional Johnson-Cook material model was tested not to work accurately. For machining simulation a modification to the conventional Johnson-Cook model was developed. The modified model with obtained parameters was used for numerical simulation of orthogonal cutting of the Ti-15-3 alloy. The model was cable of producing segmented chips as seen in the physical experiments;

4) for the sake of efficiency, Alloy 625 was experimentally characterized only for the region of high strain rate at room and elevated temperatures,

5) It was experimentally verified and proved for Ti-15-3 to produce segmented chips in the orthogonal cutting experiments by the quick-stop set-up. With a cutting speed of 20 m/s that is corresponding to the range of high speed cutting for the material.

6) for practical cutting stress measurements, the idea of a U-shaped specimen together with cutting tool was implemented on the Split Hopkinson Pressure Bar system. Preliminary tests show a good agreement with the results gained from numerical simulations. This also gives an indication about the quality of the constitutive model used for simulations. Cutting stress value for Ti-15-3 with a cutting speed of 15 m/s was experimentally determined to be 2200 MPa. Value from simulations was 2000 MPa. This difference of 10% is most probably because of the non-uniform conditions of friction. Experimentally measured cutting stress value for Alloy 625 is 1650 MPa.

REFERENCES

Apostol M. Strain Rate and Temperature Dependence of the Compression Behavior of FCC and BCC Metals, Ph.D. thesis, Department of Materials Science, Tampere University of Technology, 2007

Apostol M., Vuoristo T., Kuokkala V.-T. High temperature high strain rate testing with a compressive SHPB, *Journal de Physique* IV 110 (2003) p. 459–464.

Bhattacharjee A. *et al.* Room temperature plastic flow behaviour of Ti-6.8Mo-4.5Fe-1.5Al and Ti-10V-4.5Fe-1.5Al: Effect of grain size and strain rate in *Materials Science and Engineering: A* Volumes 452–453, 15 April 2007, Pages 219–227

Boyer R., Collings E.W., Welsch G. Material properties handbook: titanium alloys, ASM int., 1994.

Calamaz M., Coupard D., Girot F. A new material model for 2D numerical simulation of serrated chip formation when machining titanium alloy Ti-6Al-4V. *Int. J. of Machine Tools and Manufacture*, Vol. 48, Issue 3–4, Mar 2008, Pages 275–288

Calamaz M., Coupard D., Girot F. Numerical simulation of titanium alloy dry machining with a strain softening constitutive law. *Machining Science and Technology*, Vol. 14, Issue 2, April 2010, Pages 244–257

Courtney T. Mechanical behaviour of materials, 2nd edition, McCraw-Hill Companies, Singapore 2000

Curtze S. Characterization of the Dynamic Behavior and Microstructure Evolution of High Strength Sheet Steels, Ph.D. thesis, Department of Materials Science, Tampere University of Technology, 2009.

Davies E., Hunter C. The Dynamic compression testing of solids by the method of the split Hopkinson pressure bar. *Journal of Mechanics and Physics of Solids*, 11 (1963)

Dudzinski D. *et al.* A review of developments towards dry and high speed machining of Inconel 718. *International journal of Machine tools & manufacture*, 44, 2004, 439–456.

Ezugwu E.O., Bonney J., Yamane Y. An overview of the machinability of aeroengine alloys. *Journal of materials processing technology*, 134, 2003, 223–252.

Ezugwu E.O., Wang Z.M., Machado A.R. The machinability of nickel-based alloys: a review. *Journal of materials processing technology*, 86, 1999, 1–16.

Fang N., Wu Q. A comparative study on the cutting forces in high speed machining of Ti-6Al-4V and Inconel 718 with a round cutting edge tool. *Journal of materials processing technology* 209, 2009, 4385–4389.

Gorman D., Wu X. An empirical method of dispersion correction in the compressive Hopkinson bar test. *Journal de Physique IV*, 7 (1997)

Hartung P.D. *et al.* CIRP Ann. Manuf. Technol. 31 (1982) 75-80.

Hirth J., Lothe J. Theory of dislocations, McGraw-Hill, New York 1968

Hokka M. Effects of Strain Rate and Temperature on the Mechanical Behavior of Advanced High Strength Steels. Ph.D. thesis, Department of Materials Science, Tampere University of Technology, 2008

Hosford W. Mechanical behavior of materials, Cambridge University Press 2006

Hua J., Shivpuri R. Prediction of chip morphology and segmentation during the machining of titanium alloys. *J. of Materials Processing Technology*, Vol. 150, Issues 1–2, 1 July 2004, Pages 124–133

Isaac R., Granato A. Rate theory of dislocation motion: Thermal activation and inertial effects. Physical Review B, 37 (1998)

Jawaid A. *et al. J. Mater. Process. Technol.* 92–93 (1999) 329–334.

Khan A.S., Liang R. Behaviors of three BCC metal over a wide range of strain rates and temperatures: experiments and modeling, *International Journal of Plasticity,* 15 (1999), pp. 1089–1109

Klepaczko J.R., Lodygowski T. Advances in Constitutive Relations Applied in Computer Codes, Springer Wien New York, 2009.

Kocks U.F., Argon A.S., Ashby M.F. *Progr. Mater.Sci.*, 19 1975 1.

Kuokkala V.-T., Apostol M., Hokka M. High and Low Temperature Techniques in Hopkinson Split Bar Testing. In the Proceedings of the annual IMPLAST annual Conference, Providence RI, USA, 2010.

Lee W.S., Lin C.F. Impact properties and microstructure evolution of 304L stainless steel. *Materials Science and Engineering A*, 308 (2001)

Leyens C., Peters M. (eds.). Titanium and Titanium Alloys – Fundamentals and Applications, Wiley VCH, 2003.

Liang R., Khan A. S. A critical review of experimental results and constitutive models for BCC and FCC metals over a wide range of strain rates and temperatures, *International Journal of Plasticity*, 15 (1999), pp. 963-980

Meyers M. Dynamic material behaviour, John Wiley and Sons, Canada 1994

Nemat-Nasser S. Introduction to high strain rate testing, In ASM Handbook Vol. 8, Mechanical Testing and Evaluation, 2001, Materials Park, Ohio, pp. 427-518

Nemat-Nasser S., Guo W.G. Thermomechanical response of HSLA-65 steel plates: experiments and modeling. *Mechanics of Materials*, 37, (2005), p. 379-405

Ogawa K. Mechanical Behaviors of β-Titanium Alloy at High Rates of Strain. *J.PHYS IV FRANCE* 7 (1997), C3-599

Rahman M. *et al. JSME Int. J.* Ser. C 49 (1) (2006).

Rokicki P. *et al.* Chip formation process of Ti-15V-3Al-3Sn-3Cr alloy. In the Proceedings of the Metal 2010: 19TH International Metallurgical and Materials Conference, 2010, pp. 844–849

Rämo J. *et al.* Influence of strain rate and adiabatic heating on the deformation behavior of cold heading steels. *Journal of Materials Processing Technology* 209 (2009) 5186–5194

Rösler J., Bäker M., Siemers C. Mechanisms of Chip Formation. In: H.-K. Tönshoff and F. Hollmann (eds.), High Speed Machining, VCH-Wiley, 2005, pp. 492–512.

Samantary D., Mandal S., Bhaduri A.K. A comparative study on Johnson Cook, modified Zerilli-Armstrong and Arrhenius-type constitutive models to predict elevated temperature flow behavior in modified 9Cr-1Mo steel. *J. Comp. Mater. Sci.* 47 (2009), pp. 568–576

Shrot A., Bäker M. Determination of Johnson-Cook parameters from machining simulations. *Comp. Materials Science*, Vol. 52, Issue 1, Feb. 2012, Pages 298–304

Shrot A., Bäker M. *Is it possible to identify Johnson-Cook law parameters from machining simulations?* Proceedings of the 13th international ESAFORM conference on material forming, Brescia, Italy, 07–09 April, 2010

Siemers C. *et al.* Chip Formation and Machinability of Nickel-Base Superalloys. *J. Advanced Materials Research* Volume 278, 2011, pp. 460–465

Siemers C. *et al.* Development of Advanced and Free-Machining Titanium Alloys by Micrometer-size Particle Distribution. *Journal Materials Science Forum*, 2011, Vol. 690, pp. 262–265

Sima M., Özel T. Modified material constitutive models for serrated chip formation simulations and experimental validation in machining of titanium alloy Ti-6Al-4V. *Int. J. of Machine Tools and Manufacture*, Vol. 50, Issue 11, November 2010, Pages 943–960

Sims C.T., Stoloff N.S., Hagel W.C. Superalloys II, Wiley & Sons, Canada 1987

Spotz Z., Leemet T., Rokicki P., Fusova Z.L., Saksl K., Siemers, C., Kuokkala, V.-T. Analysis of Microstructure of Annealed Alloy Ti-15V-3Cr-3Sn-3Al after Deformation. *Chemicke Listy*. Nr. 105 (2011), pp. 586–588.

Totten E.G., Xie L., Funatani K. Modeling and Simulation for Materials Selection and Mechanical Design. Marcel Dekker, 2004, New-York

Zener C., Hollomon J.H. *J. Appl. Phys*., 15 (1944), 22.

SUMMARY

Because of their excellent mechanical, physical and chemical properties even at elevated temperature, titanium and nickel-base alloys are the materials suitable for the production of several parts and components in the aerospace and power generation industry and for implants and tools in medical engineering. However, these materials are known as difficult-to-machine materials and in extreme cases up to 50% of the manufacturing costs are related to the machining. The current study is motivated by the idea of finding ways to improve the machinability of difficult-to-machine materials, as there have already been many projects aimed at advancing general material properties. Reduction of the production costs by the possible optimisation and higher efficiency of the cutting process should be of great interest for manufacturing companies.

Chip formation is one of the key factors influencing the machinability of these materials. The aim of the research presented in this thesis was to investigate essential features of the mechanical behaviour of the materials under compression and relate them to the chip formation and cutting in general, as input for simulations. Titanium alloy Ti-15-3 was the primary target of the study, and the nickel-base Alloy 625 was also studied to an extent.

List of the tasks to be solved to achieve the aim were:

1. Experimental verification of the chip formation process and chip morphology for Ti-15-3 alloy (**I**).
2. Experimental investigation of the mechanical behaviour in a wide range of strain rates and temperatures for Ti-15-3 alloy (**II-V**). Preliminary characterization of Alloy 625 in the region of high strain rates at room and elevated temperatures and low strain rates at room temperature.
3. Modelling mechanical behaviour in compression in a wide range of strain rates and temperatures. Modification and tuning of the model for reliable orthogonal cutting simulation results (**II-V**).
4. Experimental cutting force measurements and comparison with magnitudes seen with model implementations in the simulations (**V**).

Quick-stop experiments were performed to study the chip formation and morphology. For strain rate and temperature dependent dynamic plasticity characterization i.e. mechanical behaviour, the Split Hopkinson Pressure Bar technique was used together with industrial servohydraulic testing machines to perform compression tests. Ti-15-3 proved to have a considerable dependence on the strain rate and temperature. Johnson-Cook material model was chosen for modelling, as it is having a considerably clear format and reasonable number of parameters in the original format. In the vicinity of the chip formation in metal cutting, strains around 800% and temperatures of 900 °C are present. Meaningful extrapolative behaviour of the model is needed. Adiabatic heating was taken as a primary cause for chip segmentation and the original Johnson-Cook model was modified accordingly. In addition to chip morphology, cutting forces were compared in the experiment and simulation. Novel U-type specimen was tested with the SPHB technique.

Results and conclusions:

1. Ti-15-3 proved to produce segmented chips in orthogonal cutting tests performed in the range of high cutting speed (>40 m/min). Development of adiabatic shear bands was also evident from the chips.

2. Ti-15-3 was characterised in a wide range of temperatures and strain rates under uni-axial compressive loading. Temperature and strain rate proved to have noticeable effect on the mechanical properties of Ti-15-3, with the effect of temperature being more significant than that of strain rate. Alloy 625 was characterized only in the high strain rate condition for different temperature.

3. No single unique set of original Johnson-Cook model parameters was found to be capable of describing the whole range of tested strain rates and temperatures. The empirical fitting model was used instead.

4. Adiabatic model modification proved to work for performing cutting simulations. A satisfactory match between physical results and simulations was achieved by comparing chip morphology and cutting forces.

KOKKUVÕTE

Masinaehituses, nagu näiteks energia- ja lennukitööstuses, kasutatakse masinaelemente ja detaile, mis peavad käitluses taluma suuri koormusi ning olema võimelised säilitama mehaanilist kandevõimet kõrgetel temperatuuridel või säilitama vastupidavuse keemiliselt agressiivses keskkonnas. Laastu tekkeprotsess ning laastu voolamine on lõiketöötlemise seisukohalt olulised tehnoloogilise protsessid. Põhilisteks probleemideks raskesti lõiketöödeldavate metallisulamite juures on pidev voolav laast ning lõikuri kiire kulumine. Esimene neist on takistuseks lõikeprotsessi automatiseerimisele, pidev voolav laast võib keerduda ning sattuda ebasobivalt lõikuri ja detaili vahele, kahjustades sellega lõikurit, mõjudes mittesoovitavalt töödeldava detaili geomeetrilistele kvaliteedile ning nõudes operaatorilt pidevat füüsilist sekkumist töötlemisel. Lõiketöödeldavuse parendamist võib kaaluda lähtudes erinevatelt alustelt, näiteks:

– materjali omadusi muutes. Kirjandusest on tuntud rida tehnilisi ja tehnoloogilisi lahendusi, milles materjali struktuuris tekitatakse soovitult kunstlikke defekte. Selle eesmärgiks on muuta lokaalselt materjali omadusi nii, et suureneks tõenäosus laastu murdumiseks ning pidevalt voolav laast asenduks murdlaastuga. Viimane on soovitav tootmise optimeerimiseks;
– muuta ja parendada lõikurite pinnakatete kulumiskindlust, misläbi suureneb vastupidavus kiirlõikerežiimi kasutamisel ning lõikuri kestvus;
– arendada innovatiivseid lõiketehnoloogiaid. Klassikalisel lõikamisel on lõikur pidevas kontaktis toorikuga. Kirjandusest on tuntud ühe võimaliku arendusena ultraheli sagedusel võnkuv ja seega toorikuga vahelduvas kontaktis olev lõikur;
– võimalikud parendused lõiketehnoloogias saavad tekkida lähtuvalt laastutekkeprotsessi põhjalikumast mõistmisest. Oluliseks teguriks on seejuures laastutüübi ning lõikejõudude kvantitatiivne hindamine. Otstarbekas on seejuures kasutada numbrilisi simulatsioone. Adekvaatsed ja füüsiliste tulemustega kokkulangevad simulatsioonid on head vahendid efektiivsema lõikeprotsessi leidmiseks.

Antud doktoritöös käsitletakse lõiketöötlemise probleeme lähtuvalt viimases punktis esitatud ideedest. Konkreetselt võeti uurimise alla kaks teadaolevalt raskesti lõiketöödeldavat sulamit ning jõuti järelduste ja tulemusteni laastutekkeprotsessi simuleerimiste võimalikkusest ja kvaliteedist.

Selleks, et numbriline simulatsioon oleks korrektne ning lähtuks antud materjalile iseloomulikest parameetritest, peab sisendiks olema materjali mudel, mis sisaldab endas informatsiooni materjali mehaanikalistest omadustest seotuna uuritava protsessiga. Teadaolevalt on makrofüüsikalised tingimused vahetus laastutekkimise tsoonis ekstreemsed, suhteline deformatsioon suurusjärgus 800%, temperatuur kuni 900 °C ning deformatsiooni kiirused piirkonnas 10^5 s^{-1}. Sellistel tingimustel laboratoorne katsetamine on praktiliselt komplitseeritud. See tähendab, et otseste katseandmete põhjal materjali füüsikalist käitumist kirjeldava matemaatilise mudelite koostamine on problemaatiline. Käesolevas doktoritöös püstitati eesmärgiks alustada materjali mudeli koostamisega võimalikult laia eksperimentaalsete andmete spektri põhjal. Katsete klassifitseerimise aluseks võeti suhtelise deformatsiooni kiirus ja katsekeha temperatuur. Suhtelise deformatsiooni osas viidi katsed läbi füüsikaliste piirideni, mille tingis olemasolev katsetehnika ja uuritav materjal. Kirjeldati uuritavate materjalide plastset deformatsiooni sõltuvalt suhtelise deformatsiooni kiirusest ja temperatuurist. Võrdluses mudeli põhjal simuleeritud laastu ja füüsikalise laastu vahel tuli koostada mudeli modifikatsioonid. Samuti seati eesmärgiks eksperimentaalselt uurida laastu morfoloogiat, lõikejõude ning nende vastavust mudeliga simuleeritule.

Kirjeldatud metoodikat rakendati uurimistöös peamiselt titaani sulami Ti-15V3Cr3Al3Sn (Ti-15-3) puhul. Lisaks tehti eeluuringud niklisulamiga Alloy 625. Samaväärselt konkreetsete sulamite uurimisega oli eesmärgiks metoodika väljatöötamine ja selle parandamine.

Töö eesmärgi saavutamiseks olid ettenähtud järgmised ülesanded:

1. Uurida eksperimentaalselt laastutekkeprotsessi Ti-15-3 materjalide puhul. Katsetused sooritada kiirlõikerežiimi piirkonnas < 40 m/min, teha kindlaks tekkiva laastu tüüp ning anda hinnang laastutüübi tundlikkusele lõikekiiruse suhtes (**I**).

2. Eksperimentaalselt uurida ja kirjeldada laias temperatuuride ja suhtelise deformatsiooni ettenähtud kiiruste vahemikus Ti-15-3 plastse deformatsiooni käitumist. Viia läbi eksperimentaalsed eeluuringud materjali Alloy 625 osas. Teha järeldused temperatuuri ja suhtelise deformatsiooni kiiruste mõjust (**II-V**).

3. Koostada matemaatiline mudel Ti-15-3 plastse deformatsiooni modelleerimiseks laias temperatuuride ja suhtelise deformatsiooni kiiruste

vahemikus. Arendada, modifitseerida mudelit saavutamaks kooskõla simulatsioonidega (**II-V**).

4. Eksperimentaalselt määrata lõikejõud uuritavatele materjalidele Hopkinsoni katseseadet kasutades (**II-V**).

Laastutekkeprotsessi uurimine Ti-15-3 sulami osas viidi eksperimentaalselt läbi Braunschweigi Tehnikaülikooli materjalitehnikainstituudis Saksamaal. Katsetööd sooritati nn Quick Stop materjali ortogonaalse lõikamise katseseadmel. Nimetatud süsteemis kiirendatakse uuritavast materjalist katsekeha kuni see põrkub jäigalt kinnitatud lõikuri imitatsiooniga. Kokkupõrke tulemusena tekib laast. Seejärel uuriti laastu morfoloogiat valgus- ja elektronmikroskoopidega ning tehti järeldused saadud laastu tüübi kohta.

Uuritavate materjalide plastset deformatsiooni uuriti eksperimentaalselt surveteimil. Madalatel kiirustel viidi katsetused läbi tööstuslikke servohüdraulilisi katsetussüsteeme kasutades. Kõrgemate suhteliste deformatsioonikiiruste uurimiseks rakendati Tampere Tehnikaülikooli materjaliteaduse osakonnas olevat Hopkinsoni katsetussüsteemi, mis võimaldab teostada katsetusi kiirustega kuni 10^5 s^{-1}. Eksperimentaalselt uuriti protsessi kiiruste vahemikus 10^{-3} kuni $3 \cdot 10^3$ s^{-1} ja temperatuuride vahemikku toatemp kuni 1000 °C.

Materjali mudeli koostamisel valiti aluseks Johnson-Cooki mudel. Kontrolliti selle sobivust kogu piirkonna modelleerimisel. Selgus, et vajalik on mudelit modifitseerida. Muudatuse aluseks võeti adiabaatilise soojenemise efekt ning sellest lähtuvalt pakuti simulatsioonidesse modifitseeritud mudel, kusjuures parameetrite määramiseks teisendati mõõdetud nö. adiabaatilised andmed arvutuslikult isotermilisteks.

Katseliseks lõikejõudude hindamiseks viidi läbi U-kujuliste katsekehadega Hopkinsoni katsetussüsteemil.

Doktoritöö tulemused:

1. Nn. Quick Stop katseseadme eksperimentide tulemuste põhjal saab väita, et Ti-15-3 sulami lõikamisel tekib lülilaast. Lülid on omavahel eraldatud piirkonnaga (nn. adiabatic shear band), mille struktuur on selgelt erinev ülejäänud laastu omast ja mida on ilmsesti deformeeritud rohkem kui muud materjali.

2. Erinevatel temperatuuridel ja suhtelise deformatsiooni kiirustel on märgatav mõju Ti-15-3 plastsele deformatsioonile. Lisaks tugevusele muutub kalestumise kulg. Temperatuuri mõju on märgatavam kui kiiruse oma. Niklisulami Alloy 625 kirjeldamisel jäid eksperimentaalsetest survekatsetustest kõrvale madalad kiirused kõrgtemperatuuridel. Mõõdetud tulemustest järeldub märkimisväärne kalestumise intensiivsuse jätkuvus kõrgetel temperatuuridel. Muutub käitumine voolavuspiiril.

3. Ti-15-3 sulami kirjeldamisel klassikalise Johnson-Cooki materjalimudeliga ei olnud võimalik koostada ühte, unikaalset parameetrite kogumit, mis võimaldaks järgida plastse deformatsiooni kulgu kogu katse ulatuses. Samuti ei olnud võimalik saavutada kokkulangevust simulatsioonide ja füüsilise laastu tüübi osas. Mudeli modifitseerimiseks kitsendati esiteks parameetrite leidmise aluseks olevat katseruumi. Sisse jäi ainult surveteimide tulemused suurtel kiirustel, lähtuvalt toatemperatuurist. Tulemusi võib pidada adiabaatilisteks, mudelisse viidi sisse temperatuuri parandusliige ning parameetrite määramiseks kasutati tuletatud isotermilisi andmeid. Simulatsioonid modifitseeritud mudeliga näitavad kokkulangevust laastu tüübi ja lõikejõudude osas. Praktilises inseneriasjanduses kasutamiseks võib selline meetod leida kasutamist. Kogutud katseandmete täies ulatuses modelleerimiseks koostati empiiriline lähendusvõrrand. Tegemist on esialgse numbrilise mudeliga, mille rakenduseks võib olla näiteks materjali vormimine. Selle puhul on teada, et suhteline deformatsioon ja kiirus jäävad samasse järku katselisega.

4. Lõikejõudude määramine Hopkinsoni katseseadmel spetsiaalsete U-kujuliste katsekehadega andis piisava kokkulangevuse simulatsiooniga.

ACKNOWLEDGEMENTS

The research leading to these results has received funding from the European Union Seventh Framework Programme (FP7/2007-2013) under grant agreement No. PITN-GA-2008-211536, project MaMiNa.

The experimental work and analyzes of the results for thesis were completed in the Tampere University of Technology, Department of Materials Science. Special gratitude and acknowledgement goes to dr. tech. Mikko Hokka. Without his guidance and scientific supervision this thesis project would have not been finished at all. All the former colleagues at Tampere are to be recognized for their kind help and assistance in all kind of matters.

I would like to thank my supervisor Prof. Jüri Olt for his support by concluding the process of preparation of the present thesis and arranging the process of defence of the thesis. I am thankful to head of the institute M.Sc Margus Arak for encouragement and for giving the extra push needed for the completion of the project. Assistant Prof. Jaak Jaaniste, for his mentorship and guidance in the academic terrain for several years already.

Last but not least, I am indebted to my family, especially to my wife and children, for their support, understanding and patience.

PUBLICATIONS

I

Siemers, C., Zahra, B., **Leemet, T.**, Rösler, J.
Development of Advanced beta-Titanium Alloys.

Proceedings of the 8th AMMT'09 Conference, St. Petersburg, Russia, (Vol. 1; 2009; 1; pp. 461-468).

Development of Advanced beta-Titanium Alloys

Carsten Siemers[1)], Badya Zahra[1)], Tonu Leemet[2)], Joachim Rösler[1)]

[1)]Institute of Materials Science, Technische Universität Braunschweig, 38106 Braunschweig, Germany
[2)] Department of Materials Research, Tampere University of Technology, 33101 Tampere, Finland

Abstract

As the chip formation process of beta-titanium alloys like Ti-15V-3Al-3Sn-3Cr is not yet completely understood, this process has been investigated in high-speed quick-stop experiments. At these cutting speeds Ti-15V-3Al-3Sn-3Cr alloy forms segmented chips which are separated by shear bands. Within fully developed shear bands a nano-crystalline microstructure is observed. Small amounts of the rare-earth metal element lanthanum have been added to Ti-15V-3Al-3Sn-3Cr alloy to improve its machinability. Due to the formation of precipitates of lanthanum and tin instead of the precipitation of metallic lanthanum particles, the machinability has not been improved. Nevertheless, grain growth is hindered by the La-Sn-precipitates which make the new alloys very interesting for applications at elevated temperatures.

Key Words**:** beta-titanium alloys, Ti-15V-3Al-3Sn-3Cr, chip formation, phase analyses

1. Introduction

Due to their unique combination of low density, high strength and ductility, beta-titanium alloys like the alloy Ti-15V-3Al-3Sn-3Cr (Ti-15-3-3-3) are getting more and more important in mechanical engineering, especially in the fields of airframe applications. The high strength of Ti-15-3-3-3 components can be further improved by precipitation hardening [1]. In addition, beta-titanium exhibits the lowest Young's modulus of all classes of titanium alloys which makes them interesting for the medical implant technology.

During the component manufacturing for airframe parts, up to 50% of the material has to be removed by different metal machining processes, especially, if complex geometries have to be produced [2]. The introduction of high-speed machining would therefore be very interesting to increase the efficiency of Ti-15-3-3-3 metal cutting operations.

Machining and especially high-speed machining of beta-titanium alloys involves high production costs due to their poor machinability [3]. This difficulty arises from the physical, mechanical and chemical, properties of titanium. Due to the relatively poor thermal conductivity of titanium, heat generated by the cutting action cannot diffuse quickly into the chip's material. As a result, heat is concentrated in front of the rake face of the tool leading to tool softening. The low Young's modulus in combination with the high strength of beta titanium causes chatter and tolerance problems. The high strength of beta-titanium alloys only allows relatively low cutting speeds compared to the machining of aluminium and steels. Additionally, during the cutting action fresh metallic titanium surfaces are produced. Due to the high chemical reactivity of titanium, chemical reactions occur between the tool and the workpiece leading built-up edge formation, to rapid destruction of the cutting tool and to a decrease of the quality of the finished workpiece. Finally, metal cutting operations of Ti-15-3-3-3 cannot be automated as the machining process must be interrupted as often as it is necessary to remove the long chips from the process zone by an operator [4].

Earlier studies have shown that the addition of rare earth elements like lanthanum to (alpha + beta)-titanium alloys leads to an improvement of metal cutting operations as short breaking chips tend to form [5].

As the chip formation mechanism is the key factor influencing the machinability of a material like Ti-15-3-3-3, only a thorough understanding of this mechanism can lead to the optimisation of the cutting process by alloy modification.

In the present study, the chip formation process of Ti-15-3-3-3 has therefore been studied by high-speed quick-stop experiments. Based on this study, alloy modifications have been developed with respect to improved machinability, namely by adding 0.9% and 1.8% lanthanum to Ti-15-3-3-3. The microstructure of the lanthanum containing Ti-15-3-3-3 alloys has been investigated by optical microscopy and scanning electron microscopy (SEM) including chemical analyses by energy dispersive X-ray (EDX). In addition, the different phases have been analysed by means of hard-X-ray (synchrotron radiation). Finally, metal cutting experiments have been performed to check the chip formation process of the different alloy modifications.

2. Machining of Ti-15-3-3-3 Alloy

2.1 Theory of Chip Formation

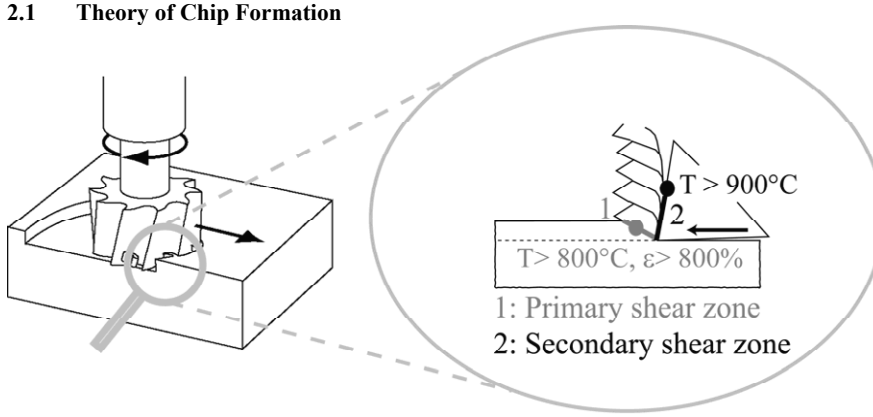

Fig. 1: Theory of chip formation. During the chip formation process (left), continuous (not included in the figure) and segmented chip formation (right) have to be distinguished.

The chip formation process during metal machining can be described as follows: In the beginning of the cutting action, the tool is penetrating the workpiece and the material is dammed in front of the tool. The plastic deformation is concentrated in a narrow zone, the so-called primary shear zone (point 1 in fig. 1), leading from the tool tip to the upper surface of the workpiece. Most of the energy used for the plastic deformation is transformed into heat in the primary shear zone. The rate of the heat dissipation into the surrounding material strongly depends on the material properties (e.g. heat conductivity and the flow curve) and the cutting parameters (e.g. the cutting speed, cutting depth and feed rate). In case the heat can dissipate quickly into the areas surrounding the primary shear zone, the material is deformed homogeneously leading to the formation of a continuous chip with constant chip's thickness. The cutting force remains almost constant. On the other hand, if the heat cannot dissipate quickly into the material surrounding the primary shear zone, heat is concentrated there, the material locally softens and the deformation therefore localises. In the end, the material is deformed in a narrow zone of a few microns (the so-called adiabatic shear band) which leads to the formation of segmented chips, (fig. 1, right). The temperature in the shear band of titanium alloys can easily exceed 900°C [6]. The chip is afterwards guided along the rake face of the tool, the so-called secondary shear zone, leading to an increase in temperature in the

contact area due to friction between tool and chip. The temperature at the end of the secondary shear zone (point 2 in fig. 1) can also rise to more than 900°C [6].

From earlier studies it is known that (alpha + beta)-titanium alloys like Ti-6Al-4V (Ti-6-4) form segmented chips for almost all cutting speeds and cutting depths [7]. The addition of rare earth metals like lanthanum to Ti-6-4 leads to the formation of short breaking chips [8]. This effect can be explained as follows: The solvability of lanthanum in alpha-titanium at room temperature is negligible. Hence, after melting and casting, lanthanum precipitates form in the titanium matrix, mainly located on the grain boundaries. During the segmented chip formation, the lanthanum particles in the shear bands soften drastically or might even melt as the melting point of lanthanum is 918°C. The coherence in the shear bands is therefore diminished so that during further progress of the tool the chips separate into small fragments. Ti-15-3-3-3 forms continuous chips at low cutting speeds, segmented chips are produced at higher cutting speeds and in the high-speed cutting regime. Hence, the addition of lanthanum to Ti-15-3-3-3 might lead to the formation of short breaking chips (if similar effects occur in beta-titanium), especially in the high-speed cutting regime.

2.2 Quick-Stop Experiment

To investigate the chip formation process of Ti-15-3-3-3 quick-stop metal cutting experiments have been performed. The experimental set-up is shown in figure 2 [9].

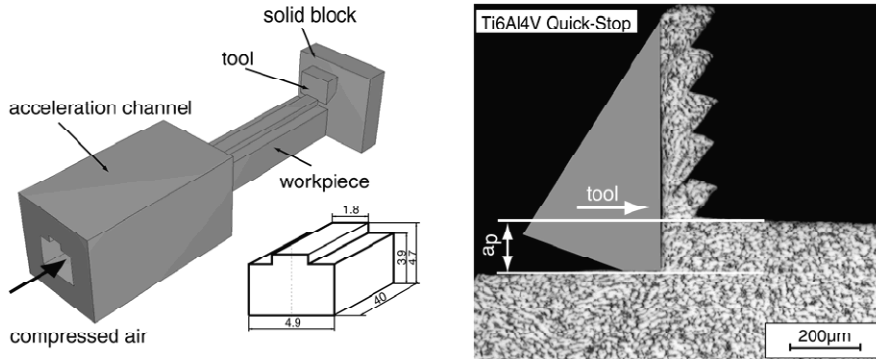

Fig. 2: Experimental set-up of the quick-stop experiment (left). An example of a resulting root-chip of Ti-6-4 is shown on the right hand side. The segments are clearly visible. Similar root-chips develop during high-speed machining experiments of Ti-15-3-3-3 alloy.

During the quick-stop experiment, a specimen (4.9mm x 4.7mm x 40mm) is fed into an acceleration channel and accelerated by compressed air which is provided from a gas tank. The velocity of the workpiece is controlled by the air pressure which is controlled by high precision valves. The workpiece is guided through the acceleration channel, reaches its steady-state speed after a short distance of acceleration and the upper part of the specimen contacts a fixed tool made of cemented carbide so that an orthogonal cut is performed. After a predetermined length of cut of a few millimetres, the lower part of the workpiece hits a solid block of cemented carbide so that the cut is interrupted immediately. Strong metallic springs prevent spring-back of the workpiece and hence protect the root-chip and the cut surface.

Within the current study, a cutting speed (v_c) of 20m/s (high-speed cutting regime) has been chosen, the depths of cut (a_p) has been fixed to 0.1mm. Several quick-stop experiments have been performed to freeze different stages of chip formation. The cross-section of the resulting root-chips has been investigated by means of optical microscopy to verify the stage of

segment formation and by scanning electron microscopy to analyse the microstructure and the state of deformation.

2.3 Chip Formation of Ti-15-3-3-3 Alloy

All quick-stop experiments carried out at the cutting speed of 20m/s lead to the formation of segmented chips, continuous chip formation has not been observed.

In the beginning of the cutting action, the material is deformed in front of the tool tip. This leads to a damming of material at the workpiece surface, see fig 3, left. The deformation itself is concentrated in individual grains located in the primary shear zone where strong lines of flow are visible, see fig. 3, right. During further progress of the tool, the deformation localises in the primary shear zone and strongly deformed grains are visible.

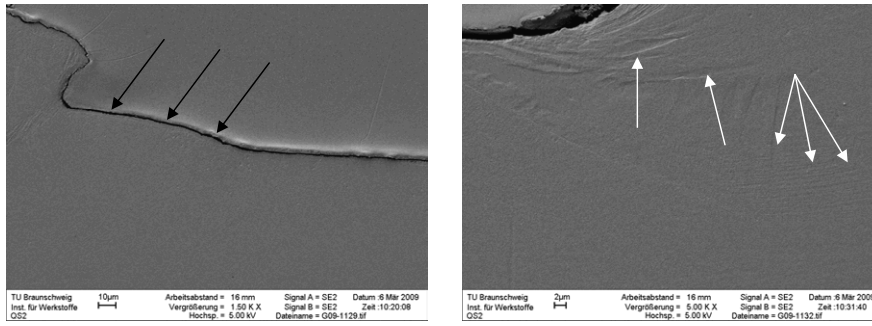

Fig 3: Scanning electron microscopic analyses of quick-stop experiments of Ti-15-3-3-3 alloy. Left: Early stage of segment formation, the material is dammed (black arrows). Right: Flow lines are visible in well oriented grains of the primary shear zone (white arrows).

In a fully developed shear band, see fig 4, left, a nano-crystalline structure of beta-titanium grains can be found, see fig. 4, right. The shear band can be clearly distinguished from the surrounding material, as the deformation of the shear band material is significantly larger compared to the surrounding regions. Crack formation has not been observed in any of the quick-stop samples.

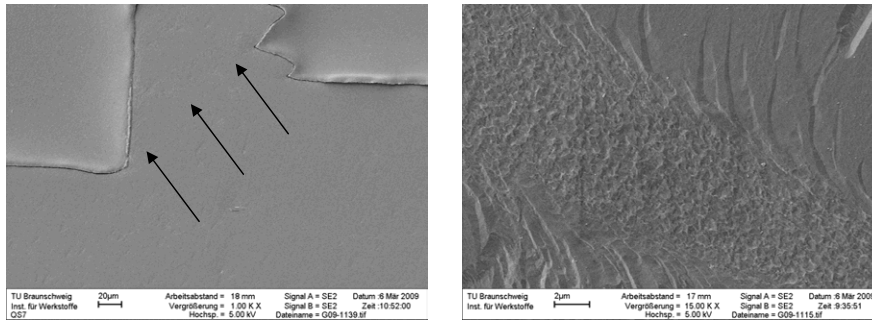

Fig 4: Scanning electron microscopic analyses of quick-stop experiments of Ti-15-3-3-3 alloy. Left: Final stage of segment formation (black arrows). Right: A nano-crystalline structure develops in the shear bands; the shear band can be clearly distinguished from the surrounding regions.

From the different quick-stop experiments it can be concluded that the shear band formation is driven by a deformation process followed by recrystallisation of the structure. Due to the high strength of Ti-15-3-3-3 the energy needed to deform the material in the primary shear zone is high. As the heat conductivity of Ti-15-3-3-3 is low the material softens in the shear zone, the deformation therefore localises and a shear band is formed.

In earlier investigations, the temperature in the shear bands of Ti-6-4 has been measured to more than 900°C [10]. As the microstructure in shear bands of Ti-6-4 and Ti-15-3-3-3 formed during chip formation is similar, it can be speculated that high temperatures also occur during the shear band formation of Ti-15-3-3-3. The addition of lanthanum to Ti-15-3-3-3 might therefore also lead to short breaking chips during metal cutting operations, which will be discussed in the following sections.

3. Ti-15-3-3-3 Alloy containing Lanthanum

3.1 Alloy Production

In order to improve the machinability of Ti-15-3-3-3, 0.9% and 1.8% of the rare earth metal element lanthanum have been added. In addition, Ti-15-3-3-3 without lanthanum addition has been investigated as reference material, see fig. 5, left. As starting materials for the alloy production, the commercially available alloy Ti-15-3-3-3 following ASTM B348 and pure Lanthanum (purity 99.9%) have been used. The alloys were fabricated by plasma arc melting in a laboratory furnace of a capacity of 300g, followed by casting the material into a water cooled copper crucible (fast cooling). The alloys have been either investigated in the as-cast state or have been deformed in compression tests at temperatures between 650°C and 850°C followed by a solution treatment at 790°C / 15 min / AC.

3.2 Microstructure Analyses

Due to the fast cooling all alloys consist of beta-grains with an average grain size of about 100µm. In addition, round precipitates distributed on the grain boundaries as well as in the grains can be observed in all lanthanum containing alloys, see fig 5, right. The particle distribution in lanthanum containing Ti-15-3-3-3 alloy is different compared to lanthanum containing Ti-6-4 alloy, in which almost all particles are located on the grain boundaries [11]. The average particle size of the precipitates in Ti-15-3-3-3 is about 5µm, whereas few particles have a diameter of more than 10µm. The volume fraction of particles increases with increasing lanthanum content from 0.4% (Ti-15-3-3-3 + 0.9% La) to 0.9% (Ti-15-3-3-3 + 1.8% La) whereas the particle size remains almost constant.

EDX-analyses of the particles indicate the presence of lanthanum (as expected) and tin (not expected). The binary phase diagram La-Sn shows different La-Sn-intermetallics, namely La_3Sn, La_3Sn_5, La_2Sn_3, LaSn**,** La_5Sn_4 and La_5Sn_3 [12]. All the La-Sn-intermetallics have a melting point higher than 1140°C. Due to the relatively small diameter of the particles, EDX-analyses are difficult to interpret as the matrix material is also exited by the electrons. Hence, none of the possible intermetallic phases could be clearly identified. The lanthanum content changed from 40% to 63% in individual particles and the tin content changed from 60% to 37%, respectively.

During microstructure analyses of lanthanum-free and lanthanum containing alloys exposed to different thermo-mechanical or thermal treatments above 700°C, it has been observed that no grain growth occurred in the lanthanum containing alloys whereas strong grain growth occurs in the standard material. This effect could be explained by the presence of the thermodynamically stable La-Sn-precipitates.

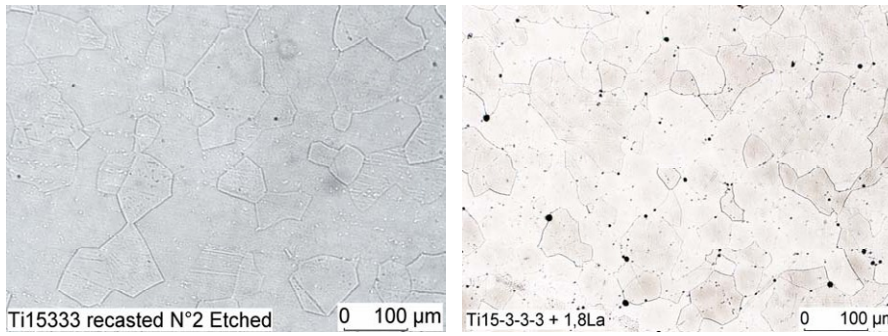

Fig 5: Microstructure of Ti-15-3-3-3 alloy (left) and Ti-15-3-3-3 containing 1.8% of lanthanum (right). Here, discrete La-Sn-rich particles precipitate after melting and casting.

3.3 Phase Composition

To understand the mechanisms leading to the formation of La-Sn-precipitates in Ti-15-3-3-3 alloy, samples of lanthanum-free (as a reference material) and the two lanthanum containing Ti-15-3-3-3 alloys have been exposed to hard-X-ray measurements at beam line BW5 of HASYLAB, DESY. The wavelength has been chosen to $\lambda = 0.014427$nm, the related energy was E = 83.93keV. Due to the high energy, specimens of 7mm thickness have been analysed in transmission (Debye-Scherrer-Configuration). The related spectra have been recorded by a position sensitive detector (image plate), the two-dimensional 2θ-Intensity diffraction pattern have been calculated by closed-loop integration.

Even if the diffraction patterns have not been analysed in detail so far, it can be stated that the peaks (additional to those matching to beta-titanium) neither belong to pure lanthanum nor to pure tin. Hence, the presence of one or more of the La-Sn-intermetallics in the lanthanum containing alloys is very likely as described above.

3.4 Machinability

The machinability of the lanthanum containing alloys has been investigated in straight turning experiments. The cutting speed, cutting depth and feed rate have been chosen in a way that segmented chips were supposed to form. In the alloys containing 0.9% or 1.8% of lanthanum no change in the chip formation process has been observed compared to the standard Ti-15-3-3-3 alloy. Short breaking chips have not been observed at all.

4. Conclusions and Future Work

During high-speed metal cutting experiments of Ti-15-3-3-3 segmented chips are formed. The addition of lanthanum most likely leads to the formation of La-Sn-intermetallics which have a melting point higher than 1140°C. The heat produced in the primary shear zone during the shear band formation is not sufficient to significantly soften the particles, melting of the intermetallics can be excluded at all as no molten structures have been found. Therefore, long chips form during metal cutting operations so that turning and drilling processes still cannot be automated for lanthanum containing Ti-15-3-3-3 alloys. Nevertheless, the La-Sn-precipitates improve the behaviour during thermo-mechanical treatments, as the presence of particles on the grain boundaries prevents grain growth (which is a serious problem for many beta-titanium alloys).

Future work will therefore on the one hand concentrate on the development of Sn-free beta-titanium alloys with improved machinability. On the other hand, the lanthanum containing Ti-15-3-3-3 alloys will be further investigated. First the existing diffraction pattern will be analysed in detail to finally identify the La-Sn-phases. Afterwards, in-situ high-temperature phase analyses at the La-Sn-containing alloys will clarify the thermal stability of the La-Sn-intermetallics. In addition, the lanthanum content will be subsequently diminished to identify the lower limit for the grain stabilising effect. Finally, the mechanical properties of this new class of alloys will be tested as improved strength combined with good ductility can be expected at room temperature even in the solution treated state. In addition, even applications at elevated temperature might be feasible.

5. Acknowledgement

The work presented in this paper has been carried out within the 7th Framework Programme of the Commission of the European Communities, section PEOPLE, Marie Curie Actions, Initial Training Networks, Project "MAMINA", Grant Agreement PITN-GA-2008-211536. Financial support of the European Commission is therefore gratefully acknowledged. The hard-X-ray investigations have been carried out at HASYLAB (DESY), Germany, beam line BW5. The authors thank Mr. Marco Girelli from the Institute for Production Technology of the Technische Universität Braunschweig for the quick-stop experiments.

6. References

[1] C. Leyens and M. Peters (eds.), *Titanium and Titanium Alloys – Fundamentals and Applications*, Wiley VCH, 2003.
[2] G. Lütjering et. al., *Titan*, Springer-Verlag, 2003.
[3] J. Donarchie (ed.), *Titanium – A Technical Guide*, ASM International, 2000.
[4] H.-K. Tönshoff, *Spanen – Grundlagen*, Springer, 1995.
[5] C. Siemers, P. Jencus, M. Bäker, J. Rösler; *A New Free-machining Titanium Alloy Containing Lanthanum*, in Proc. of the Titanium 2007, Kyoto, Japan, article in press.
[6] J. Rösler, M. Bäker, C. Siemers; *Mechanisms of Chip Formation* in: H.-K. Tönshoff and F. Hollmann (eds.), *High Speed Machining*, VCH-Wiley, 2005, pp. 492 - 512.
[7] F. Nakayama, *The Formation of Saw Tooth Chips*, Proc. of Int. Conf. on Prod. Eng., 1974.
[8] Technische Universität Braunschweig, J. Roesler, M. Baeker and C. Siemers, German Patent DE 103 32 078, *Method for Machining a Workpiece from a Titanium Base Alloy*, DPMA publications, 2005.
[9] H. Hoffmeister and T. Wessels; *High-Speed Machining of Titanium and Nickel-base Superalloys*, in: H. K. Tönshoff and F. Hollmann (eds.), *High Speed Machining*, VCH-Wiley, 2005, pp. 470 - 491.
[10] C. Siemers, P. Jencus, M. Baeker, J. Roesler, F. Feyerabend, *A new free machining Titanium alloy containing Lanthanum*, Proceedings of the Titan 2007 world conference, Vol. I, pp. 709 – 712, Kyoto, Japan, 2007.
[11] S. Benfer, C. Siemers, P. Jencus, J. Rösler, W. Fürbeth, *Corrosion properties of a new free machining titanium alloy*, Proceedings of the EUROCORR 2008 conference, September 7th – 11th, Edinburgh, United Kingdom, 2008.
[12] Landolt-Börnstein, *Numerical Data and Functional Relationships in Science and Technology, Group IV Physical Chemistry*, Springer, 1997.

II

Leemet, T., Hokka, M., Kuokkala, V.T., Olt, J.
Behavior of Ti-15-3 alloy at wide range of strain rates and temperatures.

Proceedings of 8th International Conference of DAAAM Baltic Industrial Engineering. 19-21st April 2012, Tallinn, ESTONIA, pp. 668-673.

8th International DAAAM Baltic Conference
"INDUSTRIAL ENGINEERING
19-21 April 2012, Tallinn, Estonia

BEHAVIOR OF TI-15-3 ALLOY AT A WIDE RANGE OF STRAIN RATES AND TEMPERATURES

Leemet, T.; Hokka, M.; Kuokkala, V.-T.; Olt, J.

Abstract: *Increasing number of practical applications, such as many high-rate manufacturing processes, involve large plastic deformations at high strain rates and at the same time at elevated temperatures. Therefore, future designs and improvements in the existing technological processes and applications are difficult without proper understanding of the material response to high-rate loadings at different temperatures. In addition, development of improved material models and validation of FE simulation results using these models require reliable experimental data at these conditions. This paper presents a computer controlled system for compression testing at high strain rates and high temperatures. The mechanical behavior of Ti-15-3 alloy was studied using this setup at wide ranges of strain rates and temperatures. Also, the Johnson-Cook plasticity model was used to simulate the material behavior.*

Key words: strain rate, high temperature, Split Hopkinson Pressure Bar, Ti-15V-3Al-3Sn-3Cr.

1. INTRODUCTION

Today there is an increasing number of applications where high rate deformations occur. Good examples are high-speed material forming and cutting operations, car crashes, vibrations of structures and buildings during earthquakes, and various aerospace applications. Especially in these kind of applications, the dependence of material properties on strain rate must be known to justify materials selection and to facilitate modeling and simulation of the material behavior.

Titanium alloy Ti-15V3Cr3Al3Sn, commercially known as 15-3, is a metastable beta-titanium alloy, first introduced in 1978 by American company USAF. Beta-titanium alloys like Ti15-3 show a unique combination of high strength, high ductility, and low density. The most important industries using these alloys are the aerospace, power generation, and chemical industries. Continuous demand for higher safety and lower CO_2 emissions make titanium alloys attractive for automotive industry as well, but so far their use has been rather limited due to the high cost of the material [1, 2]. The relatively high price of titanium alloys, compared to other construction materials, has two principal reasons: 1) the production costs of the raw material and 2) the costs related to the manufacturing of the components. In some instances, up to 50% of the material has to be removed with different machining processes [3], which can be very time consuming and therefore expensive due to the generally poor machinability of titanium alloys. Automated high speed machining of Ti-15-3 is hampered by two key factors: first, the continuous chip production, due to which the operator must continuously interfere with the process to remove the chips manually, and second, the accelerated wear of the cutting tools due to the adiabatic heating and poor heat conductivity of the metal, which in turn causes insufficient geometrical and surface tolerances of the workpiece [3].

The machinability of titanium alloys can be improved by developing so-called free machining alloys with better chip formation properties, by developing better tools, and by enhancing machining procedures, which can be greatly assisted by proper modeling of the material behavior and simulation of the machining process.

1.1 Deformation and testing at high strain rates and high temperatures

The strain rate dependence of flow stress in crystalline materials at low and intermediate strain rates is explained by the thermally activated dislocation motion, but a steep upturn in the flow stress is often observed at higher strain rates. This rapid increase of strength can be explained by phenomena caused by viscous drag on dislocations at higher dislocation velocities. Also temperature affects the material behavior by changing the available thermal energy and character of the obstacles for the dislocations. Changes in the material temperature can, in turn, happen for both external and internal reasons. During deformation only 5 to 10 % of imparted energy is consumed for restructuring the defect (dislocation) structure of the material, and most of the work is dissipated as heat. When strain rate increases, there simply is not enough time for the heat to escape from the deforming material, and the isothermal conditions of low strain rate deformation change towards more adiabatic during deformation at higher strain rates. As a consequence, the deformation may become highly localized at very narrow regions or adiabatic shear bands.

Split Hopkinson Pressure Bar (SHPB) is the most widely used technique for conducting high strain rate tests in the range of 10^2 to 10^4 s^{-1}. The compression test apparatus consists of two symmetrical slender bars, between which the small cylindrical specimen is sandwiched. The actual test is performed by impacting a striker bar to the free end of the first (incident) bar and by the consequent travel of the elastic stress pulse through the specimen, deforming it at a high rate.

Conducting high strain rate tests at elevated temperatures is rather challenging due to several practical and scientific reasons. The test setups found in the literature can be divided into two basic methods: 1) heating up all or short sections of the incident and transmitted bars together with the specimen, and 2) heating the specimen only while keeping the bars at room temperature throughout the test. The first method involves an inherent problem that limits its usable temperature range: when heating up the bars their physical properties change, which affects the strength of the bars and the speed of the elastic waves distorting the measured stress pulses. The change in the speed of the wave is difficult to account for and the necessary mathematical or mechanical corrections are complicated. Restrictions to the second technique are set by the allowed contact time of the hot specimen with the cold bars before the impact. The contact time can be minimized by a special manipulation system for the bars and the specimen and using, for example, a furnace or a radiation heater outside the axis of the bars. The essence of this method is to bring the hot specimen and the cold bars into contact just a fraction of a second before the impact of the striker on the input bar. Both the control and timing of the specimen heating and the movements of the bars and the specimen are very critical and can only be done using computer controlled systems.

2. DESCRIPTION OF THE HT-SHPB SYSTEM

The following Chapters describe the high temperature Split Hopkinson Pressure Bar device designed and built at the Department of Materials Science of Tampere University of Technology.

2.1 SHPB device

The device typically consists of two 1-2 m long metal bars with a diameter of 10-25 mm, and a striker bar, usually made of the same material and with the same diameter as the stress bars. When the striker bar is shot against the free end of the incident stress bar, the impact generates a stress pulse that propagates in the incident bar towards the specimen, which is sandwiched between the incident and transmitted bars. As the stress pulse reaches the bar-specimen interface, part of the pulse is reflected back as a wave of tension while part of it is transmitted through the specimen into the transmitted bar. The specimen is deformed plastically at a high strain rate as the pulse travels through it. Stress, strain, and strain rate in the specimen can be calculated from the three elastic stress pulses, incident, reflected, and transmitted pulses, measured from the pressure bars using strain gages and recorded with a digital oscilloscope.

The compression SHPB test system built at the Department of Materials Science of Tampere University of Technology (TUT) uses pressure bars made of high strength steel (YS ~ 1100 MPa), Maraging steel (YS ~ 1850 MPa), or high strength aluminium alloy 7075 (YS~500 MPa). Compression behaviour of materials can be studied in a strain rate range of $2 \cdot 10^2$-$10^4 s^{-1}$ by varying the length and the impact velocity of the striker bar and the length of the specimen. For data acquisition, a pair of strain gauges is bonded on both the incident and the transmitted bars. The signals are amplified using a signal conditioner with a bandwidth of 500 kHz and recorded on a 12-bit 10 Msample digital oscilloscope. Test data is downloaded to a PC and processed further with MATLAB based calculation routines.

2.2 High Temperature (HT) System

The fully computerized high temperature SHPB (HT-SHPB) system at TUT is constructed using the idea of only heating the specimen and keeping the other components of the testing system at room temperature. The specimen is first placed in a specimen holder using a ceramic wool support ring. The specimen holder is then pushed into the furnace by a pneumatic manipulation system. When the specimen has reached the desired test temperature, the manipulator rapidly retracts the specimen at high speed from the furnace to the centerline of the bars. The striker bar is shot, and just before it hits the incident bar, a transmitted bar manipulator pushes the bars and the specimen together. This way the maximum contact time of less than 50 ms is ensured between the hot specimen and the cold bars. The specimen is heated by a small resistive tube furnace with a maximum temperature of 1000 ºC. Entrance of the furnace is shielded with a special pneumatically controlled shutter to protect the bars from the heat. During heating of the specimen, a flow of inert gas is maintained to prevent the specimen from oxidizing. The specimen temperature is measured directly from the surface of the specimen using a K-type thermocouple touching the surface of the specimen. A summary of the system capabilities is given in Table 1.

Type of loading	Compression
Duration of the loading pulse [s]	50 ... 200 10^{-6}
Strain rate range [s^{-1}]	10^2... 10^4
Load range [kN]	0...250
Temperature range [ºC]	-150...1000
Specimen dimension [mm]	D<22; h~0.5…12

Table 1. SHPB system capabilities at TUT [5, 6].

3. RESULTS

Figure 3 shows true stress-true strain curves for the 15-3 alloy at different temperatures and strain rates. A substantial decrease in the flow stress levels with increasing temperature can be clearly seen in Fig 3a. At the strain rate 1600 s^{-1} at RT (Fig 3a), strain hardening takes place in the

beginning of the test, but after a few percent of plastic deformation the material first strain softens and then shows almost ideal plastic deformation behavior. With increasing temperatures the material shows notable strain hardening also at higher strains, especially at 400 ºC, as seen in Fig. 3a.

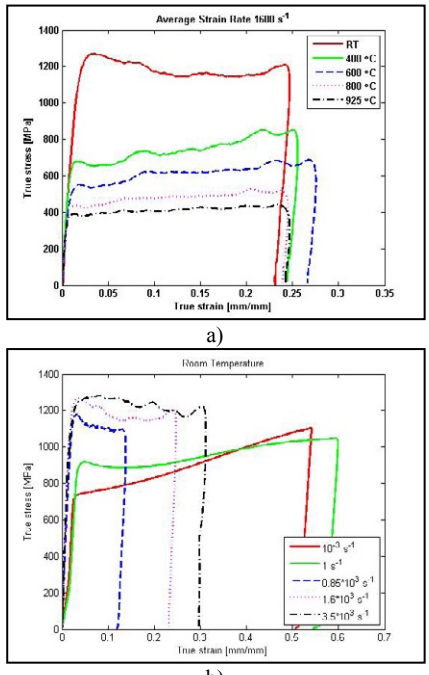

Fig. 3. Compression true stress – true strain curves for the Ti-15-3 alloy a) at different temperatures at an average strain rate of 1600 s^{-1}, and b) at different strain rates at room temperature.

The strain hardening rate, however, decreases when the temperature is further increased from 400 ºC, and at the highest test temperature of 925 ºC, the work hardening rate is already very low, most likely due to the fast dynamic recovery taking place at high temperatures.

Figure 3b shows the room temperature stress-strain response of the material at different strain rates. The flow stress levels increase notably with increasing strain rate, especially in the low strain regime, but the strain hardening rate clearly decreases at the same time. As can be seen in Fig 3b, at high strains the strength of the material at 10^{-3} s^{-1} even exceeds that at 1 s^{-1}, which is evidently related to the internal (adiabatic) heating of the material.

4. MODELING

One way to numerically describe the plastic deformation of materials is to use mathematical expressions that relate the dependencies of flow stress to variables describing the state of the material and the deformation conditions. Commonly used variables include strain, strain rate, and temperature, and the equations of state can be written in a general form as

$$\sigma = f(\varepsilon, \dot{\varepsilon}, T) \qquad (1)$$

A good model should be able to reproduce the real material behavior well enough, be mathematically simple, and to have an optimum (small) number of material parameters. Due to the interdependence of parameters on each other, setting up an ideal model is an extremely hard task. In engineering, compromises are usually needed, and typically somewhat simplified models are used that still provide the needed accuracy.

4.1 Johnson-Cook Model

The most widely used semi-empirical equation is the Johnson-Cook model

$$\sigma(\varepsilon, \dot{\varepsilon}, T) = \left(A + B \cdot \varepsilon^{n}\right)\left(1 + C \cdot \ln\left[\frac{\dot{\varepsilon}}{\dot{\varepsilon}_{ref}}\right]\right)\left(1 - \left[\frac{T - T_r}{T_m - T_r}\right]^{m}\right) \qquad (2)$$

which describes the flow stress as a multiplication of three terms. The first term represents the dependence of flow stress on strain, the second term on strain rate, and the third on temperature. It includes five material parameters that are to be determined from a set of tests performed at different strain rates and temperatures. The

model, however, has a fundamental problem that it assumes the parameters to be independent of each other, which for most materials and deformation conditions is not the case. However, the Johnson-Cook model is still broadly used mostly because of its simplicity and availability of the parameters.

The first three parameters A, B, and n are determined by fitting the Ludwik's equation, the first term in the model, on the reference stress-strain curve (often the curve obtained at room temperature at the strain rate of 1 s^{-1}, where the conditions are still isothermal for most materials). The remaining two parameters are then determined by fitting the model to the data measured at different temperatures and strain rates.

The material studied in this work, Ti-15-3, is a modest heat conductor and heats up considerably during plastic deformation. Because of this, an additional term was introduced into the model to take also the adiabatic heating into account, i.e,

$$\sigma_a(\varepsilon,\dot{\varepsilon},T)=\left(A+B\cdot\varepsilon^n\right)\left(1+C\cdot\ln\left[\frac{\dot{\varepsilon}}{\dot{\varepsilon}_{ref}}\right]\right)\left(1-\left[\frac{T+\Delta T-T_r}{T_m-T_r}\right]^m\right) \quad (3)$$

$$\Delta T=\frac{\beta}{\rho\cdot C_p}\int\sigma\cdot d\varepsilon \quad (4)$$

In this study an attempt was made to find a single set of values for the model parameters over the whole studied range of strain rates and temperatures. The first initial set of values was obtained from room temperature low strain rate tests. Several rounds of iterations were made, during which the initial set was compared to the experimental results obtained at different strain rates and temperatures. As a result of fitting, the model into the compression test data, the following set of material parameters for the Johnson-Cook (J-C) model (Table 2) was found to give the best fit at the strain rate range of 10^{-3}-4x10^3 s^{-1} and the temperature range of 295-1273 K.

A	B	n	C	m
754	992	1.3	0.02	0.7

Table 2. Parameters for the Johnson-Cook Equation for titanium 15-3 alloy.

Figure 4 shows the comparison of the experimental stress-strain curves and the curves calculated using the Johnson-Cook model (Table 2). The calculated values match extremely well with the measured data at the reference conditions, i.e., room temperature and strain rate of 10^{-3} s^{-1}. However, the model does not predict the material behavior at higher strain rates, and the calculated stresses are clearly underestimated. Furthermore, simply increasing the strain rate sensitivity of the model by increasing the parameter 'C' will lead to increasing strain hardening rate as a function of strain rate, which does not agree with the experimental observations in Figure 3, where the strain hardening rate decreases with strain rate. However, the fit is significantly improved if only relatively narrow ranges of strain rate and temperature are used. Therefore it is obvious that separate sets of J-C parameters should be used for different strain rate and temperature regimes.

The main reason for the J-C model not to be capable of reproducing the true stress-strain response of Ti-15-3 is related to the strain hardening behavior of this material that deviates considerably from the shape of the Ludwik equation. Also the general interdependence of the J-C model parameters on each other limits the usability of the model to narrower ranges of strain rates and temperatures. For any positive value of parameter 'C', the strain hardening rate predicted by the model increases with strain rate. For the titanium 15-3 alloy this seems not to be the case, as the strong adiabatic heating decreases the strain hardening rate rapidly at strain rates higher than 1 s^{-1}.

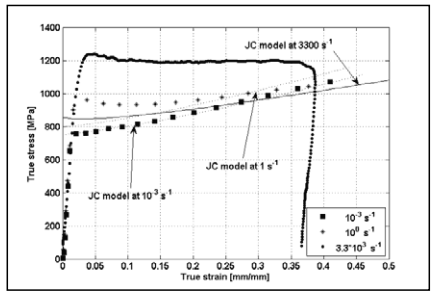

Fig. 4. The comparison of measured and calculated stress strain curves.

5. CONCLUSIONS

In this paper, a computer controlled HT-SHPB testing system is described in details, as well as some example results of the high temperature high strain rate testing of titanium 15-3 alloy. The results of the compression tests for the titanium 15-3 alloy show strong positive strain rate sensitivity at room temperature. Also the strain hardening rate is strongly affected by both the strain rate and temperature. At room temperature the strain hardening rate clearly decreases with increasing strain rate, and even becomes negative at very high strain rates and small strains.

No single set of Johnson-Cook parameter values was found to be able to describe the mechanical behavior of Ti-15-3 over the studied wide range of strain rates and temperatures. Therefore the model parameters have to be defined for narrower regions of strain rate and temperature to yield acceptable fits between the calculated and experimental stress strain curves.

6. REFERENCES

1. Leyens, C.; Peters, M. *Titanium and Titanium Alloys - Fundamentals and Applications*. Wiley VCH, 2003.

2. Bhattacharjee, A.; Ghosal, P. et al. Room temperature plastic flow behaviour of Ti–6.8Mo–4.5Fe–1.5Al and Ti-10V-4.5Fe–1.5Al: Effect of grain size and strain rate. *Mater. Sci. Eng., A.,* 2007, **452-453**, 219-227

3. Siemers, C.; Zahra, B.; Leemet, T.; Rösler, J. Development of Advanced beta-Titanium Alloys. In *Proceedings of the 8th AMMT'09 Conference*. St. Petersburg, 2009.

4. Hokka, M. testing of materials with the Hopkinson Split Bar technique. In *Proceedings of the SMP IX Conference*. Lappeenranta, 2006.

5. Apostol, M.; Vuoristo, T.; Kuokkala, V.-T. High temperature high strain rate testing with a compressive SHPB. *J. Phys. IV,* 2003, **110**, 459-464

6. Apostol, M. *Strain rate and temperature dependence of the compression behavior of FCC and BCC metals; Development of experimental techniques and their application to materials modeling.* Ph.D. thesis, Department of Materials Science, Tampere University of Technology, 2007.

7. Neelekantan, S.; Rivera-Diaz-del-Castillo, P.; v.d. Zwaag, S. Prediction of the martensite start temperature for β titanium alloy as a function of composition. *Scr. Mater.,* 2009, **60**, 611-614

8. Xu, W.; Kim, K.; Das, J.; Calin, M. Phase stability and its effect on the deformation behavior of Ti-Nb-Ta-In/Cr β alloys. *Scr. Mater.,* 2006, **54**, 1943-1948

7. ADDITIONAL DATA ABOUT AUTHORS

Tõnu Leemet Ph.d student Estonian University of Life Sciences
Behaviour and Modelling of Titanium 15-3 Alloy at a Wide Range of Strain Rates and Temperatures
Ph.d student/Kreutzwaldi 56, 51014 Tartu, Estonia/Tonu.Leemet@emu.ee/
http://te.emu.ee/+37256659869/+37274419 97
Tõnu Leemet, Kreutzwaldi 56, 51014 Tartu, Estonia. Room A416

III

Hokka, M., Shrot, A., **Leemet, T.**, Baeker, M., Kuokkala, V.-T. Dynamic Behavior and Numerical Modeling of Titanium 15-3-3-3 Alloy.

Proceedings of SEM XII International Congress & Exposition on Experimental and Applied Mechanics Measurement Challenges for New Structures and Materials. Hilton Orange County/Costa Mesa, Costa Mesa, CA USA June 11-14, 2012

Dynamic Behavior and Numerical Modeling of Titanium 15-3-3-3 Alloy

Mikko Hokka[1], Tõnu Leemet[1], Aviral Shrot[2], Martin Bäker[2], Veli-Tapani Kuokkala[1]

[1]Tampere University of Technology, Department of Materials Science
P.O.B. 589, 33101 Tampere, Finland
mikko.hokka@tut.fi
[2]Technische Universität Braunschweig, Department of Materials Science

ABSTRACT

Metastable beta titanium alloys combine excellent mechanical properties with low density, and are therefore very attractive in many mechanically demanding applications. The high strength and hardness, however, cause several challenges in the machining of these materials, and the machining costs of titanium components can be significant compared to the overall costs of the component. The cutting conditions can be optimized using finite element simulations, leading to reduced machining costs and improved machining quality. However, the simulations of the rather complex machining processes need reliable material models. The models can only be generated when the mechanical behavior of the material is understood well. In this work, the mechanical response of Ti-15-3-3-3 alloy has been characterized in a wide range of strain rates and temperatures. Johnson-Cook material model was fit to the measurement data, and the model was used to simulate orthogonal cutting of the material. The simulation results were further compared to cutting experiments at high cutting speeds. The current model is able to simulate the serrated chip formation frequently observed for titanium alloys at high cutting speeds. Also, the simulated cutting forces match well with the experimentally obtained forces. However, the model needs to be further developed to match also the fine details of the chip, such as the chip curl and thickness of the individual serrations.

INTRODUCTION

The extraordinary properties of titanium and its alloys have rapidly increased the usage of these metals and alloys in several engineering applications, especially in the aerospace industry. Typical properties of titanium alloys include low density, excellent corrosion resistance, and high strength and hardness that are retained to relatively high temperatures. Other properties typical to titanium alloys include relatively low heat conductivity and high chemical reactivity. Despite these excellent properties, the high strength and hardness combined with the overall chemical reactivity typically lead to several difficulties in the machining of these alloys [1-3]. The high strength and hardness are typically retained to high temperatures, and therefore, the machining forces are typically rather high. The hardness also increases the abrasive wear or the tools. Chemical reactions between the tool and the workpiece can lead to strong adhesion or galling of the tool and the chip leading to a rapid wear and failure of the tool. Finally, the low heat conductivity and high strength of the material typically induce strong adiabatic heating during machining, leading to higher machining temperatures and faster failure of the tool. For these reasons, most titanium alloys are considered hard-to-machine alloys.

The experimental research on machining and machinability is somewhat complicated due to the vast number of different machining operations, e.g., turning, milling, drilling etc., and the number of different conditions or machining parameters, e.g., cutting speed and depth, rake angles etc. Therefore, studying the material behavior in machining would require extensive testing with various techniques and devices. The testing can be, however, complemented by simulating the machining processes. However, the simulation results are reliable only when using accurate material models that are able to reproduce the true material behavior at the cutting conditions. These models are typically generated based on experimental data acquired from rather simple experiments, such as tension or compression tests. However, the material properties can be measured only in certain and often

quite narrow ranges of strain, strain rate, and temperature. In machining, the strains, strain rates, and temperatures are most likely to be much higher than what can be covered by the laboratory experiments, and therefore, the material model must be able to predict the properties and behavior of the material beyond the range where the model and its parameters were determined.

In this work, the behavior of titanium 15-3-3-3 alloy was extensively studied in compression, and a material model based on the Johnson-Cook equation was generated. This model was used to simulate orthogonal cutting experiment at high cutting speed.

EXPERIMENTAL

In this work, the compression behavior of the commercial metastable beta titanium alloy Ti-15V-3Sn-3Al-3Cr was studied in a wide range of strain rates and temperatures. The alloy was studied in as-received condition without any aging treatments. Cylindrical compression specimens with a diameter of 8 mm and length of 8 mm and/or 6 mm were machined using electric discharge machining. At low strain rates the mechanical testing was performed using an MTS servohydraulic materials testing machine with an induction heating system for high temperature testing. The high strain rate compression tests, on the other hand, were done with a Split Hopkinson Pressure Bar (SHPB) device equipped with high temperature test setup. The device used in this study consists of 22 mm diameter high strength Maraging steel incident, transmitted, and striker bars. Both incident and transmitted pressure bars were aligned along the same horizontal axis, and the bars were supported by three bearings on four stanchions, which can be moved in y- and z- directions to ensure proper alignment. The lengths of the incident, transmitted, and momentum trap bars were 1200 mm each, and the length of the striker bar varied between 200 mm and 400 mm. A room temperature experiment is performed simply by placing the cylindrical specimen between the lubricated ends of the incident and transmitted bars, and then impacting the striker bar to the free end of the incident bar. The impact velocity is adjusted by changing the pressure and measured using three IR sender receiver pairs. The impact of the striker creates a stress pulse that propagates in the incident bar at the speed of sound (~4900 m/s), and when the stress pulse reaches the bar-specimen interface, part of the pulse is transmitted through the specimen into the transmitted bar, whereas the remaining part of the incident stress pulse is reflected back to the incident bar as a wave of tension. The incident, reflected, and transmitted stress pulses are measured with strain gages bonded on the surface of the stress bars, and the signals are amplified and recorded using Kyowa CDV 700A series signal conditioner and Yokogawa DL 708 high sampling rate digital oscilloscope. The stress, strain, and strain rate in the specimen are calculated from the dispersion corrected stress pulses using Equations 1-3. The numerical dispersion correction used in this work was adopted from the work of Gorman [4].

Average stress in the specimen is given by:

$$\sigma(t) = \frac{A_b\, E\varepsilon_t(t)}{A_S} \tag{1}$$

Average strain in the specimen is given by:

$$\varepsilon(t) = \frac{2C_0}{L_s}\int_0^t \varepsilon_r(t)\, dt \tag{2}$$

Average strain rate in the specimen is given by:

$$\dot{\varepsilon} = \frac{2C_0\varepsilon_r(t)}{L_S} \tag{3}$$

In Equations 1-3, A_b, E, and C_0 are the cross sectional area, Young's modulus, and the speed of sound of the bar material, L_s and A_s are the length and cross sectional area of the specimen, and ε_r, and ε_t are the reflected and transmitted stress pulses. The Equations 1-3 assume stress equilibrium, i.e., that the stresses on the front and back sides of the specimen are the same. For metallic materials this assumption is true at least for strains higher that a few percent.

The high temperature compression test system at high strain rates is based on computer controlled pneumatic manipulation of the stress bars and the specimen. This system allows keeping the bars at room temperature while heating the specimen in a furnace located beside the bars. The specimen is inserted to a ceramic insulating wool ring exposing only the ends of the cylindrical specimen. The wool ring itself is very soft and does not mechanically constrain the deformation of the specimen. The wool ring is further placed to a specimen holder arm that is pneumatically pushed to the furnace. After heating the specimen holder arm quickly retracts the specimen to the centerline of the bars. The striker bar is shot, and just a fraction of a second before the impact, a second manipulator pushes the cold bars and the hot specimen into contact. The current high temperature setup limits the total time that the specimen spends outside the hot furnace before the dynamic loading to about 200 ms. More importantly the system limits the contact time of the hot specimen and the cold bars to less than 50 ms, which keeps the temperature of the specimen essentially constant. The heat flow from the specimen to its surroundings has been studied by numerical simulations, and the results show a minor temperature drop of only a few degrees at depth of less than 150 μm for a test performed at the initial temperature of 800 °C [5-6]. Figure 1 shows the testing steps during a test with the high temperature system.

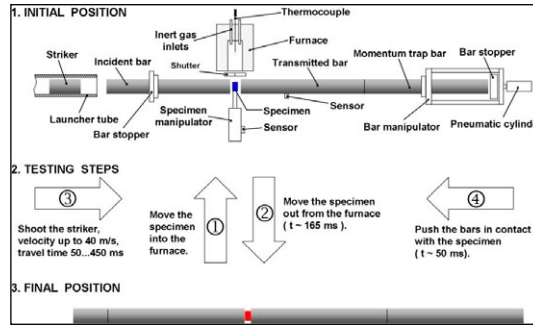

Fig 1 Schematic picture of the testing steps during a test with the high temperature setup

The simulation results were further compared to orthogonal cutting experiments with the U-shape specimens. A schematic picture of the U-shape test specimen is shown in Figure 2. The test is performed by inserting the cutting tool between the arms of the 'U', and the whole specimen-tool assembly is placed between the bars. The test is carried out by impacting the striker bar to the incident bar and obtaining the cutting forces from the transmitted signal.

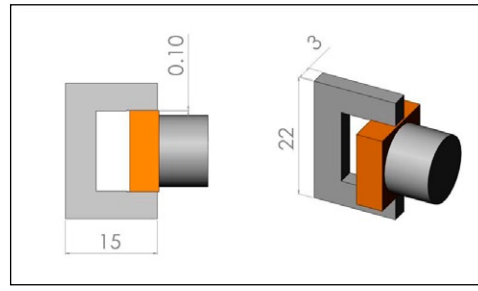

Fig 2 schematic picture of the U-shape specimen for cutting force measurement. Units are in millimeters

RESULTS AND DISCUSSION

The room temperature stress-strain curves for the titanium 15-3-3-3 alloy are shown in Figure 3a. At low strain rates the yield behavior of the material is continuous followed by strain hardening. When the strain rate is increased from 10^{-3} s^{-1} to 1 s^{-1} the strain hardening rate decreases strongly with increasing strain rate. Also, the yield behavior changes gradually and pronounced yielding is observed at strain rates 1 s^{-1} and above. At strain rates 600 s^{-1} and above the strain hardening rate of the material decreases further and the material actually softens at low strains.

Figure 3b shows the absolute strain rate sensitivity factor, $m_a=d\sigma/d\log(\ )$ and Figure 3c the relative (logarithmic) strain rate sensitivity factor, $m_r=d\log(\sigma)/d\log(\ )$, as a function of plastic strain. The sensitivity factors in Figures 3b and 3c are obtained at different temperatures and at strain rates between 10^{-3} s^{-1} and 1 s^{-1}. The absolute strain rate sensitivity (Fig. 3b) decreases strongly with plastic strain at room temperature. However, at elevated temperatures the behavior is clearly different and the sensitivity factor higher than that at room temperature. The rate sensitivity increases with plastic strain at temperatures of 800 °C and 950 °C. The highest absolute strain rate sensitivity is achieved at 800 °C. On the other hand, if the strain rate sensitivity is calculated with respect to material's strength, (Fig. 3c) the rate sensitivity increases strongly with increasing temperature and the highest rate sensitivity is achieved at 950 °C. The relative strain rate sensitivity decreases with plastic strain at room temperature, is essentially constant at 600 °C, slightly increases at 800 °C, and clearly increases at 950 °C.

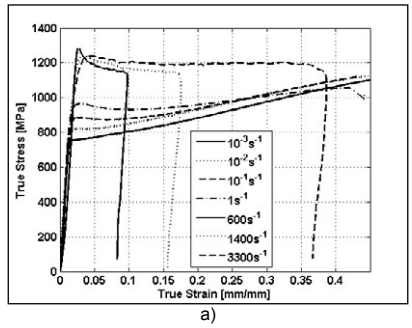

a)

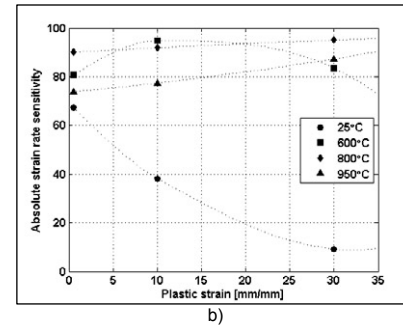

b)

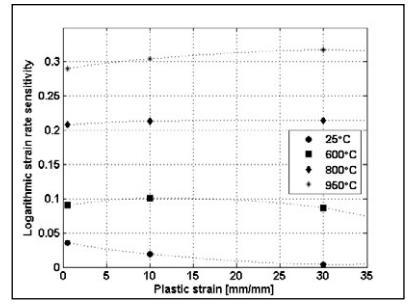

c)

Fig 3 a) true stress vs. true strain curves at different strain rates, b) absolute, and c) relative (logarithmic) strain rate sensitivity as a function of plastic strain at different temperatures

The Jonhson-Cook plasticity model was used to model the mechanical behavior of the titanium alloy. The model used for the adiabatic strength of the material is shown in Equation 4. The parameters for the model were found using the following procedure: first the parameter 'm' was obtained using Equation 5, where the yield strengths and were obtained at the reference and at an elevated temperature, respectively. Second, the adiabatic stress-strain curve obtained experimentally at the reference temperature and strain rate was converted to isothermal one using Equation 6. Third, the parameters A, B, and n were obtained by fitting a straight line to the log(σ-A) vs. log(ε) curve. Finally the parameter C was obtained by comparing the experimental stress-strain curves obtained at different strain rates and the curves calculated using Equation 4. The parameter A was determined as the yield strength of the material at the reference strain rate. However, this value overestimated the strength of the material at higher strains, and therefore, the value was decreased so that the strength calculated by the model matches the experimental stresses at higher strains. Also, the value for the parameter m that was obtained using Equation 5 did not produce a good match between the simulated and experimental stresses at higher strains. Therefore, the value was manually adjusted to improve the fit. The values for the parameters are shown in Table 1. Figure 4 shows the comparison of the experimentally obtained adiabatic stress and the values calculated using the current material model. The fit is relatively good at strains higher than about 7 percent. The initial pronounced yielding was omitted when obtaining the model parameters as this behavior is very difficult to reproduce with the current material model, and furthermore, the observed yield behavior is not likely to have a significant effect on the chip formation process.

$$\sigma_a = (A + B\varepsilon^n)(1 + C_{JC} \ln \frac{\dot{\varepsilon}}{\dot{\varepsilon}_{ref}})(1 - \left[\frac{T + (\frac{\beta}{\rho c} \int_0^{\varepsilon} \sigma d\varepsilon) - T_{ref}}{T_m - T_{ref}} \right]^m) \quad (4)$$

$$m = \log(1 - \frac{\sigma_y^{T2}}{\sigma_Y^{Tr}}) - \log(\frac{T_2 - T_r}{T_m - T_r}) \quad (5)$$

$$\sigma_i = \frac{\sigma_a}{\left[1 - \left(\frac{T + (\frac{\beta}{\rho c} \int_0^{\varepsilon} \sigma d\varepsilon) - T_r}{T_m - T_r} \right)^m \right]} \quad (6)$$

Table 1: the parameters for the Johnson-Cook models used in this work

Parameter	A	B	n	C	M	T_r [°C]	T_m [°C]	$\dot{\varepsilon}_{ref}$ [s^{-1}]	β	C_p [J/kgK]	ρ [kg/m^3]
Value	984	380	0.3	0.069	1.1	23	1669	1400	0.9	500	4760

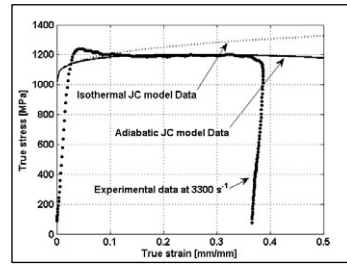

Fig 4 Comparison of the measured adiabatic stress and values calculated by the Johnson-Cook model at the strain rate of 3300 s^{-1}

Figure 5 shows the effects of the specific heat capacity on the isothermal stress-strain curves. In this work both the modeling and simulations were done using heat capacity of 500 J/Kg*K, which is a value commonly found in literature, e.g. [8], However, the heat capacity of the alloy is known to increase with temperature. In high speed cutting, the deformation induced heat increases both the temperature and the heat capacity of the material. Figure 5 shows the stress strain curves calculated from the measured adiabatic curves at room temperature at the strain rate of 3300 s^{-1} using Equation 6 with the specific heat capacities of 500 J/Kg*K and 650 J/Kg*K. At low strains the difference between the isothermal stress-strain curves is negligible, but the difference increases towards higher strains. The higher heat capacity leads to higher simulated strength as the temperature of the material increases less during deformation. In the simulations of the high speed cutting, the results were found very sensitive to small changes in the heat capacity, and the serrated chips were only produced when using the lower heat capacity value. At C_p = 650 J/Kg*K the deformation induced heat was not sufficient to localize the strain and to produce segmented chips.

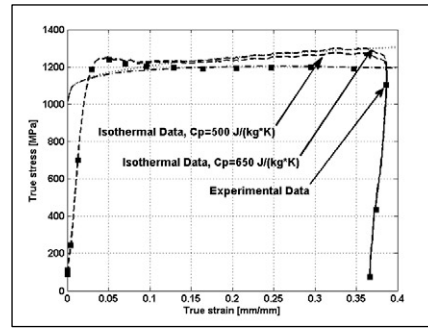

Fig 5 Effects of specific heat capacity on the isothermal stress strain curves. The dotted and dash-dot lines are stresses calculated using the Johnson-Cook model

A two dimensional explicit finite element model was created using the commercial software ABAQUS 6.9-1. The tool was assumed rigid and no heat conduction was allowed between the tool and the chip. A conservative friction coefficient of 0.1 was used between the tool and the deforming material. The workpiece was meshed very finely with CPE4R elements, and the model contained 101151 nodes and 100049 elements (Figure 6). Since the alloy has low thermal conductivity, the machining process was assumed adiabatic at the cutting speed of 15 m/s. The chip separation was modeled by using a sacrificial layer whose elements were deleted when the shear strain exceeded a value of 1.0.

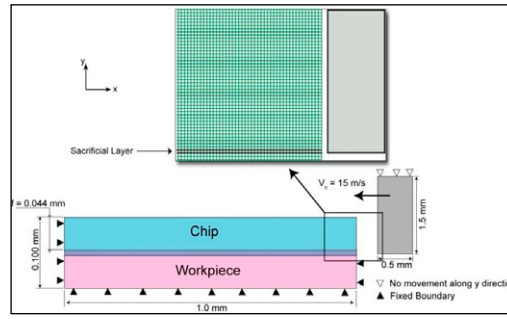

Fig 6 the finite element model

The same cutting conditions, i.e., cutting speed of 15 m/s and cutting depth of 44 µm were used in both the simulations and experiments. The simulated (Fig.7) and experimentally obtained chips show somewhat similar serrations, but the fine details such as the chip curl and the dimensions of individual segments are somewhat different. On the other hand, the cutting stresses obtained from the experiments and from the simulations were 2000 MPa and 2200 MPa, respectively. The difference in the simulated and experimentally obtained cutting forces can be explained at least partly with the differences in the frictional conditions between the simulated and experimental setups. However, the model still needs to be further developed to match also the chip shape. One possibility for optimization of the parameters is using inverse methods [7].

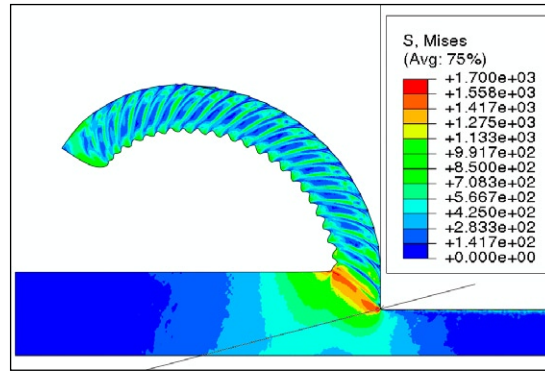

Fig 7 von Mises stress in the simulated chip

SUMMARY

The dynamic response of the titanium 15-3-3-3 alloy was studied at room and at elevated temperatures. Based on the results of the mechanical tests, material model based on the Johnson-Cook equation was generated and the model was further used in the simulations of orthogonal cutting experiment.

The strain hardening rate of the material was found to be a sensitive function of strain rate and temperature. The strain hardening rate decreases fast when strain rate is increased. Also, at higher temperatures the strain hardening rate at high strain rates was much stronger compared to that observed at room temperature. The strain

rate sensitivity of the material was also found to be a very sensitive function of temperature, and in the low strain rate region, the relative sensitivity increased rapidly with temperature.

The parameters for the Johnson-Cook plasticity model were determined from the isothermal stress strain curves. The model was further used to simulate orthogonal cutting of the alloy. The model is clearly able to produce segmented chips and to match the experimental cutting forces with high accuracy. However, more work is still needed to fine tune the model to match also the details of the chip shape.

ACKNOWLEDGEMENTS

The research leading to these results has received funding from the European Union Seventh Framework Programme (FP7/2007-2013) under grant agreement No. PITN-GA-2008-211536, project MaMiNa.

REFERENCES

[1] M. Rahman, Z. Wang, Y. Wong, JSME International Journal, Series C, 49, no.1, 2006.
[2] P.D. Hartung, B.M. Kramer, B.F. von Turkovich, CIRP Annals – Manufacturing Tech., 31 (1982), 75-80.
[3] A. Jawaid, C.H. Che-Haron, A. Abdullah, J. Mat. Proc. Tech., 92-93 (1999), 329-334.
[4] D. Gorman, J. Phys. E: Scientific Instruments, 16 (1983).
[5] M. Apostol, V.-T. Kuokkala, T. Vuoristo, In: C. Papalettere (Eds.) Advances in Experimental Mechanics, McGraw-Hill, Bari Italy, 2004.
[6] M. Apostol, T. Vuoristo, V.-T. Kuokkala, J. de Phys. IV, 110, 2003.
[7] A. Shrot, M. Bäker, J.Com.Mat.Sci. 52, (2012), 298-304.
[8] R. Boyer, G Welsch and E. W. Collings, Materials Properties Handbook: Titanium alloys, ASM International, Materials Park, OH, USA.

IV

Hokka, M., **Leemet, T.**, Shrot, A., Baeker, M., Kuokkala, V.-T.
Modeling of the Dynamic Behavior of Hard-to-Machine Alloys.

Proceedings of DYMAT 2012 - 10th International Conference on the Mechanical and Physical Behaviour of Materials under Dynamic Loading 2nd-7th, 2012, Freiburg, Germany

Modelling of the Dynamic Behaviour of Hard-to-Machine Alloys

M.Hokka[1], T. Leemet[1], A.Shrot[2], M. Bäker[2], and V.-T. Kuokkala[1]

[1]Tampere University of Technology, Department of Materials Science, Finland
[2]Technische Universität Braunschweig, Department of Materials Science, Germany

Abstract. Machining of titanium alloys and nickel based superalloys can be difficult due to their excellent mechanical properties combining high strength, ductility, and excellent overall high temperature performance and material properties. Machining of the alloys can, however, be improved by simulating the processes and by optimizing the machining parameters. The simulations, however, need accurate material models that predict the material behaviour in the range of strains and strain rates that occur in the machining processes. In this work, the behaviour of titanium 15-3-3-3 alloy and nickel based superalloy Alloy 625 were characterized in compression, and Johnson-Cook material model parameters were obtained from the results. For the titanium alloy, the adiabatic Johnson-Cook model predicts softening of the material adequately, but the high strain hardening rate of Alloy 625 in the model prevents the localization of strain and no shear bands were formed when using this model. For Alloy 625, the Johnson-Cook model was therefore modified to decrease the strain hardening rate at large strains. The models were used in the simulations of orthogonal cutting of the material. For both materials, the models are able to predict the serrated chip formation, frequently observed in the machining of these alloys. The machining forces also match relatively well, but some differences can be seen in the details of the experimentally obtained and simulated chip shapes.

1 Introduction

Metal alloys with superior mechanical properties are needed in various parts and components of the aerospace, transportation, mining and excavation, and power generation industries. In these alloys, high strength and hardness are combined with good overall ductility, high chemical and corrosion resistance, and excellent fatigue and high temperature performance. Titanium alloys and nickel based superalloys are examples of metal alloys with these extraordinary properties. However, the good mechanical performance can lead to problems in the manufacturing of parts and components. Especially machining of these materials can be challenging, time consuming, and expensive. Most titanium alloys have rather low thermal conductivity, and therefore the temperature of the deforming material often increases rapidly during high speed cutting. The increased temperature of the machining process leads to rapid tool wear and decreased machining quality. Some alloys also produce continuous chips that do not segment and break during machining leading to dangerous entanglements of sharp chips and forcing to interrupt the machining process to manually remove the chips. Also the chemical affinity of titanium can lead to severe galling of the tool and the material causing severe damage to the tool. The nickel based alloys, on the other hand, can contain extremely hard precipitates, such as carbides or intermetallic compounds, which abrade the tool during machining. For these reasons, many of the titanium and nickel based alloys are considered hard-to-machine, and the majority of the overall costs of geometrically complex components can be due to machining. For a better overview on the machining of titanium and nickel alloys see, for example, refs. [8-10].

Machining of these alloys can be improved by developing alloys that are more suitable for machining and by improving the machining processes and tools. Finite element simulations can be very useful in obtaining information about the machining processes and optimizing the machining parameters, such as cutting depth and speed. The simulations, however, require accurate material models based on real experiments. Mechanical testing, on the other hand, can usually be done only in a relatively narrow range of strain, strain rate, and temperature. In machining however, the strains and strain rates can be significantly higher than what can be studied in a controlled laboratory environment. Therefore, the material models intended for machining simulations must be able to predict the material behaviour also at much higher strains and strain rates than for which it was initially generated. In this work, the mechanical behaviour of titanium 15-3-3-3 alloy and Alloy 625, similar to Inconel 625, was characterized in compression

at a wide range of strain rates at room and elevated temperatures. The Johnson-Cook material model [6-7] parameters were obtained from the results of compression tests and the models were used to simulate orthogonal cutting of the studied alloys. This paper presents and discusses the results of the mechanical testing and modelling of the material behaviour. Preliminary cutting simulation results are also presented and the results are compared to cutting experiments.

2 Experimental

The materials studied in this work were Alloy 625 (similar to Inconel 625) and the metastable beta titanium 15-3-3-3 alloy. Both materials were studied in a fully annealed state without precipitation treatments. The mechanical behaviour of the alloys was characterized in compression in a wide range of strain rates and temperatures. The low strain rate tests were performed with an MTS servohydraulic materials testing machine with an induction heating system for high temperatures. The high strain rate tests were done using a Hopkinson Split Bar device with high temperature capabilities. The high temperature system used in this study heats the specimen in a furnace located beside the bars and utilizes two separate pneumatic manipulation systems for the specimen and the bars. The small cylindrical specimen with a diameter of 6 mm and length between 6 and 8 mm is placed in a soft ceramic wool ring. The ring and the specimen are inserted in a special specimen holder arm, which can be pneumatically pushed from the centreline of the bars inside the furnace, where it is heated to the test temperature. After heating the specimen holder quickly retracts the specimen back to the centreline of the bars. The striker bar is shot and the second pneumatic actuator pushes the cold bars into contact with the hot specimen just a fraction of a second before the impact loading. The current specimen and bar manipulation system limits the contact time between the hot specimen and the cold bars to less than 50 ms, which guarantees that only the surface temperature of the specimen drops by a few degrees [1-3]. Figure 1 shows the testing steps involved in the high temperature test.

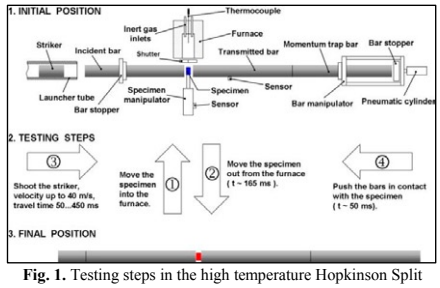

Fig. 1. Testing steps in the high temperature Hopkinson Split Bar test.

3 Results

Figure 2 shows the stress-strain curves at different strain rates and temperatures for the titanium 15-3-3-3 alloy. At room temperature, the strain hardening rate observed in the low strain rate region is significantly higher than that observed at higher strain rates. At the strain rate of 3300 s^{-1}, the strain hardening rate is essentially zero after the initial pronounced yielding. This behaviour can at least partly be explained with adiabatic heating and consequent thermal softening at high strain rates. At higher temperatures, the strength of the material clearly decreases. The strain hardening rate is also much higher at elevated temperatures compared to that at room temperature. Also the strain rate sensitivity of the material was found to increase significantly with temperature.

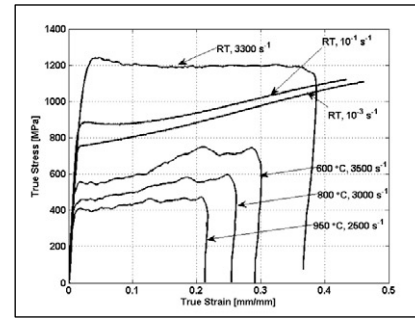

Fig. 2. Results of the compression tests for titanium 15-3-3-3 alloy.

Figure 3 shows the stress strain curves obtained at different strain rates and temperatures for Alloy 625. The behaviour of Alloy 625 is significantly different from that observed for the titanium alloy. The stress strain curves at all strain rates and temperatures are nearly linear. At room temperature, the strain hardening rate of the material is essentially constant with respect to strain rate, which also leads to constant strain rate sensitivity with respect to plastic strain. The strain hardening rate decreases slowly as the temperature is increased obviously due to increased recovery and annihilation of dislocations.

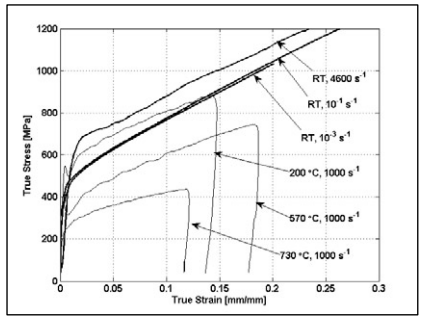

Fig. 3. Results of the compression tests for Alloy 625.

Figure 4 shows the strength of the material as a function of temperature at a constant strain rate. The strength of the titanium 15-3-3-3 alloy decreases rapidly when the temperature is increased from room temperature to 400 °C. Increasing the temperature from 400 °C to 950 °C decreases the strength even further, but the response is now nearly linear. For Alloy 625, the strength decreases with temperature steadily but there is more scatter in the results. The temperature sensitivity of the titanium alloy seems to be stronger in the low temperature region than that observed for Alloy 625, but at higher temperatures the strength of the Alloy 625 actually seems to decrease slightly faster. The relative decrease of strength for the titanium alloy is also higher than that for Alloy 625.

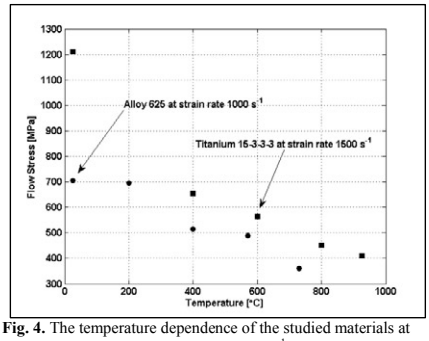

Fig. 4. The temperature dependence of the studied materials at the strain rate of 1000 s^{-1}.

3.1 Modelling

Modeling of the mechanical behaviour of the titanium alloy is complicated by its strong rate sensitivity of strain hardening. A model describing the behaviour in the whole range of strain rate and temperatures would be quite complex, because it needs to take into account the changes in the strain hardening rate with respect to strain rate and temperature. Also, the strain rate sensitivity of the material is not constant, especially at low strain rates, where the sensitivity increases strongly with temperature. Furthermore, especially at room temperature the rate sensitivity increases significantly at strain rates around 10^3 s^{-1}, when the dislocation drag mechanisms become active. The commonly used Johnson – Cook (JC) model can in general be used to model the isothermal response of the material in a narrow range of strain rates. In machining the strain rates can be very high, and therefore the parameters of the JC model were obtained from the compression tests using only the high strain rate data. However, at these high strain rates the material is likely to heat up significantly due to the adiabatic heating. Therefore, the measured adiabatic curves were first converted to isothermal ones using Equation 1. The parameter m used in this Equation was first obtained from the yield strengths of the material at the reference strain rate using Equation 2. In Equation 5, the yield stresses and were obtained at the reference temperature and at an elevated temperature, respectively. However, the obtained parameter m did not provide good results at higher strains and the value of the parameter was manually adjusted to improve the fit of the measured and calculated data also at large strains. The model used to calculate the adiabatic stress is shown in Equation 3.

$$\sigma_i = \frac{\sigma_a}{\left[1-\left(\frac{T+(\frac{\beta}{\rho c}\int_0^{\varepsilon}\sigma d\varepsilon)-T_r}{T_m-T_r}\right)^m\right]} \quad (1)$$

$$m = \log(1-\frac{\sigma_Y^2}{\sigma_Y^{Tr}}) - \log(\frac{T_2-T_r}{T_m-T_r}) \quad (2)$$

$$\sigma_a = (A+B\varepsilon^n)(1+C_{JC}\ln\frac{\dot{\varepsilon}}{\dot{\varepsilon}_{ref}})(1-\left[\frac{T+(\frac{\beta}{\rho c}\int_0^{\varepsilon}\sigma d\varepsilon)-T_{ref}}{T_m-T_{ref}}\right]^m) \quad (3)$$

The JC model was used to simulate also the behaviour of Alloy 625. The model parameters were found using a nonlinear fitting routine in Matlab and assuming the deformation to be fully adiabatic. Only the high strain rate data were used since low strain rates hardly occur in machining. However, the strain hardening rate of Alloy 625 is very high at high strain rates, and when extrapolating the material behaviour to larger strains the model predicts unreasonably high strength. In the simulations, no serrated chips were formed using this model. This is because the strain does not localize due to the strong strain hardening that effectively compensates for the thermal softening caused by the adiabatic heating. Therefore, the JC model was modified to include also softening at higher strains. An approach similar to that described by Sima and Özel [5] was used in this work by adding an a strain softening term to the Johnson-Cook model. The modified JC model is shown in Equation 4.

The parameters of the Johnson-Cook models for both materials are shown in Table 1.

$$\sigma_a = Eq(6) * \left[- \left(- \tanh(\varepsilon) \right) \right] \quad (4)$$

Table 1. Johnson – Cook model parameters for the studied materials.

Parameter	Titanium 15-3	Alloy 625
A	984	559
B	380	2201
n	0.3	0.8
C	0.069	0.0002
m	1.1	1.146
k	--	4.5
T_m	1669 °C	1350 °C
$\dot{\varepsilon}_{ref}$	1400 s^{-1}	1670 s^{-1}

The major differences in the obtained parameters for the two materials are the significantly higher yield strength of the titanium alloy and the higher strain hardening rate of Alloy 625. The strain rate sensitivity of both materials, especially Alloy 625, is very low in the high strain rate region.

The high strength and low temperature conductivity of the titanium alloy lead to higher adiabatic heating compared to that of Alloy 625. This strong adiabatic heating and consequent thermal softening combined with the relatively low strain hardening rate (parameters B and n) at high strain rates allow using the Johnson-Cook model for extrapolating the material behaviour to large strains without adding an extra strain softening term to the function. For Alloy 625, the observed strong strain hardening rate at room temperature, on the other hand, makes the extrapolation impossible without the strength becoming unreasonably high at large deformations.

Figure 5 shows the stress – strain curve obtained at the strain rate of 3300 s^{-1} for the titanium 15-3-3-3 alloy. The yield behaviour of the material at high strain rates is somewhat pronounced and the strength decreases after yielding from about 1250 MPa to about 1200 MPa. This pronounced yielding was observed at high strain rates, but it was omitted when determining the model parameters. Modelling of the pronounced yielding is somewhat difficult with such a simple model as the JC Equation. In addition, the effect of the higher strength at yielding on the chip formation is negligible and can therefore be omitted in the model. The adiabatic data calculated using Equation 6 fits well to the experimentally obtained adiabatic data at the strain rate of 3300 s^{-1}. At higher strains, the adiabatic heating decreases the strength significantly allowing modelling of the strain localization at high strains and strain rates.

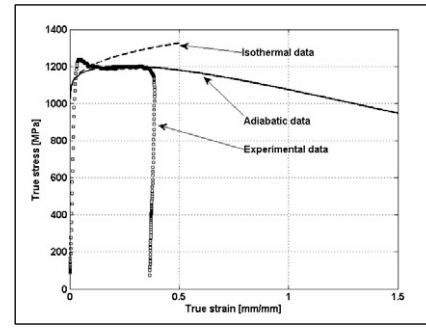

Fig. 5. Experimental data and the isothermal and adiabatic Johnson-Cook model data calculated at strain rate 3300 s^{-1} for the titanium 15-3-3-3 alloy.

Modelling of the behaviour of Alloy 625 requires using the strain softening term in the JC model. The effects of the strain softening are shown in Figure 6. Without strain softening, the parabolic hardening function of the model increases strength of the material above 2000 MPa before the thermal softening becomes a dominant factor and the adiabatic flow stress starts to decrease. This behaviour was found unsuitable for producing segmented chips and shear bands in tentative simulations of orthogonal cutting. However, introducing the strain softening exponent k=2 decreases the maximum stress to about 1550 MPa. Increasing the strain softening exponent to k=4 and k=4.5 actually increases the maximum stress, but the peak shifts to clearly lower strains and the softening following the maximum stress in much stronger than that observed for smaller values of the strain softening exponent. For k=4.5 the strength of the material decreases to about 250 MPa at strain 2. The current strain softening term does not essentially affect the simulated flow stresses at small strains, and the match between the experimental data and the simulated values is essentially the same with or without the strain softening.

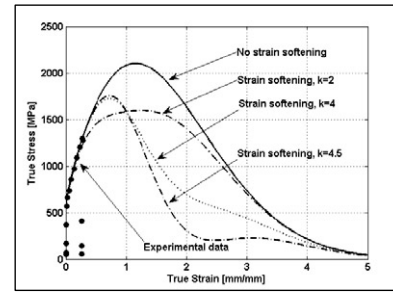

Fig. 6. Experimental data obtained at room temperature at the strain rate of 3500 s^{-1} and the simulated stress-strain curves with different values of the strain softening exponent.

4 Simulations

ABAQUS 6.9-1 software was used to create a two dimensional explicit finite element model No heat conduction was allowed between the tool and the chip. Very fine meshing was used for the workpiece, and the models contained 101151 nodes and 100049 elements, as shown in Figure 7. The separation of the chip from the workpiece was modelled using a sacrificial layer whose elements were deleted when the shear strain exceeded the value of 1.0.

The results of the simulations were compared to the cutting tests done with the Hopkinson Split Bar device using U-shape specimens. The U-shape test is carried out by inserting the cutting tool between the 'arms' of the U and placing the specimen-tool assembly between the incident and transmitted stress bars. The test is carried out by impacting the striker to the free end of the incident bar and measuring the cutting forces from the transmitted bar.

The simulations were run using the same cutting speed and depth as were used in the experiments. The simulation results for the titanium alloy and Alloy 625 are shown in Figures 8 and 9, respectively. For the titanium alloy, serrations are clearly visible, but the chip curl and overall shape is somewhat different from that observed in machining. For Alloy 625 the serrations are also clear and distinct, but much coarser than those observed for the titanium alloy. Closer inspection of the shear bands in Alloy 625 shows splitting of the shear bands near the tool edge, which is also observed in experimentally obtained chips. For both materials, however, the overall shape of the chip as well as the fine details, such as the thickness of the individual serration, are somewhat different from those observed in the experiments.

The cutting forces obtained from cutting experiments with the U-shape specimen compare quite well with the titanium alloy. At the cutting speed of 15 m/s and cutting depth of 44 µm the cutting force was 2200 MPa, while the simulated cutting force was 2000 MPa. The 10% difference in the cutting forces can at least partly be explained by the different frictional conditions in the experiments and simulations. In the simulations, a conservative friction coefficient of 0.1 was used between the tool and the chip.

For the Alloy 625, the cutting forces obtained from the simulations are significantly higher the experimentally obtained values. The experimental cutting stress was 1620 MPa, whereas the simulated force was 1900 MPa. The simulations were run without friction, and therefore, the difference in the cutting forces was even higher if friction would be included in the simulations. The overestimated cutting force is most likely due to the overestimated strength of the material at high strains.

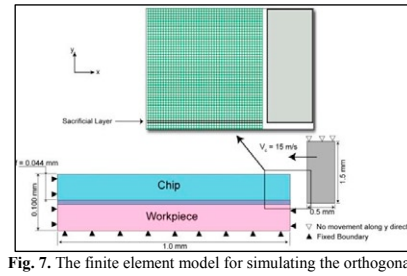

Fig. 7. The finite element model for simulating the orthogonal cutting of the titanium 15-3-3-3 alloy.

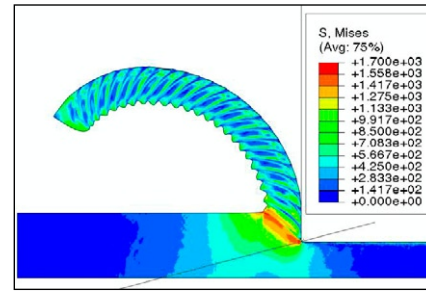

Fig. 8. Simulation results for the titanium 15-3-3-3 alloy.

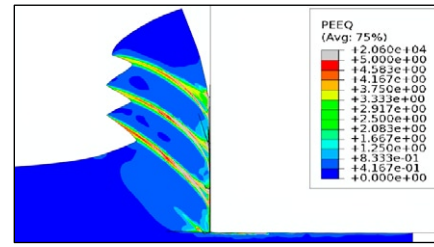

Fig. 9. Simulation results for Alloy 625.

5. Summary

Mechanical behaviour of titanium 15-3-3-3 alloy and a nickel based superalloy, similar to Inconel 625, were studied in this work. The dynamic response of the materials was studied in compression at different strain rates and temperatures. At high strain rates the titanium 15-3-3-3 alloy shows high strength and low strain hardening at room temperature. The strength of the material decreases strongly, when temperature is increased from room temperature to 400 °C. At even higher temperatures the strength decreases almost linearly with temperature. Alloy 625, on the other hand, shows strong and essentially strain rate independent strain hardening at room temperature.

Numerical material models, based on the common Johnson-Cook model, were developed for the studied materials and used in the simulations of orthogonal cutting experiments. Johnson-Cook material model parameters were obtained from the isothermal stress strain curves derived from the initial compression test data at different strain rates and temperature. For the titanium alloy, the Johnson-Cook model predicts a decrease in strength with increasing strain and adiabatic heating, but for Alloy 625 the model overestimates the strength at large deformations due to its strong parabolic strain hardening term. The model for Alloy 625 was therefore modified to include also the observed strain softening at higher strains.

The simulation results for the titanium alloy show a good match with the experimentally obtained cutting stresses. However, the chip shape and the fine details do not match perfectly and more work is needed to develop the model further. For Alloy 625, the material model predicts strain localisation and splitting of the shear bands near the edge of the tool. However, despite the added strain softening term, the strength predicted by the model is still too high and the simulated cutting stresses clearly higher than those obtained from the cutting experiments.

Acknowledgements

The research leading to these results has received funding from the European Union Seventh Framework Programme (FP7/2007-2013) under grant agreement No. PITN-GA-2008-211536, project MaMiNa.

References

1. M. Apostol, Ph.D. thesis, Tampere University of Technology (2007)
2. M. Apostol, V.-T. Kuokkala, T. Vuoristo, In: C. Papalettere (Eds.) *Advances in Experimental Mechanics* (McGraw-Hill, Bari Italy, 2004)
3. M. Apostol, T. Vuoristo, V.-T. Kuokkala, J. de Phys. IV, **110** (2003)
4. D. Gorman, J. Phys. E, **16** (1983).
5. M. Sima, T. Özel, Int. J. Mach. Tools & Manufacture, **50** (2010)
6. G. Johnson, W. Cook. Int. J. Eng. Fract. Mech. (1985)
7. G. Johnson, W. Cook, Proc. 7th International Symposium on Ballistics (1983)
8. E. O. Ezugwu, Z.M. Wang, A.R. Machado, J. Mat. Proc. Tech., **86**,(1999).
9. E.O. Ezugwu, J. Bonney, Y. Yamane,. J. Mat.Proc. Tech. **134**, (2003)
10. M. Rahman, Z. Wang, Y. Wong, JSME Int. J., Series C, **49**, (2006)

Hokka, M., **Leemet, T.**, Shrot, A., Baeker, M., Kuokkala, V.-T. Characterization and Numerical Modeling of High Strain Rate Mechanical Behavior of Ti-15-3 Alloy for Machining Simulations.

Materials Science and Engineering A. Nr. 550 (2012), pp. 350-357.

Materials Science and Engineering A 550 (2012) 350–357

Contents lists available at SciVerse ScienceDirect

Materials Science and Engineering A

journal homepage: www.elsevier.com/locate/msea

Characterization and numerical modeling of high strain rate mechanical behavior of Ti-15-3 alloy for machining simulations

M. Hokka[a,*], T. Leemet[a], A. Shrot[b], M. Baeker[b], V.-T. Kuokkala[a]

[a] Tampere University of Technology, Department of Materials Science, Finland
[b] Technische Universität Braunschweig, Institute for Materials, Germany

ARTICLE INFO

Article history:
Received 14 December 2011
Received in revised form 24 April 2012
Accepted 25 April 2012
Available online 3 May 2012

Keywords:
Titanium alloy
Hopkinson split bar
Material models
Machining

ABSTRACT

Metastable beta titanium alloys combine light weight, high strength, and excellent corrosion and fatigue resistance, and can therefore be very useful in many demanding applications. However, they are also difficult to machine and the machining costs of titanium components can be significant compared to the overall costs of the component. Finite element simulations can be used to optimize the cutting conditions and reduce the machining costs. However, any attempt to simulate the rather complex machining processes needs reliable material models that can only be generated when the mechanical behavior of the material is understood well. In this work, the mechanical properties and behavior of titanium 15-3 alloy was studied in a wide range of strain rates and temperatures, and a constitutive model was generated for simulating orthogonal cutting of the alloy. The strain-hardening rate of Ti-15-3 is a strong function of strain rate, and it decreases rapidly as the strain rate is increased. Also, the strain rate sensitivity of the material was found to depend strongly on temperature. Johnson–Cook plasticity model, based on isothermal stress–strain curves, was used to model the behavior of the material. The isothermal stress–strain response was calculated from the experimental data, and the model used in the simulations was modified to account also for the adiabatic heating and consequent thermal softening of the material. The current model is able to simulate the serrated chip formation frequently observed for titanium alloys at high cutting speeds.

1. Introduction

Metastable beta titanium alloys are very attractive materials especially for the aerospace industry. The excellent strength-to-weight ratio combined with good fatigue and corrosion resistance makes these alloys one of the best choices in, for example, different fasteners and connectors in demanding applications. However, most titanium alloys have low thermal conductivity and overall high chemical reactivity at high temperatures, which can cause problems in machining if the material adheres to the machining tools [20–22]. During machining, the adiabatic heating can easily increase the temperature of the deforming material and the tool by several hundreds of degrees and lead to rapid tool wear and increased machining expenses. In addition, at low cutting speeds the chip formation in the machining of titanium alloys can be continuous, and in the worst case the machining needs to be stopped and chip removed manually to avoid severe entanglement. For these reasons, most titanium alloys are classified as hard-to-machine materials, and majority of the total fabrication costs of geometrically complex components can be due to the high machining costs. Therefore, improving the machinability of titanium alloys by developing easy-to-machine alloys and by improving the machining technology can significantly reduce the overall manufacturing costs of titanium components.

Reliable finite element simulations always need material models that can mathematically reproduce the most essential features of the material behavior. Material behavior is influenced by strain rate and temperature, which can have significant effects on the strength and strain-hardening behavior of the material. In the literature, there are numerous mathematical models that have been generated for simulating the behavior of different materials. Probably the most commonly used material model is the one originally presented by Johnson and Cook [1,2]. This model presents the flow stress of the material as a function of strain, strain rate, and temperature with the aid of five fitting parameters, which are determined from the experimental data. Zerilli and Armstrong [3,4], in turn, presented a constitutive model vaguely based on dislocation dynamics. This model has a separate equation for each crystal structure, i.e., HCP, FCC, BCC, based on the different rate controlled deformation mechanisms in each structure. Another model, more strongly based on the underlying physics, was presented by Kocks [5] and Follansbee and Kocks [6–8]. In this Mechanical Threshold

* Corresponding author. Tel.: +358 40849 0132; fax: +358 33115 2330.
E-mail address: mikko.hokka@tut.fi (M. Hokka).

0921-5093/$ – see front matter © 2012 Elsevier B.V. All rights reserved.
http://dx.doi.org/10.1016/j.msea.2012.04.086

Stress (MTS) model, strain as a state variable is replaced by the mechanical threshold stress, which is used to describe the structure of the material. However, the Zerilli–Armstrong and MTS models are more complex and the application of these models requires special equipment as mechanical testing is required also at subzero and elevated temperatures. However, modeling of the material behavior for the machining simulations is further complicated by the need to extrapolate the material behavior determined at laboratory conditions to the actual machining conditions. Strain rates as high as $10^6\ s^{-1}$ and strains as large as 500% can occur in machining, and these ranges of strain rate and strain are very difficult to study by laboratory experiments.

Machining can be optimized by selecting optimal cutting conditions, such as tool material, rake angle, and feed rate for both maximized productivity and optimal surface quality. Optimizing the cutting conditions can be assisted by proper understanding of the plastic behavior of the material and also by numerically simulating the machining. The machining simulations of titanium alloys are, however, complicated by the material behavior, which often leads to a serrated chip shape and adiabatic shear banding in the most deformed regions. Therefore, the applied material model and the simulation have to be able to reproduce also this behavior. There are two main approaches that have been used to simulate the serrated chip shape and adiabatic shear banding; using a plasticity model and a failure criterion [17–19], or using a constitutive plasticity model with strain softening [13,14,16]. Both methods can be used to simulate the formation of the shear bands and serrated chip shape during machining. Lazoglu and Altintas [9] were able to solve the tool and chip temperatures in a continuous and discontinuous machining of different materials using different cutting conditions. Based on the calculations, they were also able to predict hazardous conditions, i.e., too high temperatures that would lead to rapid tool wear. Similar work was done by Shatla and Altan [10] using analytical modeling. Shatla et al. [11,12] also studied the mechanical properties and modeled the behavior of several metals and were able to resolve effects of tool geometry on the machining process of several steels. The machining simulations and machining research on titanium alloys has almost solely been done on the most commonly used alloy Ti–6Al–4V. Hua and Shivpuri [15] found by simulating the machining of Ti–6Al–4V that the chip breakage changes with cutting speed. The adiabatic heating at higher cutting rates increases the temperature of the material in the primary shear zone above the β transus and causes microstructural changes leading to different crack propagation. Sima and Özel [13] generated a constitutive model for the Ti–6Al–4V by adding a flow softening term to the Johnson–Cook model. Addition of the flow softening term allows the material to be deformed in the simulations to very high strains while maintaining the stress at a reasonable level. At large strains and high strain rates, it also allows the strength of the material to decrease due to the adiabatic heating of the material. Introducing the strain softening term into the model can be used to model adiabatic shear band and serrated chip formation without a separate failure model. According to Sima and Özel [13], both the degree of serrations and the chip curl increase with increasing flow softening. Similar results have also been published by Calamaz et al. [14].

In this work, the mechanical behavior and properties of the Ti-15-3 alloy were studied in compression over a wide range of strain rates and temperatures. Based on the results of the mechanical testing, Johnson–Cook model parameters were determined and the model was used for machining simulations. Both the results of the mechanical testing as well as the modeling approach are presented. The results of the mechanical testing are discussed also from the modeling point of view. Some preliminary results of the machining simulations are also presented.

2. Experimental

The material studied in this work is a commercial beta titanium alloy Ti–15V–3Sn–3Al–3Cr. The alloy was first prepared using a vacuum arc remelting (VAR) furnace, forged into a round billet with a diameter of 75 mm using rotary swaging at 850 °C, and finally water quenched from 700 °C to room temperature. The material was studied in as-received condition without any aging treatments. The cylindrical compression specimens with the diameter of 8 mm and length of 8 mm and/or 6 mm were machined using electric discharge machining.

Mechanical testing at low strain rates was performed using an MTS servohydraulic materials testing machine with a high temperature capability. High temperature tests were performed using a high power induction heater and measuring the strain with a high temperature extensometer. During the test, the temperature was kept constant by continuously adjusting the output power of the induction heater with a PID controller.

The high strain rate mechanical behavior of the titanium alloy was characterized using a Split Hopkinson Pressure Bar (SHPB) device with a high temperature setup. The device consists of 22 mm diameter high strength Maraging steel incident, transmitted, and striker bars. Both incident and transmitted pressure bars lie on the same horizontal axis supported by three bearings on four stanchions, which can be moved in y- and z-directions to ensure proper alignment of the pressure bars and the specimen. In the current setup, also a third bar is placed after the transmitted bar to capture the transmitted momentum and to prevent the transmitted pulse from reflecting back toward the specimen. The lengths of the incident, transmitted, and momentum trap bars were 1200 mm each, and the length of the striker bar varied between 200 mm and 400 mm. In a room temperature experiment, the small cylindrical specimen is placed between the lubricated ends of the incident and transmitted bars. The high strain rate test is carried out by creating a compressive stress pulse into the incident pressure bar by impacting the striker bar into its free end. The stress pulse travels in the pressure bar with the speed of sound (~4900 m/s) toward the specimen, and when the pulse reaches the bar-specimen interface, part of the pulse transmits through the specimen into the transmitted bar and part of it reflects back to the incident bar as a wave of tension. These three stress pulses are recorded using strain gages bonded on the surface of the pressure bars. The strain gage signals are then amplified using a Kyowa CDV 700A signal conditioner and recorded with a high speed Yokogawa DL 708 digital oscilloscope. The time resolved strain, strain rate, and stress in the specimen are calculated from the dispersion corrected stress pulses using Eqs. (1)–(3), assuming that the stresses in the specimen are uniform, which is true at least for strains higher than a few percent. The dispersion correction method used in this study is adopted from the work of Gorham [24].

Average stress in the specimen is given by:

$$\sigma(t) = \frac{A_b E \varepsilon_t(t)}{A_s} \tag{1}$$

Average strain in the specimen is given by:

$$\varepsilon(t) = \frac{2C_0}{L_s} \int_0^t \varepsilon_r(t)dt \tag{2}$$

Average strain rate in the specimen is given by:

$$\dot{\varepsilon}(t) = \frac{2C_0 \varepsilon_r(t)}{L_s} \tag{3}$$

In Eqs. (1)–(3), A_b, E, and C_0 are the cross sectional area, Young's modulus, and the speed of sound of the bar material, L_s and A_s are the length and cross sectional area of the specimen, and ε_r, and ε_t are the reflected and transmitted stress pulses.

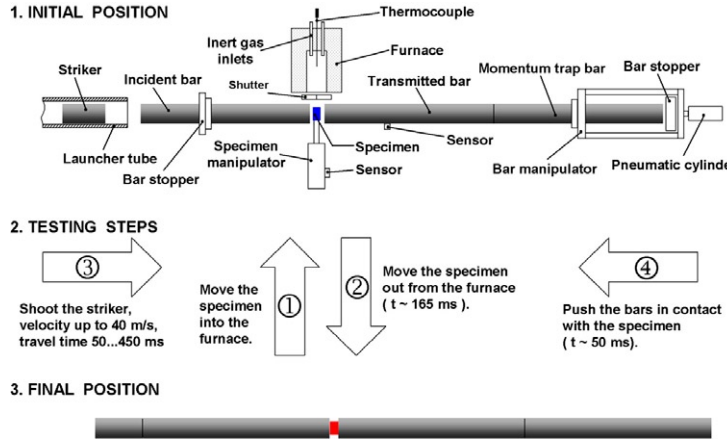

Fig. 1. Schematic illustration of the testing steps during a test with the high temperature setup.

The high strain rate tests at high temperatures were conducted using a furnace located beside the bars to heat the specimen to the desired temperature and mechanically manipulating the bars and the specimen during the heating and the actual compression test. The specimen is surrounded by a ceramic insulating wool ring exposing only the ends of the cylindrical specimen. The wool ring is placed in a specimen holder arm that can move the specimen inside the tube furnace. In this setup, the bars are kept at room temperature and only the specimen is heated. When the specimen reaches the desired test temperature, the specimen holder arm quickly retracts the specimen to the centerline of the bars. At this stage, the hot specimen is not touching the room temperature pressure bars. Immediately when the specimen reaches the centerline of the bars, the striker bar is shot, and just a fraction of a second before the impact, a second pneumatic manipulator pushes the bars and the specimen into contact. This setup limits the total time that the specimen spends outside the hot furnace before being dynamically deformed to about 200 ms, and more importantly, it limits the contact time between the hot specimen and the cold bars to less than 50 ms. Under these conditions, numerical simulations of the heat flow from the specimen to its surrounding show a temperature drop of only less than 9 °C in depth of less than 150 μm for a test performed at the initial temperature of 800 °C [23,26,27]. Fig. 1 shows the testing steps during a test with the high temperature system.

The high temperature testing performed in the described way assumes that the structure of the sample material does not change significantly during the heating up of the specimen and holding it at elevated temperatures before testing. For metastable β titanium alloys this is not necessarily true, and several phase transformations can take place at higher temperatures, especially in the current study because the tested material was not age hardened. Aging of the titanium 15-3 alloy is usually done in the temperature range of 500–550 °C [25], and therefore, the material behavior was studied at temperatures 600 °C and above. However, during extended periods at higher temperatures the structure can also change significantly by grain growth, leading to altered mechanical properties and behavior. In this work, some tests were also performed using a rapid heating system that uses the same specimen and bar manipulation system as the high temperature system described above. In the rapid heating system, however, the furnace is replaced by two copper electrodes that are connected to a high power DC welding transformer. With this setup, the specimen can be heated to the test temperature in only a few seconds by running a high amperage DC current through the specimen. The structural changes taking place prior to the actual compression test can, therefore, be largely minimized. However, preliminary testing revealed that the differences in the mechanical behavior of the Ti-15-3 alloy measured with the two different high temperature setups were negligible. Based on these tests, the microstructure was concluded to be reasonably stable in the tested temperature range, and the high strain rate mechanical testing was done using the high temperature setup shown in Fig. 1.

3. Results and discussion

The compression stress strain curves for the titanium 15-3 alloy at different temperatures and strain rates are shown in Fig. 2. At room temperature and strain rates below 1 s^{-1}, the yield strength of the material increases steadily as a function of strain rate. A significant increase in strength can be observed when strain rate is increased from 1 s^{-1} to 600 s^{-1}. The material shows relatively strong strain hardening at strain rates 10^{-4} s^{-1} and 10^{-3} s^{-1}, but the strain-hardening rate quickly decreases as the strain rate is increased. At higher strains the stress–strain curves obtained at the strain rates of 10^{-4} s^{-1} and 10^{-3} s^{-1} actually show higher stresses than the curves measured at strain rates 10^{-1} s^{-1} and 1 s^{-1}. At even higher strain rates (>600 s^{-1}) the stress–strain curves actually show a negative slope at small strains, and at larger strains the strain-hardening rate is essentially zero.

The stress–strain behavior changes significantly when temperature is increased from room temperature to 600 °C. The pronounced yield behavior consistently observed at high strain rates at room temperature is not observed anymore at higher temperatures. Also the shape of the curves changes and the overall strength

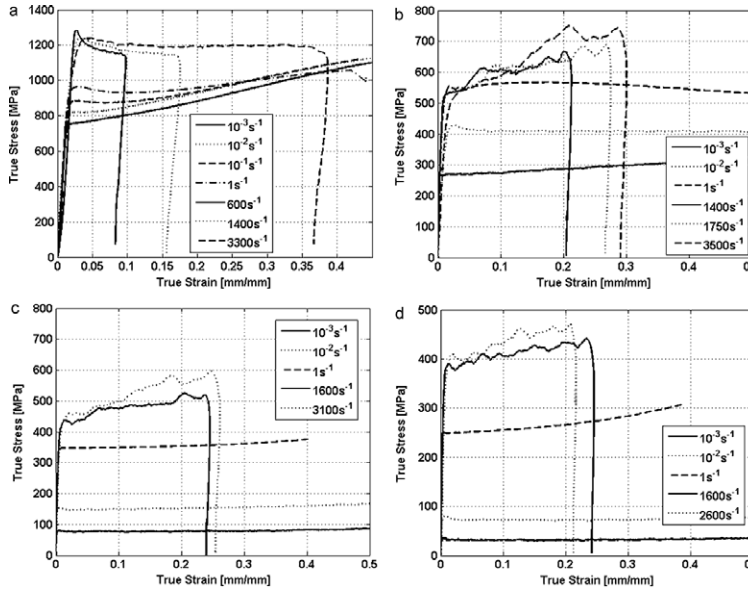

Fig. 2. Compression stress–strain curves for the titanium 15-3 alloy measured at (a) room temperature, (b) 600 °C, (c) 800 °C, and (d) 950 °C.

level decreases significantly, when the temperature is increased. At 600 °C at the strain rate of $10^{-3}\,s^{-1}$ (Fig. 2b) the strain-hardening rate slightly decreases compared to that observed at room temperature. At strain rate $10^{-1}\,s^{-1}$ the strain-hardening rate is essentially zero, and at strain rate $1\,s^{-1}$ the material strain hardens at low strains but strain softens at larger strains. At strain rates above $1\,s^{-1}$, the material shows strong strain hardening, which was not observed in the room temperature experiments. At 800 °C and 950 °C (Fig. 2c and d) the strength of the material decreases further, and the only significant change in the flow behavior compared to that at 600 °C is the slightly increasing strain-hardening rate at the strain rate of $1\,s^{-1}$ at larger strains.

The strain rate sensitivities of Ti 15-3 at strain rates $<1\,s^{-1}$ at different temperatures are shown in Fig. 3. At room temperature, the logarithmic strain rate sensitivity, $m = \partial \log\sigma / \partial \log\dot{\varepsilon}$, is very low and decreases slightly toward higher strains. The overall strain rate sensitivity increases significantly when temperature is increased. At 600 °C and 800 °C the strain rate sensitivities are almost constant with respect to plastic strain, while at 950 °C the strain rate sensitivity slightly increases with increasing amounts of deformation.

In contrast to the low strain rate region, the apparent strain rate sensitivity in the high strain rate region is higher at room temperature than at elevated temperatures. The sensitivity is lowest at 600 °C and then increases slightly toward higher temperatures. This can be seen in Fig. 4, where the flow stress at 10% of plastic strain is plotted as a function of logarithmic strain rate. It should, however, be noted that the comparison of the strain rate sensitivities presented in Figs. 3 and 4 is not straightforward. The logarithmic strain rate sensitivity in Fig. 3 is based on the relative change in stress, whereas the strain rate sensitivity indicated by the slope of the plotted curves in Fig. 4 shows only the absolute change of stress due to changing strain rate.

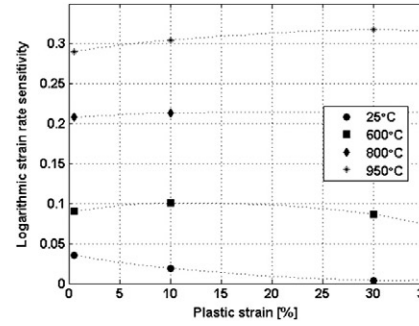

Fig. 3. Logarithmic strain rate sensitivity for strain rates between $10^{-4}\,s^{-1}$ and $1\,s^{-1}$ as a function of plastic strain at different temperatures.

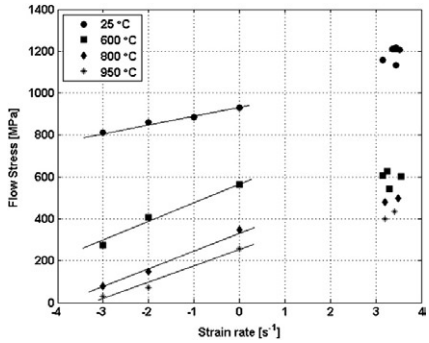

Fig. 4. Flow stress at 10% of plastic strain at different temperatures.

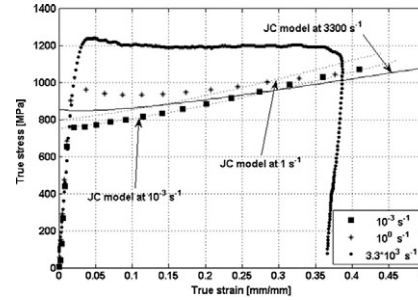

Fig. 5. Measured true stress vs. true strain curves and the corresponding values calculated with the Johnson–Cook model. The parameters of the model were determined using the experimental data for the entire studied temperature and strain rate regime (first row in Table 1).

3.1. Modeling approach

The mechanical behavior of Ti-15-3 alloy presents several challenges regarding the mathematical modeling of that behavior. At room temperature, the relatively strong strain-hardening rate observed at low strain rates quickly decreases as the strain rate is increased, and at strain rates around 3000 s^{-1} the behavior at strains above 10% is nearly ideally plastic showing essentially no hardening or softening with plastic strain. Also the strain rate sensitivity of the material increases at low strain rates but decreases at high strain rates with temperature. Therefore, it is very difficult to generate only one equation of state describing this complex behavior in such a wide range of strain rates and temperatures.

In this work, the Johnson–Cook plasticity model was used to describe the material behavior at different strain rates and temperatures. However, there are some inherent problems with the Johnson–Cook equation and its fitting to the measurement data. For the titanium 15-3 alloy, the strain-hardening rate clearly decreases with strain rate, whereas the Johnson–Cook model predicts an increasing strain-hardening rate with strain rate for any material with positive strain rate sensitivity or parameter C. If the Johnson–Cook model is fitted to the studied range of strain rates and temperatures, its predictions are not very good outside the reference temperature and strain rate. This can be seen in Fig. 5, where experimental data are shown with the stress values calculated with the Johnson–Cook model. The model fails to predict the material behavior at higher strain rates and clearly underestimates the strength of the material at the strain rate of 3300 s^{-1}. However, in machining the ranges of temperature and strain rate are slightly different from those covered by the experiments of this study, which needs to be considered when choosing the Johnson–Cook model parameters. Low strain rate deformations at high temperatures are not likely to occur during machining, and therefore, more accurate model can be generated using only the high strain rate data at different temperatures. Also, the studied strain rate and strain regions are too low compared to the machining. Therefore, the predictive power of the model needs to be strong enough to enable extrapolation of the material behavior to much higher strains and strain rates. The conventional Johnson–Cook equation does not take into account the thermal softening due to the adiabatic heating of the material during deformation. Therefore, the model needs to be modified to also include the thermal softening due to adiabatic heating, which can be done simply by adding Eq. (4) into the temperature term of the Johnson–Cook model and making $T = T(\varepsilon)$. The Johnson–Cook model used in the simulations is presented by Eq. (5). In this equation, β is the fraction of the mechanical energy that is converted to heat; ρ and c are the density and specific heat capacities of the material. The value for β was chosen based on the literature, where typical values range from 0.9 up to 1. It should be noted that the model is unmodified Johnson–Cook equation for calculating adiabatic stress. There are various material models presented in the literature, e.g., by Calamaz [14,16] and Sima and Özel [13], which are modified Johnson–Cook equations with extra parameters and terms for stronger strain softening. These modifications are needed when the thermal softening alone is not strong enough to localize deformation and to produce segmented chips.

$$\Delta T = \frac{\beta}{\rho c}\int \sigma d\varepsilon \tag{4}$$

$$\sigma_a = (A + B\varepsilon^n)\left(1 + C\ln\frac{\dot{\varepsilon}}{\dot{\varepsilon}_{ref}}\right)\left(1 - \left[\frac{T + ((\beta/\rho c)\int_0^{\varepsilon}\sigma d\varepsilon) - T_{ref}}{T_m - T_{ref}}\right]^m\right) \tag{5}$$

For the model used in the simulations, the parameters A, B, and n of the Johnson–Cook model were determined from the isothermal stress vs. strain curve obtained at the reference temperature and strain rate. The isothermal stress strain curves were obtained from the measured adiabatic stress strain curves using Eq. (6), where σ_i and σ_a are the calculated isothermal and measured adiabatic stresses, ρ and c are the density and specific heat of the material.

$$\sigma_i = \frac{\sigma_a}{[1 - ((T + ((\beta/\rho c)\int_0^{\varepsilon}\sigma d\varepsilon) - T_r)/(T_m - T_r))^m]} \tag{6}$$

The parameter m was first determined using Eq. (7), where the yield strengths σ_{Tr}^{Y} and σ_{T2}^{Y} are obtained at the reference strain rate at reference temperature and at elevated temperature, respectively. The values given by this equation were, however, found not to produce a good match between the calculated and experimental data at higher strains. Therefore, the value of the parameter m was slightly adjusted by simple trial and error method by comparing the calculated and measured stress strain curves obtained at the reference strain rate and at different temperatures.

$$m = \frac{\log(1 - (\sigma_{T2}^{Y}/\sigma_{Tr}^{Y}))}{\log(T_2 - T_r/T_m - T_r)} \tag{7}$$

Parameter A in the conventional JC model is the yield strength obtained at reference temperature and reference strain rate. For the

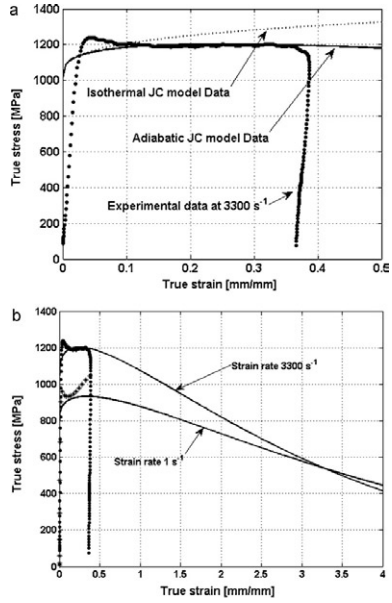

Fig. 6. Experimental data and data produced by the high strain rate Johnson–Cook model: (a) isothermal and adiabatic true stress vs. true strain curves at the strain rate of 3300 s^{-1}, and (b) experimental data and values calculated by the model and extrapolated to large strains at strain rates 3300 s^{-1} and 1 s^{-1}.

titanium 15-3-3-3 alloy, however, the yield strength is somewhat pronounced at high strain rates, and the parameter A was determined simply so that the stress calculated by the model matches better the experimental stress at higher strains. Parameters B and n were determined by fitting a line to the $\log(\sigma - A)$ vs. $\log(\varepsilon)$ plot, and the parameter C was determined by comparing the experimentally obtained stress strain curves with the curves calculated by the model at reference temperature and different strain rates. The procedure for determining the Johnson–Cook model parameters is explained in more details in, for example, Ref. [29].

The parameters for the Johnson–Cook models that were used in this work are shown in Table 1. The measurement data and both the isothermal and the adiabatic stresses calculated with the high strain rate model are shown in Fig. 6a, and Fig. 6b shows the data extrapolated to higher strains. The fit at the strain rate of 3300 s^{-1} with this model seems to be very accurate after the first 10% of strain. The pronounced yielding that occurs at high strain rates is very difficult to model, but it only has a small effect on the overall behavior of the material and was therefore omitted. The thermal softening produced by the adiabatic heating can be clearly seen in Fig. 6b. If the measured data is extrapolated using the current Johnson–Cook model, the strength of the material clearly decreases toward higher strains. The strength of the material at the strain rate 3300 s^{-1} approaches the strength at 1 s^{-1} and the two lines actually cross at around strain of 3.25. The stronger softening of the material at higher strain rates is of course due to the higher strength and therefore faster adiabatic heating of the material.

3.2. Simulations

A two dimensional explicit finite element model was created using the commercial software ABAQUS 6.9-1. The tool was assumed rigid and no heat conduction was allowed between the tool and the chip. A friction coefficient of 0.1 was used between the tool and the deforming material. The workpiece was meshed very finely and the model contains 101,151 nodes and 100,049 elements (Fig. 7). Since the alloy has low thermal conductivity, the machining process was assumed adiabatic at the cutting speed of 15 m/s. The workpiece was modeled using CPE4R elements and the cutting depth was 44 μm. The chip separation was modeled by using a sacrificial layer whose elements were deleted when the shear strain exceeded a value of 1.0. The material parameters for the high strain rates listed in Table 1 were used in the model.

To verify the simulation results, orthogonal cutting experiments were carried out with the Hopkinson Split Bar device using 'U-shape' specimens. A schematic picture of the U-shape test specimen is shown in Fig. 8. In this test, the cutting tool is simply inserted between the arms of the 'U'-shaped specimen, and the specimen-tool assembly is placed between the incident and transmitted bars.

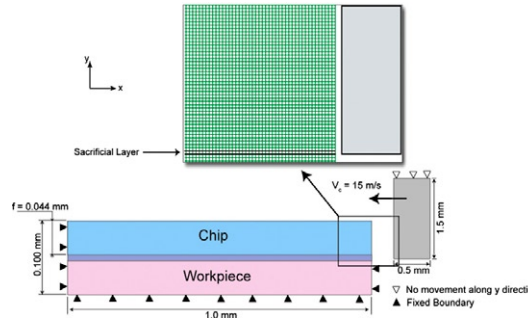

Fig. 7. The finite element model.

Table 1
The parameters for the Johnson–Cook models used in this work.

Model with the parameters determined for	A [MPa]	B [MPa]	n	C	m	T_r [°C]	T_m [°C]	$\dot{\varepsilon}_{ref}$ [s^{-1}]	β	C_p [J/(kgK)]	ρ [kg/m^3]
Whole studied range of T and $\dot{\varepsilon}$	754	882	1.3	0.02	0.7	23	1669	0.001	–	–	–
High strain rates only	984	380	0.3	0.069	1.1	23	1669	1400	0.9	500	4760

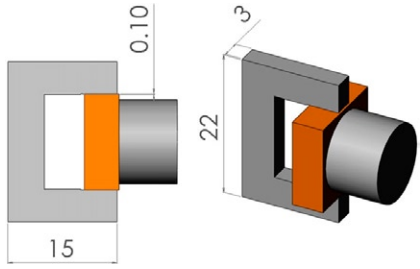

Fig. 8. Schematic picture of the U-shape specimen for cutting force measurement. Units are in millimeters.

Impacting the striker bar to the incident bar will force the tool forward between the arms of the 'U' leading to controlled chip formation. The cutting force can be easily calculated from the transmitted bar signal. The drawback of these simple experiments is the fact that the chips cannot usually be recovered after the experiment. In this study the comparison of the experimental and simulated chip shapes are based on the chips recovered from the U-shape experiments and quick-stop cutting experiments performed at Technische Universität Braunschweig, but the chip with an exact match to the simulated conditions, i.e., cutting speed and cutting depth was not available. For these reasons, a very conservative and simplified approach was chosen for the discussions concerning the comparison of the simulated and experimental chip shapes.

The cutting speed in the simulations and experiments was 15 m/s and the cutting depth 44 μm. The simulated (Fig. 9) and experimentally obtained chips show somewhat similar serrations, but some differences can be observed in the chip curl, overall chip shape, and in fine details such as the dimensions of individual segments. On the other hand, the average cutting stresses obtained from the simulations compare very well with the experimentally determined cutting stresses. The average cutting stress obtained from the simulations was 2000 MPa, whereas the experimentally determined stress was 2200 MPa. The 10% difference in the cutting stresses can be explained at least partly with the small differences

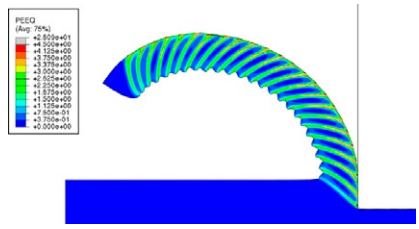

Fig. 9. The plastic equivalent strain in the simulations. Cutting speed 15 m/s and cutting depth 44 μm.

in the frictional conditions between the simulated and experimental setups. Despite the good agreement of the simulated and experimentally determined cutting stresses, the model needs to be further developed to match also the chip shape. The model can be further improved by, for example, optimization of the parameters using inverse methods [28].

4. Conclusions

The mechanical behavior of titanium 15-3-3-3 alloy was studied in a wide range of strain rates and temperatures. The parameters for the Johnson–Cook material model were determined from the test results, and the model was used to simulate machining of the material.

The strain-hardening rate of the Ti-15-3 alloy depends strongly on both strain rate and temperature. At low strain rates and at room temperature, the strain-hardening rate was rather high, but it quickly decreased when the strain rate was increased. At strain rates above 600 s^{-1}, the material showed slight strain softening at low strains, and at higher strains the slope of the stress strain curve was essentially zero. At higher temperatures, the strain-hardening rate at low strain rates was lower than at room temperature, but at higher strain rates the strain-hardening was much stronger compared to than observed at room temperature. At strain rates less than 1 s^{-1}, the strain rate sensitivity of the material increases strongly with temperature.

The Johnson–Cook model parameters were determined from the isothermal stress strain curves. The obtained model was used to simulate orthogonal cutting of the titanium 15-3 alloy. The model was capable of producing segmented chips and the simulation results match well with the cutting experiments. The cutting stress obtained from the simulations and from the experiments was around 2000 MPa and 2200 MPa, respectively.

Acknowledgements

The research leading to these results has received funding from the European Union Seventh Framework Programme (FP7/2007-2013) under Grant Agreement No. PITN-GA-2008-211536, project MaMiNa.

References

[1] G. Johnson, W. Cook, Proceedings of the 7th International Symposium on Ballistics, 1983.
[2] G. Johnson, W. Cook., Int. J. Eng. Fract. Mech. (1985).
[3] F. Zerilli, R. Armstrong, J. Appl. Phys. 61 (1987).
[4] F. Zerilli, R. Armstrong, J. Phys. IV 10 (2000).
[5] U. Kocks, J. Eng. Mater. Technol. 98 (1976).
[6] P. Follansbee, in: L. Murr, K. Staudhammer, M. Meyers (Eds.), Metallurgical Applications of Shock-Wave and High-Strain-Rate Phenomena, Marcel Dekker Inc., New York, 1986.
[7] P. Follansbee, U. Kocks, Acta Mater. 36 (1988).
[8] P. Follansbee, G. Gray, Mater. Sci. Eng. A 138 (1991).
[9] I. Lazoglu, Y. Altintas, Int. J. Mach. Tools Manuf. 42 (2002) 1011–1022.
[10] M. Shatla, T. Altan, J. Mater. Process. Technol. 98 (2000) 125–133.
[11] M. Shatla, C. Kerk, T. Altan, Int. J. Mach. Tools Manuf. 41 (2001) 1511–1534.
[12] M. Shatla, C. Kerk, T. Altan, Int. J. Mach. Tools Manuf. 41 (2001) 1659–1680.
[13] M. Sima, T. Özel, Int. J. Mach. Tools Manuf. 50 (2010) 943–960.
[14] M. Calamaz, D. Coupard, F. Girot, Int. J. Mach. Tools Manuf. 48 (2008) 275–288.
[15] J. Hua, R. Shivpuri, J. Mater. Process. Technol. 150 (2004) 124–133.
[16] M. Calamaz, D. Coupard, F. Girot, Mater. Sci. Technol. 14 (2010) 244–257.
[17] G. Chen, C. Ren, X. Yang, X. Jin, T. Guo, Int. J. Adv. Manuf. Technol. (March 2011), http://dx.doi.org/10.1007/s00170-011-3233-6.

[18] E. Ceretti, P. Fallböhmer, W.T. Wu, T. Altan, J. Mater. Process. Technol. 59 (1996) 169–180.
[19] E. Ceretti, M. Lucchi, T. Altan, J. Mater. Process. Technol. 95 (1999) 17–26.
[20] M. Rahman, Z. Wang, Y. Wong, JSME Int. J. Ser. C 49 (1) (2006).
[21] P.D. Hartung, B.M. Kramer, B.F. von Turkovich, CIRP Ann. Manuf. Technol. 31 (1982) 75–80.
[22] A. Jawaid, C.H. Che-Haron, A. Abdullah, J. Mater. Process. Technol. 92–93 (1999) 329–334.
[23] M. Apostol, Ph.D. thesis, Tampere University of Technology, 2007.
[24] D. Gorham, J.E. Phys, Sci. Instrum. 16 (1983).
[25] J. Ma, Q. Wang, Mater. Sci. Eng. A243 (1998) 150–154.
[26] M. Apostol, V.-T. Kuokkala, T. Vuoristo, in: C. Papalettere (Ed.), Advances in Experimental Mechanics, McGraw-Hill, Bari, Italy, 2004.
[27] M. Apostol, T. Vuoristo, V.-T. Kuokkala, J. Phys. IV 110 (2003).
[28] A. Shrot, M. Bäker, J. Com. Mater. Sci. 52 (2012) 298–304.
[29] D. Samantaray, S. Mandal, A. Bhaduri, J. Commun. Mater. Sci. 47 (2009) 568–576.

CURRICULUM VITAE

First name: Tõnu
Last name: Leemet
Date of Birth: 09 November 1979
Address: Estonian University of Life Sciences Institute of Technology, Fr.R.Kreutzwaldi 56, Tartu 51014, Estonia
Phone: +372 56 659 869
E-mail: Tonu.Leemet@emu.ee

Education:

1986 – 1998	Tartu Mart Reiniku High School
1998 – 2003	B.Sc. applied physics, University of Tartu
2003 – 2007	M.Sc. production engineering, Estonian University of Life Sciences
2009 – 2012	Doctoral studies, Tampere University of Technology (FIN). Faculty of Automation, Mechanical and Materials Engineering.
2007 – 2012	Doctoral studies, Estonian University of Life Sciences.

Professional employment

2003 – 2008	Estonian University of Life Sciences, Institute of Technology. Started as teaching assistant. At 2007 elected as a lecturer. College teacher for the subjects of applied physics, CAD
2004 – 2008	Est-Doma, project manager. Sales of scientific and industrial measuring equipment
2008 – 2011	Tampere University of Technology, Finland. Research scientist, materials science
2011 –	Tartu Science Park Foundation. Development manager at semi-industrial CNC workshop “Protolab”, project manager

Supplementary courses and training:

2009	Workshop “Titanium and Titanium Alloys” March 16-23, 2009 2010 at the Technische Universität Braunschweig Institut für Werkstoffe

2009	Workshop “Machining and Machine Tools” March 9-14, 2009 at the Lodz University of Technology, Faculty of Mechanical Engineering
2010	Workshop “Scientific Presentations / Networked Collaboration” January 19-21, 2010 at the Technische Universität Braunschweig Institut für Werkstoffe
2010	Workshop “Acting professionally in Teams” February 22-25, 2010 Volkswagen AG
2010	Workshop “Introduction to Computer Simulation of Alloys” May 3-8th 2010 National e-Science Centre, Edinburgh 15 South College St.
2010	Workshop “PROGRESSIVE CUTTING METHODS” 13-17 September 2010, Loughborough University, UK
2010	Workshop “European Projects/European Patents” December 1-3, 2010, Brussels
2011	Workshop “Nickel-base superalloys” at ALSTOM Switzerland Ltd. (ALS) March 14-16 2011, Baden, Switzerland

Research projects

2012 – 2014	Project “Advanced thin hard coatings in tooling”, researcher

Dissertations supervised

2009	Erich Tohvre, Master’s Degree
2007	Pearu Orusalu, Bachelors Degree
2007	Marten Madissoo, Bachelors Degree

Knowledge of foreign languages

English

ELULOOKIRJELDUS

Eesnimi: Tõnu
Perekonnanimi: Leemet
Sünniaeg: 09. novembril 1979
Aadress: Eesti Maaülikool, Tehnikainstituut, Fr.R.Kreutzwaldi 56, Tartu; Eesti
Telefon: +372 56659869
E-post: Tonu.Leemet@emu.ee

Haridustee:

1986 – 1998	Tartu Mart Reiniku Gümnaasium
1998 – 2003	B.Sc. Tartu Ülikool, Füüsikaosakosakond, rakendusfüüsika suund, füüsikalise infotehnoloogia eriala
2003 – 2007	M.Sc. tootmistehnika erialal Eesti Maaülikool/EPMÜ
2009 – 2012	Doktoriõpe, Tampere Tehnikaülikool, Soome. Automaatika, Materjalitehnika ning Mehhaanika teaduskond
2007 – 2012	Doktoriõpe, Eesti Maaülikooli Tehnikainstituut

Täiendharidus:

2009	Workshop “Titanium and Titanium Alloys” March 16-23, 2009 2010 at the Technische Universität Braunschweig Institut für Werkstoffe
2009	Workshop “Machining and Machine Tools” March 9-14, 2009 at the Lodz University of Technology, Faculty of Mechanical Engineering
2010	Workshop “Scientific Presentations / Networked Collaboration” January 19-21, 2010 at the Technische Universität Braunschweig Institut für Werkstoffe
2010	Workshop “Acting professionally in Teams” February 22-25, 2010 Volkswagen AG
2010	Workshop “Introduction to Computer Simulation of Alloys” May 3-8th 2010 National e-Science Centre, Edinburgh 15 South College St.
2010	Workshop “PROGRESSIVE CUTTING METHODS” 13-17 September 2010, Loughborough University, UK.

2010	Workshop “European Projects/European Patents” December 1-3, 2010, Brussels.
2011	Workshop “Nickel-base superalloys” at ALSTOM Switzerland Ltd. (ALS) March 14-16 2011, Baden, Switzerland.

Teenistuskäik

2003 – 2008	Eesti Põllumajandusülikool/ Eesti Maaülikool. Laborant. Alates 2007 kuni lõpp, lektor
2004 – 2008	Est-Doma, projektijuht. Mõõtetehnika müük
2008 – 2011	Tampere Tehnikaülikool. Teadur materjalitehnika suunal, materjalide mehhaaniliste omaduste uurimine
2011 –	Tartu Teaduspark. Pooltööstusliku peenmehaanika labori “Protolab” arendusjuht, projektijuht

Uurimisprojektid

2012 – 2014	Projekt “Advanced thin hard coatings in tooling”, teadur

Juhendatud väitekirjad

2009	Erich Tohvre, magistritöö
2007	Pearu Orusalu, bakalaureusetöö
2007	Marten Madissoo, bakalaureusetöö

Võõrkeelte oskus

Inglise

VIIS VIIMAST KAITSMIST

HANNO JAAKSON

INSULIN RESISTANCE IN DAIRY COWS IN REFERENCE TO BREED, BODY CONDITION AND MILK YIELD

INSULIINIRESISTENTSUSEST PIIMALEHMADEL JA SELLE SEOSTEST TÕU TOITUMUSE JA PIIMA TOODANGUGA

prof. emer. **Olav Kärt**, vanemteadur **Katri Ling**

13. detsember 2012

KAI GINTER

THE DIET OF JUVENILE PIKEPERCH *SANDER LUCIOPERCA* IN LAKES PEIPSI AND VÕRTSJÄRV: RELATIONS BETWEEN LONG-TERM CHANGES IN THE FISH COMMUNITIES AND FOOD RESOURCES IN LARGE SHALLOW LAKES

KOHA *SANDER LUCIOPERCA* NOORKALADE TOITUMINE PEIPSIS JA VÕRTSJÄRVES: SEOSED KALASTIKU KOOSSEISU JA TOIDUVARUDE PIKAAJALISTE MUUTUSTEGA MADALATES SUURJÄRVEDES

vanemteadur **Külli Kangur**, vanemteadur **Andu Kangur**, teadur **Peeter Kangur**

18. detsember 2012

RENE FREIBERG

HOW PHYTOPLANKTON PIGMENTS REFLECT HISTORICAL AND CONTEMPORARY STATUS OF LARGE SHALLOW LAKES?

KUIDAS FÜTOPLANKTONI PIGMENDID PEEGELDAVAD SUURTE MADALATE JÄRVEDE AJALOOLIST JA TÄNAPÄEVAST SEISUNDIT?

vanemteadur **Arvo Tuvikene**, vanemteadur **Ilmar Tõnno**

18. detsember 2012

KAUPO TOOM

POSSIBILITIES FOR BALANCING WIND GENERATORS OUTPUT POWER

TUULIKUTE VÄLJUNDVÕIMSUSTE BALANSSEERIMISE VÕIMALUS

prof. **Andres Annuk**

18. detsember 2012

JÜRGEN AOSAAR

THE DEVELOPMENT AND BIOMASS PRODUCTION OF GREY ALDER STAND ON ABANDONED AGRICULTURAL LAND IN RELATION TO NITROGEN AND CARBON DYNAMICS

ENDISELE PÕLLUMAALE RAJATUD HALL-LEPIKU ARENG, BIOMASSI PRODUKTSIOON JA LÄMMASTIKU- NING SÜSINIKU DÜNAAMIKA

dotsent **Veiko Uri**

20. detsember 2012

ISBN 978-9949-484-62-1